STUDIA
UNIVERSITATIS BABEŞ-BOLYAI

PHYSICA

1

1987

CLUJ-NAPOCA

ANUL XXXII 1987

STUDIA

UNIVERSITATIS BABEŞ-BOLYAI

PHYSICA

1

Redacţia: 3400 CLUJ-NAPOCA, str. M Kogălniceanu, 1 Telefon ☎ 1 61 01

SUMAR — CONTENTS

C. BĂLEANU, S COLDEA, J. KARACSONY, Effect of a Spatially Uniform External Periodic Magnetic Field on Wave Propagation Through Plasma 3

M. COLDEA, I. POP, V. CRIŞAN, Quadrupole Interactions in $Hf_{1-x}Zr_xV_2$ Intermetallic compounds 11

L. POP, C. MARALOIU, L. STĂNESCU, I POP, Magnetic Behaviour of the α (Fe_2O_3—Al_2O_3) Oxidic System 16

AL. NICULA, S. AŞTILEAN, Transverse Response of the Spin System in Magnetic Spin Imaging by Density Matrix Method 24

V. CRISTEA, E TRIF, AL NICULA, Dependence of the Electrical Resistance of a Synthetic Zeolite Upon the Ambient Atmospheric Pressure 30

M. CRIŞAN, Critical Dynamics of the Cluster Model of the Spin Glass State 33

V. CRIŞAN, Spin Waves for Ferrimagnetic Collinear Structures 40

V. CRIŞAN, I. POP, V. TOŞA, M POPESCU, 4f States in Gd_2Ni_{17} Intermetallic Compounds 46

Z. NÉDA, Z GÁBOS, On the Applicability of the Joos-Weinberg Equations 49

S SIMON, V SIMON, AL NICULA, Magnetic Resonance on Borate Glasses with High Copper Oxide Content 56

V. IONCU, S SIMON, V. SIMON, E. TĂTARU, I. ARDELEAN, Dispozitiv de măsurare a fazei în amplificatorul-detector sincron ● Device for the Measurement of Phase Relation in the Sinchron Amplifier-Detector 63

D. DĂDÂRLAT, E. DĂDÂRLAT, Photothermal Methods for the Study of the Solids 67

H. SZŐCS, Contributions to the Electrical and Magnetical Methods of the Physical-Mechanical Parameter Determination the Machine Parts Made of Ferromagnetic and Non-Ferrous Materials 71

T. PETRIŞOR, A. GIURGIU, I. POP, High Temperature Superconductivity in Y—Ba—Cu—O System 74

I. CĂPLĂNUŞ, M GUŢUL, C. MANDRAVEL, AL NICULA, Physical and Chemical Studies of the Polymerization Product of Pyrol with Phosphoric Acid . . . 76

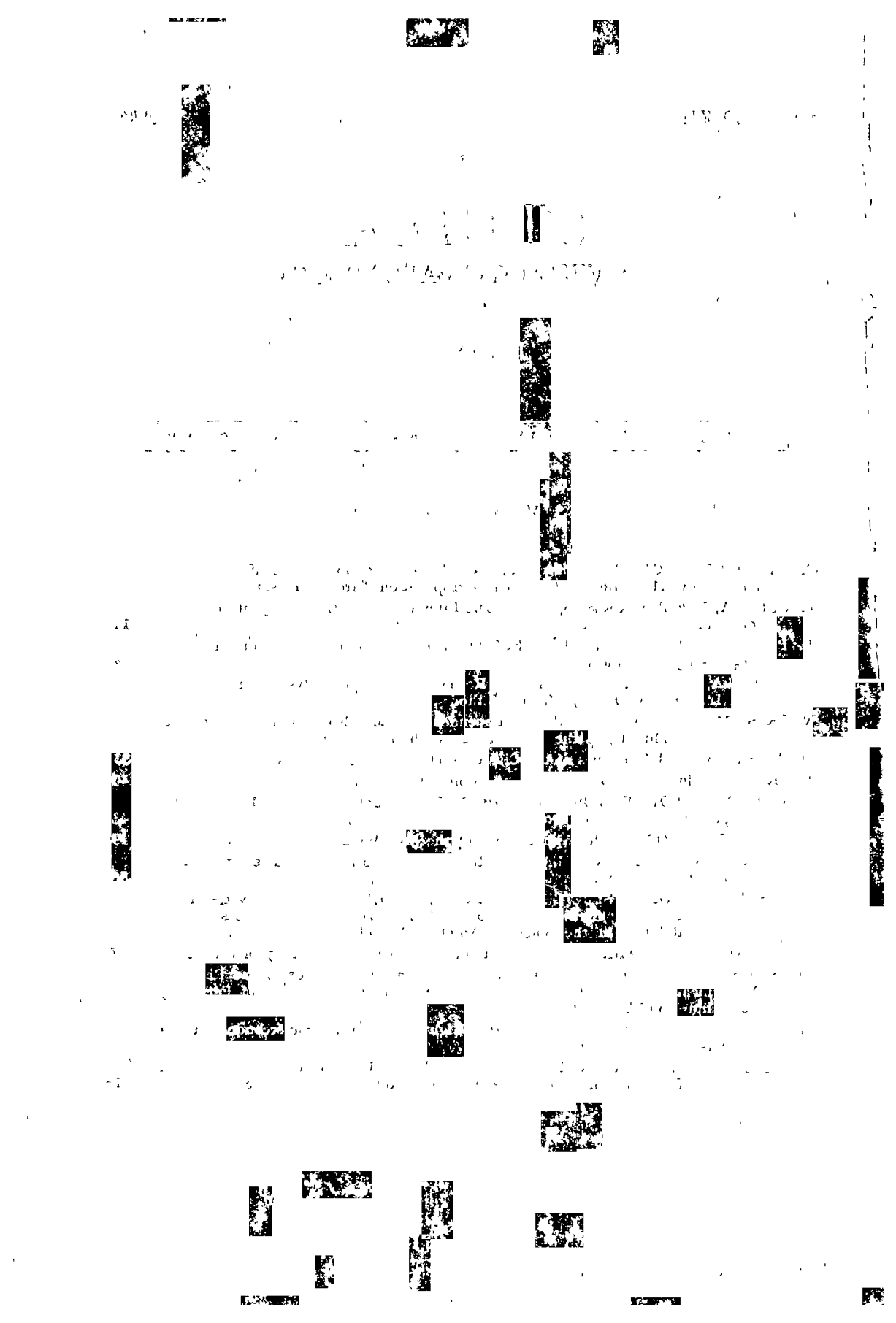

STUDIA UNIV BABEŞ—BOLYAI, PHYSICA, XXXII, 1, 1987

EFFECT OF A SPATIALLY UNIFORM EXTERNAL PERIODIC MAGNETIC FIELD ON WAVE PROPAGATION THROUGH PLASMA

C. BĂLEANU*, S. COLDEA* and J. KARACSONY*

Received November 18, 1986

ABSTRACT. — The effect of a spatially uniform external periodic magnetic field on wave propagation through an electron-ion plasma was studied It was found that the ions produce modifications of pump frequency and were recovered the growth rates previously defined [3] when ions motion was neglected A new case for onset of instabilites was obtained By another method — that of many time scale perturbation [4] — it was found that there was no possibility of appearance of instabilities due to coupling of electrostatic and electromagnetic modes, as an effect of the pump magnetic field

The parametric instabilites of plasma waves due to magnetic pump fields have been intensively studied [1—5] because of their applications in supplementary heating method [3] of tokamak plasmas. By applying a previously used method [3] we will study in the present paper the effect of spatially uniform magnetic fields on wave propagation through plasma, taking into account the ions dynamics. The many time scale perturbation method [4] will be also applied for the same problem, in view of obtaining new possibilities of parametric excitations

The solutions for zero order field quantities are of the form:

$$\vec{B}^{(0)} = \hat{z} \quad B_0 \cdot \cos w_0 \cdot t$$

$$\vec{E}^{(0)} = \vec{v}_e^{(0)} = \vec{v}_i^{(0)} = p_e^{(0)} = p_i^{(0)} = n_s^{(0)} = n_i^{(0)} = 0 \tag{2}$$

where the subscripts e and i reffer to the plasma electrons and ions.

From Maxwell's equations and motion equations, written in cylindrical coordinates, we have found that the Eqs (1)—(2) are exact solutions of the zero order field equations, only if the following conditions are fulfiled

$$r^2 \ll \frac{c^2}{w_0^2 - w_p^2} \quad (3) \text{ and } \frac{eB_0 r}{Mc^2} \ll \frac{eB_0 r}{mc^2} \ll 1 \tag{4}$$

where c is the light velocity, r is the distance from the axis of symmetry, $-e$, e, m, M beeing the electron and ion charges and mass w_p is the electron-ion plasma frequency:

$$w_p^2 = w_e^2 + w_i^2 \tag{5}$$

* *University of Cluj-Napoca, Physics Department, 3400 Cluj-Napoca, Romania*

with

$$w_e^2 = 4\pi n_0 e^2/m \quad (6a) \text{ and } w_i^2 = 4\pi n_0 e^2/M \quad (6b)$$

From Maxwell's equations and hydrodynamic equations, linearized about the time dependent state, given in (1)—(2), making the following assumtions for space dependence of the field quantities and for time dependence of z-component of the magnetic field:

$$X = X^+ \cdot e^{iKx} + X^- \cdot e^{-iKx} \tag{7}$$

$$B_z^+ = \sum_{\nu=-\infty}^{\infty} (B_z^+)_\nu \cdot e^{i(w+\nu w_0)t} \tag{8}$$

it is obtained an infinite set of equations for B_z^+

$$a_\nu - 2(B_z^+)_{\nu-2} + (1 + c_\nu)(B_z^+)_\nu + l_{\nu+2}(B_z^+)_{\nu+2} = 0 \tag{9}$$

where

$$a_\nu = -\frac{\Omega_e^2}{4w_0^2} \frac{1}{(z+\nu+2)\,[(z+\nu+2)^2 - \Omega_k^2/w_0^2]} \times$$

$$\times \frac{\left[(z+\nu)^2 - \dfrac{c^2K^2 + w_i^2}{w_0^2}\right](z+\nu+1) \cdot \left[(z+\nu+1)^2 - \dfrac{w_i^2}{w_0^2}\right]}{[(z+\nu+1)^2 - w_i^2/w_0^2]\;[(z+\nu+1)^2 - w_{Le}^2/w_0^2] - \dfrac{w_e^2 w_i^2}{w_0^4}} \tag{10}$$

$$c_\nu = -\frac{\Omega_e^2}{4w_0^2} \cdot \frac{[(z+\nu)^2 - (c^2K^2 + w_i^2)/w_0^2]}{(z+\nu)\,[(z+\nu)^2 - \Omega_k^2/w_0^2]} \times$$

$$\times \left\{ \frac{(z+\nu-1)\,[(z+\nu-1)^2 - w_i^2/w_0^2]}{[(z+\nu-1)^2 - w_i^2/w_0^2]\;[(z+\nu-1)^2 - w_{Le}^2/w_0^2] - w_e^2 w_i^2/w_0^4} + \right.$$

$$\left. + \frac{(z+\nu+1) \cdot [(z+\nu+1)^2 - w_i^2/w_0^2]}{[(z+\nu+1)^2 - w_i^2/w_0^2]\;[(z+\nu+1)^2 - w_{Le}^2/w_0^2] - w_e^2 w_i^2/w_0^4} \right\} \tag{11}$$

and

$$l_\nu = -\frac{\Omega_e^2}{4w_0^2} \frac{1}{(z+\nu-2)\,[(z+\nu-2)^2 - \Omega_K^2/w_0^2]} \times$$

$$\times \frac{\left[(z+\nu)^2 - \dfrac{c^2K^2 + w_i^2}{w_0^2}\right](z+\nu-1)\left[(z+\nu-1)^2 - \dfrac{w_i^2}{w_0^2}\right]}{[(z+\nu-1)^2 - w_i^2/w_0^2] \cdot [(z+\nu-1)^2 - w_{Le}^2/w_0^2] - w_e^2 w_i^2/w_0^4} \tag{12}$$

where

$$\Omega_e = eB_0/mc \quad (13); \quad z = w/w_0 \quad (14), \quad \Omega_k^2 = c^2K^2 + w_e^2 + w_i^2 \quad (15)$$

$$w_{ke}^2 = w_e^2 + \gamma k^2 v_{Te}^2 \tag{16}$$

γ beeing the ratio of the two specific heats of electrons and v_{Te} is the thermal velocity of electrons.

The assumptions that the ions are cold is made because we could neglect the effect of magnetic field on ion motion by virtue of

$$\Omega_s = eB_0/Mc \ll \Omega_e \tag{17}$$

The obtained expressions (10)—(12) include the ion contributions and differ from the expressions previously given (3). As a consequence in the infinite determinant of Eq. (9), together with the simple poles $z = n$ and $z = n \pm w_k/w_0$, the second order poles $z = n \pm w_L/w_0$ and $z = n \pm \pm w_s/w_0$ appear, where

$$w_s = \sqrt{\gamma} K \cdot v_s ; \; w_L^2 = w_i^2 + w_{Le}^2 \tag{18}$$

$$v_s = v_{Te} \, (m/M)^{1/2} \tag{19}$$

are the ion-acoustic frequency and velocity, which are due to the plasma ions. (n is any integer, positive, negative or zero).

We can apply a previously developped method [3] to the determinant of Eq. (9) and obtain the following dispersion relation·

$$\left(\sin^2\pi z - \sin^2\pi \cdot \frac{\Omega_k}{w_0}\right)\left(\sin^2\pi z - \sin^2\pi \cdot \frac{w_L}{w_0}\right)\left(\sin^2\pi z - \sin^2\pi \cdot \frac{w_s}{w_0}\right) =$$

$$= \varepsilon^2\lambda_1 \cdot \sin 2\pi \cdot \frac{\Omega_k}{w_0}\left(\sin^2\pi z - \sin^2\pi \cdot \frac{\Omega_L}{w_0}\right)\left(\sin^2\pi z - \sin^2\pi \cdot \frac{w_s}{w_0}\right) +$$

$$+ \varepsilon^2\lambda_2 \cdot \sin 2\pi \cdot \frac{w_L}{w_0}\left(\sin^2\pi z - \sin^2\pi \cdot \frac{\Omega_k}{w_0}\right)\left(\sin^2\pi z - \sin^2\pi \cdot \frac{w_s}{w_0}\right) +$$

$$+ \varepsilon^2\lambda_3 \cdot \sin 2\pi \cdot \frac{w_s}{w_0}\left(\sin^2\pi z - \sin^2\pi \cdot \frac{w_L}{w_0}\right)\left(\sin^2\pi z - \sin^2\pi \cdot \frac{\Omega_k}{w_0}\right) \tag{20}$$

where

$$\varepsilon^2 = \Omega_e^2/w_0^2 \ll 1 \tag{21}$$

$$\lambda_1 = \frac{w_e^2}{2\Omega_k^2} \cdot \left\{ \frac{(\Omega_k/w_0 - 1)\,[(\Omega_k/w_0 - 1)^2 - w_i^2/w_0^2]}{[(\Omega_k/w_0 - 1)^2 - w_i^2/w_0^2]\;\;[(\Omega_k/w_0 - 1)^2 - w_{Le}^2/w_0^2] - w_e^2 w_i^2/w_0^4} + \right.$$

$$\left. + \frac{(\Omega_k/w_0 + 1)\quad[(\Omega_k/w_0 + 1)^2 - w_i^2/w_0^2]}{[(\Omega_k/w_0 + 1)^2 - w_i^2/w_0^2]\cdot[(\Omega_k/w_0 + 1)^2 - w_{Le}^2/w_0^2] - w_e^2 w_i^2/w_0^4} \right. \tag{22}$$

$$\lambda_1 = \lambda_1^{(0)} + \frac{w_i}{\Omega_k^{(0)}}\left\{\frac{3\Omega_k^{(0)}}{w_0} - 1 - \frac{4\Omega_k^{(0)}/w_0(\Omega_k^0/w_0 - 1)^2 + 2w_k^2\Omega_k^0/w_0^3}{(\Omega_k^2/w_0 - 1)^2 - w_{Le}^2/w_0^2} \times \right.$$

$$\left. \times \frac{\lambda_{11}^0}{\frac{\Omega_k^{(0)}}{w_0} - 1} + \left[\frac{3\Omega_k^0}{w_0} + 1 - \frac{4\Omega_k^0/w_0\left(\frac{\Omega_k^0}{w_0} + 1\right)^2 + 2\frac{w_{Le}^2}{w_0^2}\cdot\frac{\Omega_k^0}{w_0}}{(\Omega_k^{(0)}/w_0 + 1)^2 - w_{Le}^2/w_0^2}\right]\right\} \frac{\lambda_{12}^{(0)}}{\left(\frac{\Omega_k^{(0)}}{w_0} + 1\right)} \tag{23}$$

with

$$\lambda_{11}^0 = \frac{w_e^2}{2\Omega_k^{02}} \cdot \frac{(\Omega_k^0/w_0 - 1)}{[(\Omega_k^0/w_0 - 1)^2 - w_{ke}^2/w_0^2]} \tag{24a}$$

$$\lambda_{12}^0 = \frac{\Omega_k^0/w_0 + 1}{(\Omega_k^0/w_0 + 1)^2 - w_{Le}^2/w_0^2} \tag{24b}$$

$$\lambda_2 = \frac{[(w_L/w_0 + 1)^2 - (c^2k^2 + w_t^2)/w_0^2] \cdot (w_L^2/w_0^2 - w_t^2/w_0^2}{(w_L/w_0 + 1) \cdot [(w_L/w_0 + 1)^2 - \Omega_k^2/w_0^2] \cdot 2(w_L^2/w_0^2 - w_s^2/w_0^2)} +$$

$$+ \frac{\left[\left(\frac{w_L}{w_0} - 1\right)^2 - (c^2k^2 + w_t^2)/w_0^2\right]\left(\frac{w_L^2}{w_0^2} - \frac{w_t^2}{w_0^2}\right)}{2(w_L/w_0 - 1) \cdot [(w_L/w_0 - 1)^2 - \Omega_k^2/w_0^2] \cdot (w_L^2/w_0^2 - w_s^2/w_0^2]} =$$

$$= \lambda_0^2 + \frac{w_t}{w_0}\left\{\frac{1}{\left[\left(\frac{w_L}{w_0} + 1\right)^2 - \Omega_k^2/w_0^2\right]} \cdot \left[(w_{Le}^2/w_0^2 + 1)^2 - \frac{\Omega_k^{02}}{w_0^2} - \frac{3}{2}\right] + \right.$$

$$\left. + \frac{1}{[(w_{Le}/w_0 - 1)^2 - \Omega_k^{02}/w_0^2]} \cdot \left[\left(\frac{w_{Le}^2}{w_0^2} - 1\right)^2 - \frac{\Omega_k^{02}}{w_0^2} - \frac{3}{2}\right]\right\} \tag{25}$$

$$\lambda_3 = \frac{[(w_s/w_0 - 1)^2 - (c^2k^2 + w_t^2)/w_0^2] \cdot (w_s^2/w_0^2 + w_t^2/w_0^2)}{(w_s/w_0 + 1) \quad [(w_s/w_0 + 1)^2 - \Omega_k^2/w_0^2] \cdot 2(w_s^2/w_0^2 - w_L^2/w_0^2)} +$$

$$+ \frac{(w_s/w_0 - 1)^2 - (c^2k^2 + w_t^2)/w_0^2 \cdot [(w_s^2/w_0^2 + w_t^2/w_0^2)]}{2\left(\frac{w_s}{w_0} - 1\right) \cdot \left[\left(\frac{w_s}{w_0} - 1\right)^2 - \Omega_k^2/w_0^2\right] \cdot \left(\frac{w_s^2}{w_0^2} - \frac{w_L^2}{w_0^2}\right)} \tag{26}$$

The quantities with the supperscript 0 are those in which the effect of ions motion is neglected. By using the substitutions:

$$x = \operatorname{tg} \pi z; \tag{27a}$$

$$a_1 = \operatorname{tg} \frac{\pi\Omega_k}{w_0}; \quad a_2 = \operatorname{tg} \frac{\pi\Omega_L}{w_0}; \quad a_3 = \operatorname{tg} \frac{\pi w_s}{w_0} \tag{27b}$$

the Eq. (20) can be transformed into an algebraic equation

$$(x^2 - a_1^2)(x^2 - a_2^2)(x^2 - a_3^2) = (1 + x^2)2\pi\varepsilon^2 \cdot \{\lambda_1 a_1(x^2 - a_2^2) \times$$

$$\times (x^2 - a_3^2) + \lambda_2 a_2(x^2 - a_1^2)(x^2 - a_3^2) + \lambda_3 a_3(x^2 - a_1^2)(x^2 - a_2^2)\} \tag{28}$$

For $x = a_3$, taking into account that

$$\frac{\lambda_3}{\lambda_{1,2}} = \mathcal{O}(m/M) \tag{29}$$

the equation (28) reduces to a biquadratic equation for which the stability conditions are obtained from Eqs. (38)—(39) of paper (3), taking the corresponding expressions for λ_1, λ_2, given by Eqs. (22) and (25). The conditions for the onset of instabilities are the following:

1. $$\Omega_k/w_0 = n \pm \Delta/\pi \quad \text{or} \quad n \pm \frac{1}{2} \pm \frac{\Delta}{\pi} \tag{30}$$

where n is any positive integer and Δ is small. The growth rate has its maximum when

$$\Delta = \varepsilon^2 \pi(\lambda_1) \tag{31}$$

with the following expression

$$r_1 = \varepsilon^2 w_0(\lambda_1) \tag{32}$$

2. $$w_L/w_0 = n \pm \frac{\Delta}{\pi} \quad \text{or} \quad n \pm \frac{1}{2} \pm \frac{\Delta}{\pi} \tag{33}$$

here the growth rate reaches its maximum

$$r_2 = w_0 \varepsilon^2(\lambda_2) \tag{34}$$

if

$$\Delta = \varepsilon^2 \pi(\lambda_2) \tag{35}$$

3. $$\frac{\Omega_k \pm w_L}{w_0} = n \pm \frac{\Delta}{\pi} \tag{36}$$

The condition for a maximized growth rate is

$$\Delta = 2\pi\varepsilon^2(\lambda_1) \tag{37}$$

and the maximum growth rate is

$$r_3 = w_0 \varepsilon^2(\lambda_1) \tag{38}$$

Replacing $\lambda_1 \to \lambda_2$ in the Eqs. (37—38) the results for longitudinal waves are obtained

If the condition $x \neq a_3$ is not fulfilled, when

$$\frac{w_s}{w_0} = n \pm \frac{\Delta}{\pi} \quad \text{or} \quad n \pm \frac{1}{2} \pm \frac{\Delta}{\pi} \tag{39}$$

from the equality

$$\sin^2 \pi z - \sin^2 \pi \cdot \frac{w_s}{w_0} = \varepsilon^2 \lambda_3 \cdot \pi \sin 2\pi \cdot \frac{w_s}{w_0} \tag{40}$$

we can obtain the maximum growth rate as

$$r_5 = \varepsilon^2 \cdot w_s(\lambda_3) \tag{41}$$

with

$$\Delta = \varepsilon^2 \cdot \pi(\lambda_3) \tag{42}$$

In the above considerations the assumption $n \neq 1$ was made.

When the many time scale perturbation method [4] is applied to the considered problem we obtain the following results: taking in the basic equations the following expressions:

$$\vec{E} = E^T \cdot \hat{e}_z + E^L \cdot \hat{e}_x; \quad \vec{B} = B \cdot \hat{e}_y \tag{43a}$$

and

$$\vec{v} = v^T \cdot \hat{e}_z + b^L \cdot \hat{e}_x \tag{43b}$$

and considering for the field quantities a spatial dependence exp (ikx), we come to the following system of coupled equations for the Fourier transforms of longitudinal and transverse quantities of a cold plasma, without collisions $(\nu_e = \nu_i = T_e = T_i = 0)$.

$$\frac{dv_{ek}^L}{dt} + \frac{e}{m} E_k^L = \Omega_e \cdot v_{ek}^T \cdot \cos w_0 t \tag{44a}$$

$$\frac{dn_{ek}}{dt} + iKn_0 \cdot v_{ek}^L = 0 \tag{44b}$$

$$\frac{dn_{ik}}{dt} + iKn_0 \cdot v_{ik}^L = 0 \tag{44c}$$

$$\frac{dv_{ik}^L}{dt} - \frac{e}{M} \cdot E_k^L = -\Omega_i v_{ik}^T \cdot \cos w_0 t \tag{44d}$$

$$iK \cdot E_k^L + 4\pi e(n_{ek} - n_{ik}) = 0 \tag{44e}$$

$$\frac{dE_k^L}{dt} - 4\pi e n_0 \cdot v_{ek}^L + 4\pi e n_0 \cdot v_{ik}^L = 0 \tag{44f}$$

$$\frac{dv_{ek}^T}{dt} + \frac{e}{m} \cdot E_k^T = -\Omega_e v_{ek}^L \cdot \cos w_0 t \tag{45a}$$

$$iKB_k - \frac{1}{2} \frac{dE_k^T}{dt} + \frac{4\pi e}{c} n_0 \cdot v_{ek}^T - \frac{4\pi}{c} n_0 v_{ik}^T = 0 \tag{45b}$$

$$icK \cdot E_k^T = dB_k/dt \tag{45c}$$

$$\frac{dv_{ik}^T}{dt} - \frac{e}{M} \cdot E_k^T = \Omega_i \cdot v_{ik}^L \cdot \cos w_0 t \tag{45d}$$

The magnetic field is sufficiently weak so that the many time scale perturbation can be applied to Eqs. (44) and (45), the quantities which

contain Ω_e and Ω_i beeing small compared with the others. Doing the well known assumptions [4]:

$$E^L(t, \varepsilon t, \varepsilon^2 t, \ldots) = E_0^L(t, \varepsilon t, \varepsilon^2 t, \ldots) + \varepsilon \cdot E_1^L(t, \varepsilon t, \varepsilon^2 t, \ldots) + \varepsilon^2 \cdot E_2^L(t, \varepsilon t, \varepsilon^2 t, \ldots) \tag{46}$$

where

$$\frac{d}{dt} = \frac{\partial}{\partial t} + \varepsilon \cdot \frac{\partial}{\partial(\varepsilon t)} + \ldots \tag{47}$$

$$\frac{d^2}{dt^2} = \frac{\partial^2}{\partial t^2} + \varepsilon \cdot \left[2 \frac{\partial}{\partial(\varepsilon t) \partial t}\right] + \ldots \tag{48}$$

$$E_{ok}^L(t, \varepsilon t) = A_L^+(t, \varepsilon t) \exp(i w_L t) + A_L^-(t, \varepsilon t) \exp(-i w_L t) \tag{49}$$

$$E_{ok}^T(t, \varepsilon t) = A_T^+(t, \varepsilon t) \cdot \exp(i\Omega_k t) + A_T^-(t, \varepsilon t) \cdot \exp(-i\Omega_k t) \tag{50}$$

and eliminating the secularities we obtain the following results:

(i) when $w_0 = w_L + \Omega_k$

$$\frac{dA_L^+}{d(\varepsilon t)} + \frac{1}{4 w_p \Omega_k}(w_e^2 \cdot \Omega_e - w_i^2 \cdot \Omega_i) A_T^- = 0 \tag{51a}$$

and

$$\frac{dA_T^+}{d(\varepsilon t)} - \frac{1}{4 w_p \Omega_k}(w_e^2 \cdot \Omega_e - w_i^2 \cdot \Omega_i) \quad A_L^+ = 0 \tag{51b}$$

(ii) When $w_0 = \Omega_k - w_L$ (52a)

$$\frac{dA_L^-}{d(\varepsilon t)} - \frac{1}{4 w_p \Omega_k}(w_e^2 \cdot \Omega_e - w_i^2 \quad \Omega_i) A_L^- = 0 \tag{52b}$$

and

$$\frac{dA_T^-}{d(\varepsilon t)} + \frac{1}{4 w_p \Omega_k}(w_e^2 \cdot \Omega_e - w_i^2 \cdot \Omega_i) A_L^- = 0 \tag{52c}$$

In both of the two cases we obtain an oscillatory solution, without growth:

$$A_L^+, \; A_T^+, \; A_L^-, \; A_T^- \sim \exp(i\gamma \varepsilon t) \tag{53}$$

and

$$\gamma = \frac{1}{4 w_p \Omega_k}(w_e^2 \cdot \Omega_e - w_i^2 \cdot \Omega_i) \tag{54}$$

As a conclusion of our calculations it results that the ions introduce a modification of the pump frequencies, Eq. (30) and Eqs. (33—34), at which instabilities can appear.

As can be seen from the expressions (32), (34), (38), (22) and (25) there are situations in which the growth rates are increased and others in which they are decreased On the other hand, the last possibility for excitation, given by Eq. (40), at integer and semiinteger subharmonic frequencies of ion sound frequency is experimentally very difficult to observe, because of the conditions (21) and (29).

By applying the many time scale perturbation method we reach Eqs. (53—54) and so we have recovered a previous result (5) due to the pump magnetic field; the appareance of instabilities due to the coupling of electrostatic and electromagnetic modes is not possible

REFERENCES

1 N F Cramer; M. C Sy, *J Plasma Phys*, **22**, 549 (1979)
2 N F Cramer, *Phys Letters*, **61A**, 314 (1977)
3 K P Das, *J Plasma Phys*, **5**, 151 (1971)
4 K F Lee, *J Plasma Phys*, **13**, 317 (1975)
5 B K Shivamoggi, *Czechoslovak J Phys*, **335**, 1341 (1985).

STUDIA UNIV BABEŞ—BOLYAI, PHYSICA, XXXII, 1, 1987

QUADRUPOLE INTERACTIONS IN $Hf_{1-x}Zr_xV_2$ INTERMETALLIC COMPOUNDS

M. COLDEA*, I. POP* and V. CRIŞAN*

Received January 30, 1987

ABSTRACT. — The lattice (q_{latt}) and conduction electron (q') contributions to the electric field gradient on V nuclei in the intermetallic compounds HfV_2, $Hf_{0.5}Zr_{0.5}V_2$ and ZrV_2 are analysed It was found that $q' \simeq -20q_{latt}$.

The measurements of the electric-quadrupole interaction in the intermetallic compounds pointed out that between the magnitude of the electric field gradient q at the given site and the density of electronic states at the Fermi energy $N(E_F)$ there is a strong correlation. The conduction electron contributions to an electric field gradient in a metal or an intermetallic compound, analysed by Watson, Gossard and Yafet [1], are linearly related to $N(E_F)$ and are of experimental significance in many ordered metals Futhermore, it was also found that such a correlation is to be found between the electric field gradient and the critical temperature of the superconductors. There is a general trend for the superconductors having higher T_c to also have larger q [2,3]. It is the point of the present paper to study the quadrupole interactions in $Hf_{1-x}Zr_xV_2$ intermetallic compounds and to illustrate the role of the conduction electrons from the immediate vicinity of the V nuclei in the measured electric field gradient q at the V sites

The intermetallic compounds $Hf_{1-x}Zr_xV_2$ crystallize in the cubic lattice of Cu_2Mg type, space group $Fd3m$, with eight formula units per unit cell as is shown in Fig. 1 [4] The local symmetry at a V site is noncubic and a nonzero electric field gradient may occur These compounds are superconductors, and the critical temperatures T_c, determined by Wallace, Craig and Rao [5], are shown in Fig 2

In order to find the charges of the ion cores in these compounds we have measured their magnetic susceptibility versus temperature between 80 and 1 000 K

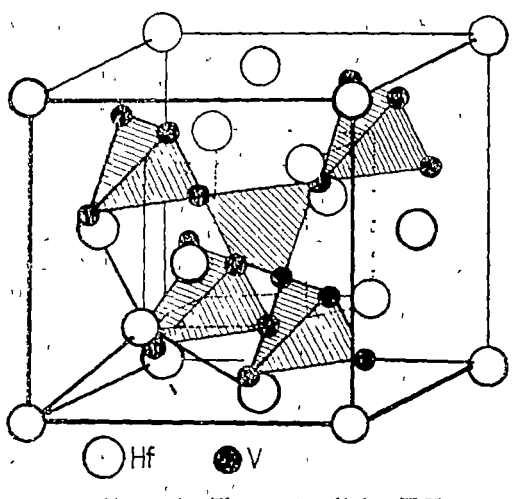

Fig 1 The unit cell for HfV_2

* University of Cluj-Napoca, Physics Department, 3100 Cluj-Napoca, Romania

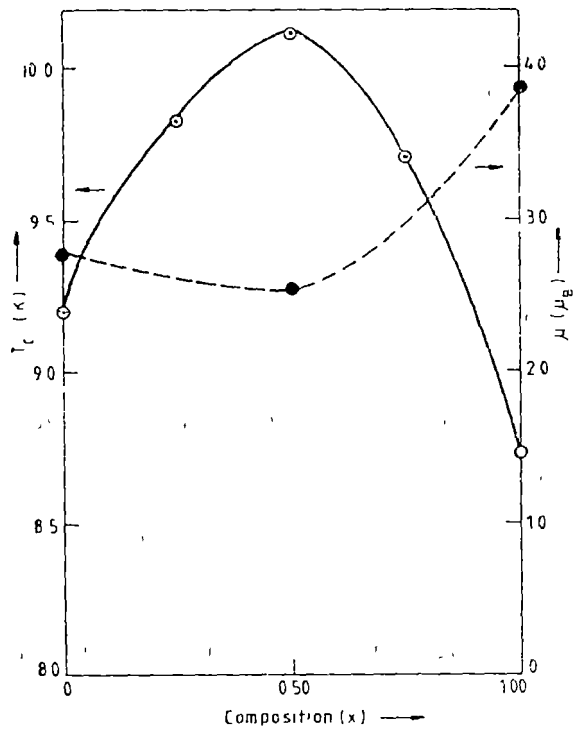

Fig. 2. The variation of the critical temperature and the magnetic moment with composition in $Hf_{1-x}Zr_xV_2$

The magnetic susceptibility obeys the Curie-Weiss law $\chi = C/(T - \theta_p)$, with $\theta_p < < 0$, and from the slopes of the curves χ^{-1} (T) the following values were determined for the magnetic moments per unit formulas · 3.92 μ_B for HfV_2, 3.61 μ_B for $Hf_{0\,5}Zr_{0\,5}V_2$ and 5.49 μ_B for ZrV_2. Taking into account that Hf and Zr do not carry magnetic moments in the metallic state [6], the obtained values of the magnetic moments may be attributed only to the V atoms. So, the effective magnetic moments per V atom in these compounds are as follows: 2.78 μ_B in HfV_2, 2 56 μ_B in $Hf_{0\,5}Zr_{0\,5}V_2$ and 3 89 μ_B in ZrV_2. The minimum value of the magnetic moment for $Hf_{0\,5}Zr_{0\,5}V_2$ compound is in good agreement with the largest super — conducting temperature (Fig 2). Is is to note that the magnetic moment values per V atom in HfV_2 and ZrV_2 compounds are very close to the values 2.82 μ_B and 3.87 μ_B, which correspond to the values of the magnetic moments for V^{3+} and respectively V^{2+} ions. On the other hand, from the value of the magnetic moment in $Hf_{0.5}Zr_{0\,5}V_2$ compound was found that one V atom carry on an average in the conduction band 3.13 electrons

The NMR spectra of ^{51}V nuclei were recorded by a JNM-3 spectrometer at 9.212 MHz, improved by a broad-line attachment JNM—BH—2. The spectra for all investigated compounds may be described in terms of the first-order quadrupole splitting with a nonvanishing asymmetry parameter. The values of the quadrupole constants e^2qQ/h are given in Table 1 and their dependence of the composition is shown in Fig. 3, revealing a maximum for $Hf_{0\,5}Zr_{0\,5}V_2$ compound. The asymmetry parameter has approximately the same value for all compounds, namely $\simeq$ $\simeq$ 0.23. In the second column of Table 1 the experimental values of the electric field gradients at the V sites are given, obtained from e^2qQ/h constants, using for the nuclear-quadrupole moment the value $Q = 0.032$b, determined by Chids and Goodman [7,8]. Following the treatment of Watson, Gossard and Yafet, we write the measured electric field gra-

dient as

$$q = (1 - \gamma_\infty)q_{\text{latt}} + (1 - R_Q)q' \tag{1}$$

where $(1 - \gamma_\infty)$ and $(1 - R_Q)$ are the Sternheimer antishielding and shielding factors, respectively; q_{latt} is the point-charge contribution and q' is a local field gradient caused by the redistribution of occupied conduction-electron states near the Fermi surface q' is the shielding response of the conduction electrons within the spherical potential of the APW sphere to the external potential imposed by the field gradient of point charges. It is therefore linear in $-q_{\text{latt}}$ and related to the densities of states at the Fermi level for the various bands, through the expression [1]

$$q' \simeq -2e^2q_{\text{latt}}N(E_F)\sum_i f_i\langle r^2\rangle_i\langle r^{-3}\rangle_i(\langle P_2^0(\cos\theta)\rangle_i)^2 \tag{2}$$

where f_i is the fraction of states at the Fermi surface having particular spatial character and P_2^0 (cos θ) the second order Legendre polynomial. For purely d orbitals and for orbital symmetry $d_{xy} + d_{yz} + d_{zx}$ with $f_i = 1/3$ for each orbital (equal numbers of xy, yz and zx orbitals), the equation (2) has the form [1]

$$q'/e^2q_{\text{latt}}N(E_F)\langle r^2\rangle\langle r^{-3}\rangle = -4/49 \tag{3}$$

Table 1

Values of the quadrupole constants, the contributions to the field gradients and the Sternheimer factors for $Hf_{1-x}Zr_xV_2$

Compound n	e^2qQ/h (KHz)	q_{exp} (10^{23}cm^{-3})	q_{latt} (10^{23}cm^{-3})	q'/q_{latt}	$1 - \gamma_\infty$
HfV_2	357 62	1 97	2 96	−19	20
$Hf_{0\,5}Zr_{0\,5}V_2$	414 15	2 29	3 43	−26 5	27
ZrV_2	371 82	2 05	0 30	−20 5	27

The lattice sums on the point charges Z_V and Z_{Hf} (or Z_{Zr}), associated with the V and Hf (or Zr) lattice sites, from a sphere of radius $2.3a_0$ which comprise 760 vanadium and 380 hafnium atoms, yield for the electric field gradient at the V site the value

$$q_{\text{latt}} = \frac{1}{a_0^3}(107\,6Z_V - 50.6\,Z_{Hf}) \tag{4}$$

In order to estimate the contribution q' in the electric field gradient at the V site in these compounds we have also calculated the density of states $N(E_F)$ at the Fermi level (Table 2) from the electronic specific-heat data determined by Rapp and Vieland [9] and Inoue and Tachikawa [10].

Table 2

Values of the lattice parameters a_0 [4,5], the γ coefficient of the electronic specific-heat and the density of states at the Fermi level for $Hf_{1-x}Zr_xV_2$

Compond	Lattice parameter (Å)	$\gamma \times 10^{-4}$ (erg/cm³ K²)	$N(E_F)$ (states/eV)
HfV_2	7 400	1 89	1 22
$Hf_{0.5}Zr_{0.5}V_2$	7 310	2 60	1 70
ZrV_2	7 445	1 60	1 32

The values of q_{latt} and q'/q_{latt}, as deduced from equation (3), taking for $\langle r^2\rangle\langle r^{-3}\rangle$ the value of 7a u. [1], are listed in Table 1. The contribution q' of the conduction electrons in the measured electric field gradient for the investigated compounds is significance being approximately 20 times the lattice contribution q_{latt}

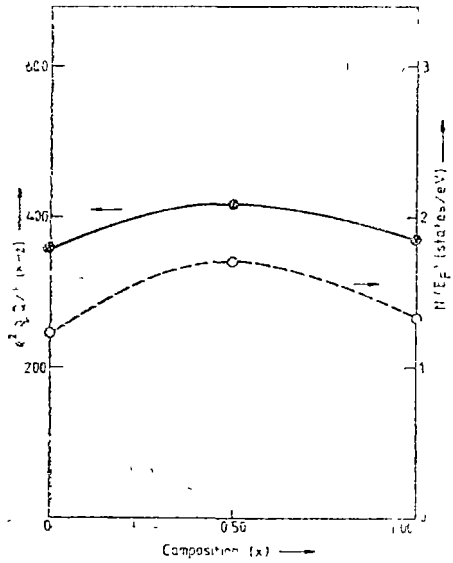

Fig 3 The variation of the the quadrupole constant and the density of states at the Fermi level with composition for $Hf_{1-x}Zr_xV_2$

In equation (1) we can set $1 - R_Q$ equal to unity with no greater than 20% uncertainty [1], so that for $1 - \gamma_\infty$ one obtains the values given in the las tcolumn of Table 1 These values are very close to that determined by Fradin and Zamir for V_3X compounds [2].

The existence of a maximum in the quadrupole constant e^2qQ/h versus composition for the ternary system $Hf_{1-x}Zr_xV_2$ is the result of the maximum in the density of states at the Fermi level $N(E_F)$ (Fig 3), which is also responsible for the maximum in the critical temperature, T_C [11]. It is interesting to note that these maximum values appear at the composition $x = 0.5$, where the lattice parameter show a minimum.

REFERENCES

1 R. E Watson, A C Gossard and Y Yafet, *Phys Rev*, **140,** A375 (1965)
2 F Y Fradin and D Zamir, *Phys Rev*, B **7,** 4861 (1973)
3 F Y Fradin and J D Williamson, *Phys Rev*, B, **10,** 2803 (1974)
4. W B Pearson, A Handbook of Lattice Spacings and Structures of Metals and Alloys, Vol 2, Pergamon Press, 1967, p 401
5 W E Wallace, R S Craig, and V U. S Rao, Solid State Chemistry: A Contemporary Overview, Advances in Chemistry Series, No **186,** 1980 (p 206), Ed. Smith L Holt, Joseph B Milstein and Murray Robbins
6 S V Vonsovski, Magnetism, Izd Nauka, Moskva, 1971 (p 124)
7 W J Childs and L S Goodman, *Phys Rev*, **156,** 64 (1967)
8 W. J Childs, *Phys Rev*, **156,** 71 (1967)
9 O Rapp and L J Vieland, *Phys Lett*, **36A,** 369 (1971)
10 K Inoue and D Tachikawa, *Proc Int Conf Low Temp Phys*, 21st, 483 (1971)
11 W L McMillan, *Phys Rev*, **167,** 331 (1968)

STUDIA UNIV. BABEŞ—BOLYAI, PHYSICA, XXXII, 1, 1987

MAGNETIC BEHAVIOUR OF THE $\alpha - (Fe_2O_3 - Al_2O_3)$ OXIDIC SYSTEM

LILIANA POP*, CAMELIA MARALOIU*, LIVIU STĂNESCU* and IULIU POP*

Received · February 4, 1987

ABSTRACT. — The $\alpha-(Fe_2O_3-Al_2O_3)$ system with the corundum crystalline structure was investigated from the magnetic view-point in the temperature range 100—1100 K.

The system is antiferromagnetic and the temperature dependence of the magnetic susceptibility is anormal and consists of three stages. The magnetic susceptibility in the paramagnetic region is almost temperature independent, that is very peculiar. The magnetic phase diagram was established for the α-$(Fe_2O_3-Al_2O_3)$ solid solutions.

1. Introduction. The oxidic system $\alpha - (Fe_2O_3-Al_2O_3)$ crystallises in the corundum type of structure. The unit cell with the rhombohedral system of crystallization contains two Me_2O_3 unit formula, and belongs to the $D_{2d}^6 - R\,\bar{3}c$ space group. The *cations* are distributed along the thernary axis in the 4*c* positions, and the *anions* in the 6*c* positions. The corundum type of structure is based on a little deformed compactness of the O^{-2} ions, where half of the octahedral positions are occupied with perfect regularity by Me^{3+} *cations*. Alternating *anionic* and *cationic* layers may be separated in the corundum structure; the *cations* being distributed along the thernary axis, while the *anions* are distributed along the $\bar{3}$ axis. As a result one obtains a structure formed from MeO_6 octahedrons disposed in an infinit chain along the direction of the rhombohedral axis. Because of the exchange and electrostatic interactions the anions and the cations are shifted from their ideal positions and the alternating layers are goffered. So, the ideal cationically centered anionic octahedrons are deformed by the supplemental atractive forces between this cations, but the three oxygen ions diverge, while the corresponding ions from the nearest neighboring anionic layers converge, determining thus a high screening of the positive electric charges. These shifts are different for the concret cases of the compounds and determine different values of the exchange energy interactions, and consequently different magnetic spin structures (1). Four types of the exchange interactions Γ_a, Γ_b, Γ_c, and Γ_d were evaluated by Ishikawa and Akimoto (2) in such kind of structure.

The higher values of the exchange energy have the first two-interactions Γ_a and Γ_b, because of the cation-anion-cation biggest angle, which allows a bigger overlapping of the d-orbitals of the cations with the p-

* *University of Cluj-Napoca, Faculty of Mathematics and Physics, 3400 Cluj-Napoca, Romania*

orbitals of the anions. The exchange energies Γ_c and Γ_d have less esential role in the direct exchange. Three possible types of ordering with an u-parameter result from the analysis of the different possible kinds of antiferromagnetic ordering in the corundum structure. Shull, Strauser and Wallan [3] pointed out that hematite, α—Fe_2O_3, at $T_N = 948$ K pass from the paramagnetic state in the antiferromagnetic state with spin magnetic moments orientated perpendicular on the c-axis, but at 250 K the spin magnetic moments are orientated antiferromagneticaly on the direction of c-axis, the rhombohedron axis as: $+ - - +$, in accordance with the first mode of the antiferromagnetic ordering, whence and the specific temperature dependence of the magnetic susceptibility, and in some cases with the superposition of the weak ferromagnetism in the natural hematite [4—19].

The oxidic system α—(Fe_2O_3—Al_2O_3) with the corundum structure, has the solid solubility only at the extremities of the concentration range, below 20 mol% α—Fe_2O_3 and α—Al_2O_3, within being a mechanical mixture of the two phases. The magnetic investigation of the system is interesting in order to see the influence of the diamagnetic component α—Al_2O_3 on the Néel temperature and on the spin reorientation temperature T_{sr} ($T_{sr} = 253$ K for α—Fe_2O_3), and also the magnetic behaviour of the two phases part.

2. Samples preparation and experimental. A set of samples was prepared from the oxidic α—(Fe_2O_3—Al_2O_3) system, with the concentrations 1, 3, 5, 7; 10, 20, 40; 60 and 80 mol% α-Al_2O_3.

For the preparation of the system α-(Fe_2O_3—Al_2O_3)$Al_2(SO_4)_3$ and $Fe(NH_4)(SO_4)_2$ was used, treated with NH_4OH in order to obtain $Al(OH)_3$ and $Fe(NH_4)(OH_2)$, respectively. After filtration, the two hydroxides were treated with HNO_3 resulting $Al(NO_3)_3 \cdot 6H_2O$ and $Fe(NO_3)_3 \cdot 6H_2O$ The obtained salts were dried in the temperature range of 333—343 K in order to avoid the crystallization water loosing

The proportions for the corresponding concentrations were established from the aluminium nitrate and iron nitrate, and mixed together and precipitated at warm with NH_3 in a weak excess After precipitation the resulted oxidic compounds were filtred, washed with distiled water and dried

In order to stabilize the structure, the samples were calcined at the temperature of 873 K, and for the elimination of the crystallization water, the samples were dried at 533 K for 5—6 hours

Finaly, the samples were pressed in pellets, sintered at the temperature of 1123 K for 7 hours and slowly cooled down. The chosen sintering temperature was 0 5 T_{Tm}(T_{Tm} — Tamman temperature) in order to be sure of the reaction in solid state After sintering the samples were heated at 773 K for 6 hours in order to eliminate the eventual Fe^{2+} ions formed in the sintering process

The temperature dependence of the magnetic susceptibility of the investigated samples in the temperature range 100—1100 K and in the magnetic field of 9,500 G intensity was pointed out using a Weiss-Forrer equipment with 10^{-8} cm³/g sensitivity.

3. Experimental results and discussion. The temperature dependence of the magnetic susceptibility for the solid solutions α—(Fe_2O_3—Al_2O_3), i.e. for the samples with the concentration of 1; 3; 5; 7; and 10 mol% of α—Al_2O_3 is given in the Fig. 1.

As one can see from the Fig. 1, the magnetic susceptibility depends anomalously of the temperature. At low temperature and up to a defi-

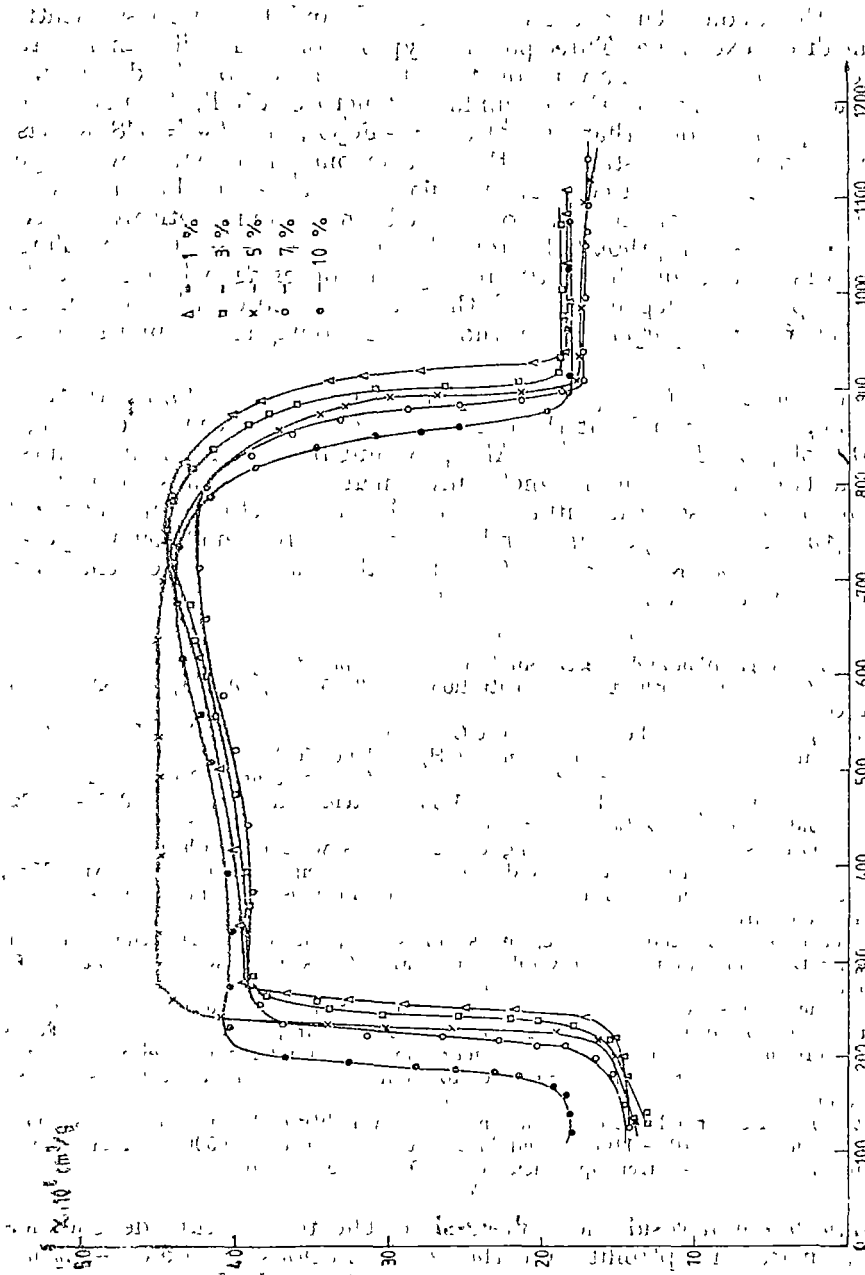

Fig. 1. — Temperature dependence of the magnetic susceptibility of the solid solutions α-(Fe_2O_3—Al_2O_3)

nit temperature, T_{sr}, depending of the samples concentration (T_{sr} = = 250 K for α—Fe_2O_3), the magnetic susceptibility is practically temperature independent. At T_{sr}, called temperature of the spin reorientation, the magnetic susceptibility value jumps more then two times, and then slowly increases with temperature increase, reaches a maximum at high temperatures (T_N= 948 K for α—Fe_2O_3) and fall off more than two times. After this anomaly, the magnetic susceptibility remains practically temperature independent, or decreases very slightly with temperature increase for any samples. The magnetic susceptibility variation in three stages for the oxidic system of solid solutions α—(Fe_2O_3—Al_2O_3) is very peculiar. The presence of the α—Al_2O_3 in the crystalline lattice of the α—Fe_2O_3 changes the aspect of the temperature dependence of the magnetic susceptibility in comparison with that of the pure α—Fe_2O_3, and even the numerical value. The magnetic spin structure of the α—Fe_2O_3 was described in the first part of this paper, so the magnetic spin structure for the solid solutions α—(Fe_2O_3—Al_2O_3) can not differ to much. Consequently, all the solid solutions α—(Fe_2O_3—Al_2O_3) behave antiferromagnetically with the temperature dependence of the magnetic susceptibility in two stages in the ordered state and the last stage in the paramagnetic state. The first stage at low temperature corresponds to the antiferromagnetic spin structure with the magnetic moments oriented along the direction parallel to *c*-axis of the rhombohedron The second stage included between temperature of the spin reorientation, T_{sr}, and the critical Néel temperature, T_N, also represents an antiferromagnetic structure with the magnetic moments oriented perpendicular on the *c*-axis, but the magnetic susceptibility has the biggest value for this stage.

It is interesting to observe that the magnetic susceptibility in the paramagnetic region, the third stage, is practically temperature independent.

As one can se efrom Fig 2, where the magnetic phases diagrams and the critical Néel temperature are given, that the spin reorientation temperature depends monotonously on the α—Al_2O_3 concentration, and decreases with increasing concentration

For the binary phase, consisting of the mechanical mixture of the two solid solutions, the magnetic susceptibility hasa specific temperature dependence, which relieves the presence of the two phases All the samples with the α—Al_2O_3 concentrations 20, 40, 60; and 80 mol% have the critical Néel

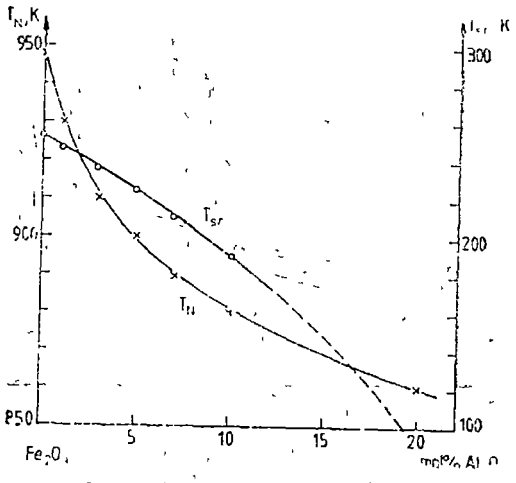

Fig 2 — Magnetic phase diagrams for α-(Fe_2O_3—Al_2O_3) solid solutions

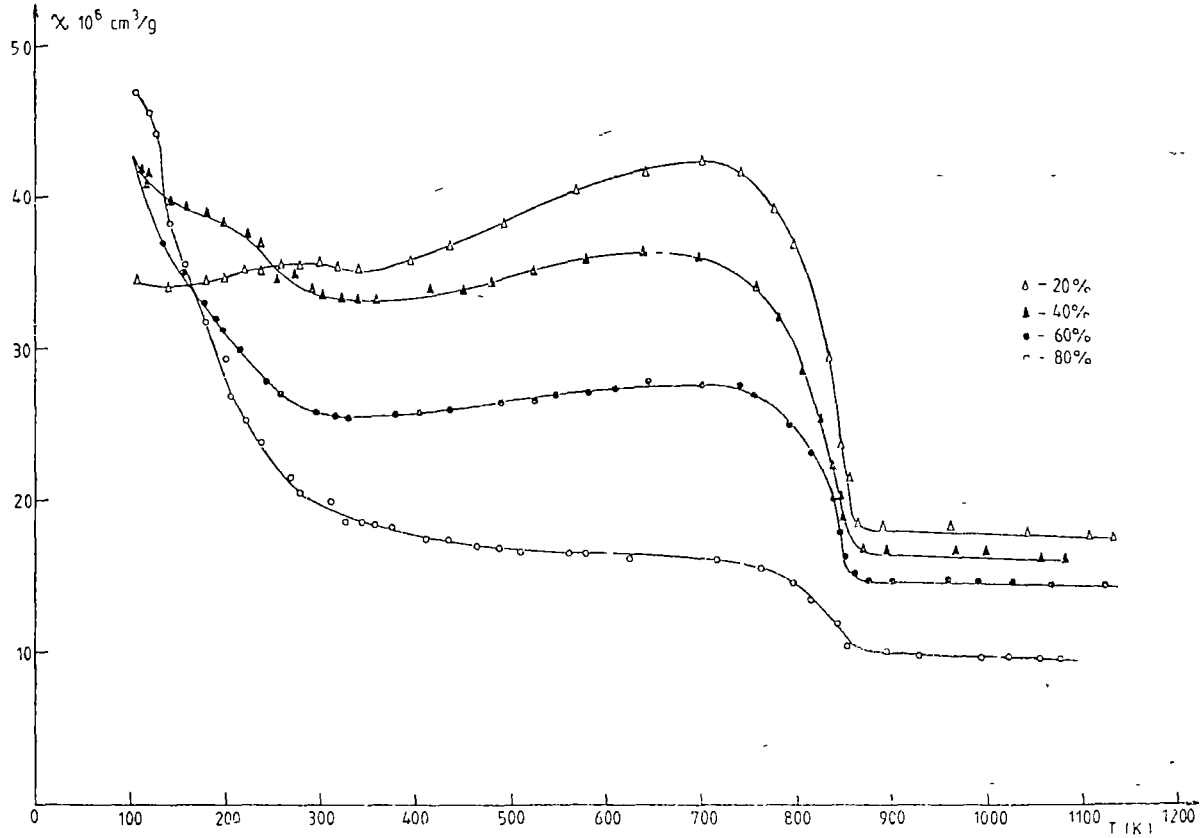

Fig. 3 — Temperature dependence of the magnetic susceptibility for α-(Fe_2O_3—Al_2O_3) mechanical mixetur

temperature at the same value $T_N = 860$ K, and below 300 K the second phase appears with the lowered Néel temperature. The magnetic susceptibility has a temperature variation in two stages for the antiferromagnetically ordered state, but different from that of α—Fe_2O_3, and has in the paramagnetic region a very easy temperature decrease. The numerical value of the magnetic susceptibility decreases with the α—Al_2O_3 concentration, increasing more than two times in the paramagnetic state and also in the antiferromagnetic state with the spin orientation perpendicular on the c-axis.

The temperature dependence of the magnetic susceptibility for the sample with 20 mol% α—Al_2O_3 is very similar to that of the solid solutions samples, being probably at the solid solubility limit and with $T_{sr} <$ $<$ 100 K, as one can see in Figs. 2 and 3

The increase of the magnetic susceptibility is very unusual, below 300 K, for the binary phase with α—Fe_2O_3 concentration it decreases where appiers the second phase more poor in α—Fe_2O_3 content .At the temperature of 100 K the sample with 80 mol% α—Al_2O_3 has the biggest value of the magnetic susceptibility, in comparison with the more concentrated in α—Fe_2O_3 samples, while in the paramagnetic region has the smallest value.

It is peculiar that the magnetic susceptibility in the paramagnetic region in a temperature range of 100—200 degrees is practically temperature independent, and after that decreases with the temperature increase obeying the Curie-Weiss law as one can see from the Fig. 4, where the

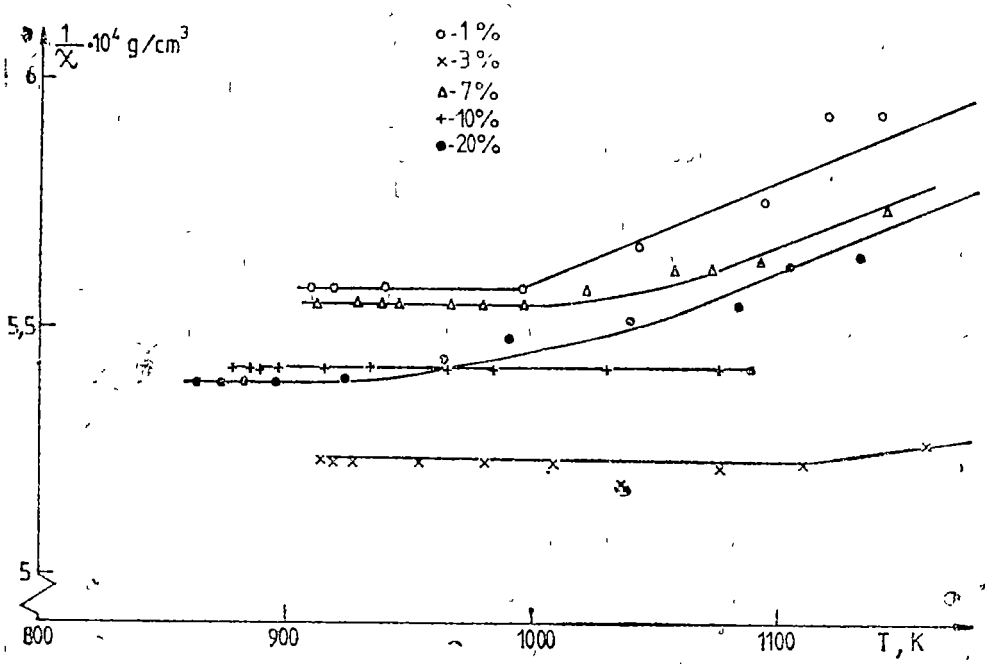

Fig. 4 — Temperature dependence of the reciprocal magnetic susceptibility

temperature dependence of the reciprocal magnetic susceptibility is given. There is a transition region from the ordered state to the paramagnetic state So, the Néel temperature accepted so far, is not probably the real Néel temperature because the magnetic order is not destroyed at this temperature, but at the higher temperature whence magnetic susceptibility abeys the Curie-Weiss law

4. **Conclusions.** The oxidic system $\alpha-(Fe_2O_3-Al_2O_3)$ crystallizes in the corundum type of structure, and up to 20 mol% of $\alpha-Al_2O_3$ give rise to the solid solutions. Between 20 mol% and 80 md% of $\alpha-Al_2O_3$ the system is biphasic and consists of the mechanical mixture of two solid solutions — one rich in $\alpha-Fe_2O_3$ and the other rich in $\alpha-Al_2O_3$. At the higher $\alpha-Al_2O_3$ concentrations the system consists of the solid solutions again

From the magnetic view-point the investigated $\alpha-(Fe_2O_3-Al_2O_3)$ system is antiferromagnetic and has a magnetic spin structure of the $\alpha-Fe_2O_3$ type. The Néel temperature for the monophasic system decreases monotonously with the $\alpha-Al_2O_3$ concentration increase, while for the biphasic system is concentration independent. The temperature of the spin reorientation for the solid solutions samples monotonously decreases with the $\alpha-Al_2O_3$ concentration increase

The magnetic susceptibility of the $\alpha-(Fe_2O_3-Al_2O_3)$ system in the paramagnetic region is practically temperature independent in a temperature range about 100—200 degrees where the magnetic order is not destroyed yet. So, the accepted Néel temperature in the oxidic compound as $\alpha-Fe_2O_3$ (T_N 948 K) probably is not the real critical temperatures for order — desorder transition, because at these temperatures the magnetic ordering is not destroyed completely. The magnetic ordering is complete destroyed only when the temperature dependence of the magnetic susceptibility obeys the Curie-Weiss law for the oxidic systems.

REFERENCES

1. Iu. A. Iziumov, R P Ozerov, „Magnitnaia neitronografia" Izd „Nauka", pp 340—359, Moskva, (1966).
2. Y. Ishikawa, S Akimoto, *J Phys Soc. Japan*, **12**, 1083 (1957)
3. C. Shull, W. Strauser, E Wollan, *Phys. Rev*, **83**, 333 (1951)
4. T. Smith, *Phys Rev*, **8**, 721 (1916)
5 H Forestier, G Chandron, *C R*, **183**, 787 (1926)

6. J L Snoek, *Physica*, **3**, 463 (1936)
7 A. Serres, *Ann de Phys*, **17**, 53 (1932)
8 K. Endo, *Sci Rep. Tohoku Imp Univ.*, **25**, 879 (1937)
9 R. Chevallier, S Mathieu, *Ann. de Phys*, **18**, 258 (1943)
10 L. Néel, *C R*, **64**, 228, (1949)
11. L Néel, *Ann. de Phys*, **4**, 249 (1949)
12. F. J. Morin, *Phys rev*, **78**, 819 (1950)
13. G High, *Phys. Mag*, **2**, 877 (1957)
14 R. Chevallier, *J. Phys et Rrad*, **12**, 172 (1951)
15 Ch. Guillaul, *J. Phys. et Rad*, **12**, 489 (1951)
16. L. Néel; *Rev Mod. Phys*, **25**, 58 (1953)
17. H Bizette, R Chevallier, B. Tsai, *C.R*, **236**, 2043 (1953)
18. Li Yin-Yuan, *Phys. rev*, **101**, 1450 (1956)
19. S T. Lin, *Phys Rev*, **116**, 1447 (1959)

STUDIA UNIV BABEŞ—BOLYAI, PHYSICA, XXXII, 1, 1987

TRANSVERSE RESPONSE OF THE SPIN SYSTEM IN MAGNETIC SPIN IMAGING BY DENSITY MATRIX METHOD

AL. NICULA* and S. AŞTILEAN*

Received: February 5, 1987

ABSTRACT. — In this paper we derive a general form for equation of magnetization and transverse response function in magnetic resonance spin imaging technique These equations, when a constant magnetic field gradient is applied were resolved both for the stationary and unstationary states The equation of magnetization from a certain sample position has been derived using the technique of density matrix developed in reference rotating frame

Introduction. A great progress has been achieved in the magnetic resonance in the last time, concerning the spatial resonance transitions in magnetic fields with constant gradients The usual effect of a gradient is to produce a free induction decay or transverse response which, through a Fourier transform, reflects bulk shape of the material, assumed to be a continuous distribution of spins This has been discussed by Mansfield [1] and Lauterbur [2]

The new research field has determined the development of the spin imaging techniques which, especially in NMR, are used as medical diagnosis methods.

Also, the spatial transitions study in a constant field gradients and dipolar fields is very recent in EPR [3]

1. **The Hamiltonian for an isolated spin in a magnetic field including a gradient.** We consider a sistem of N noninteracting spins in a constant and uniform magnetic field $\vec{B}_0 = B_0\vec{k}$ and an interacting term which is a linear magnetic field gradient [4, 5] or a dipolar magnetic field [3].

The Zeeman interaction for a isolated spin at position $\vec{r}$ in this total magnetic field, including a magnetic gradient tensor $\tilde{G}$, may be written generally as:

$$\mathcal{H} = -\hbar(\omega_0 I_z + \vec{I}\tilde{G}\vec{r}) \tag{1}$$

where $\omega_0 = \gamma B_0$ is the Larmor preccessional angular frecquency and γ is the magnetogyric ratio.

A magnetic field gradient is, in general, a tensor $\tilde{G}$ comprising nine components [7] However, if linear gradients: $G_{xz} = \frac{\partial Bz}{\partial x}$, $G_{yz} = \frac{\partial Bz}{\partial y}$ and $G_{zz} = \frac{\partial Bz}{\partial z}$ only are applied, all other tensor components being zero,

* *University of Cluj-Napoca, Faculty of Mathematics and Physics, 3400 Cluj-Napoca, Romania*

then we may define a vector gradient $\vec{G} = \vec{i}G_{xz} + \vec{j}G_{yz} + \vec{k}G_{zz}$ which completely specifies the interaction as follows :

$$\mathcal{H} = -\hbar[\omega_0 I_z + \gamma(\vec{G}\vec{r})I_z] \qquad (2)$$

For a better undestanding of this vector gradient, Fig. 1 must be observed.

Now, the transformation of Eq (2) into the coordinate system rotating with frequency ω around the direction of $\vec{k}\vec{B}_0' = \vec{k}(B_0 + \vec{G}\vec{r})$, rotating frame, is provided by the unitary operator or using the transformation properties of the spin operators to rotation about the z axis :

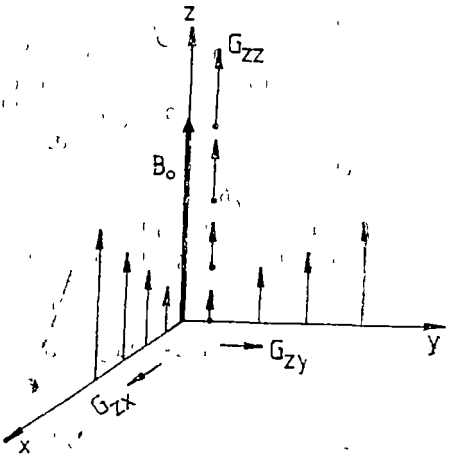

Fig 1 The linear magnetic field gradients in all three dimensions are superimposed on the "main field" B_0

$$U(t) = \exp\,(i\omega I_z t) \equiv \hat{R}_z(\varphi)$$

From the transformation of the Schrödinger equation into the rotating frame we obtain for Zeeman Hamiltonian $\mathcal{H}'$ in the rotating frame the expression .

$$\mathcal{H}' = -h[\Delta\omega I_z + \gamma(\vec{G}\vec{r})I_z] \qquad (3)$$

with $\Delta\omega = \omega_0 - \omega$.

As we shall see, the magnetizations from different parts of the specimen which now lie in slightly different static fields, precess at different frequencies : in other words, the spatial displacements are turned into resonance frequency displacements.

For example, we consider a homogeneous spin distribution in the form of a cylinder (Fig 2), the axis of which lies along the z direction. A linear static gradient G_{zz} exists over the sample. We shall assume that in the initial equilibrium state, the spin magnetization is uniformly distributed along the cylinder axis with a magnetization per unit lenght $m_0(z)$ given by

$$m_0(z) = \iint m(x, y, z)\mathrm{d}x\mathrm{d}y \qquad (4)$$

We shall apply an rf pulse of constant amplitude $\vec{i}B_1$, in a frame rotating with angular frequency ω.

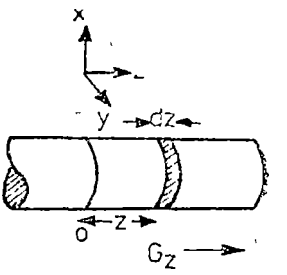

Fig 2 Slice selection from an extended abject in a gradient G_{zz}

In the case $\omega = \gamma(B_0 + G_z z)$, spins which lie in the plane z are therefore at exact resonance and interact strongly with the *rf* pulse. Spins either side of this plane will be progressively less affected the farther they lie from the isochromatic plane. The precise behavior of the spin system is best calculated for a particular pulse by considering spins displaced Δz from z which are then off resonance with respect to the pulse by $\Delta\omega_z = \gamma \cdot \Delta z \cdot G_z = \gamma b$

We consider the spins in the plane sheet of thickness dz at Δz. The equilibrium spin magnetization in the sheet is

$$\delta M_0 = m_0 dz \tag{5}$$

The motion of this magnetization:

$$M(t) = m(t)dz \tag{6}$$

in the tilted rotating frame follows a cone of precession about an effective field $\vec{B}_{eff} = B_1\vec{i} + b\vec{k}$. (see: Fig. 3). We shall turn to this discription in the next section.

2. **Equations of Motion of the Spin System.** Since the difficulties inherent in claculating the entire NMR line shape are well known, we shall restrict our discussion on imaging techniques to noninteracting or weakly interacting spin system and this paper is limited to deriving only the change in the line shape resulting from the linear magnetic field gradients, in a generale form.

The effect of applying a linear magnetic field gradient to a noninteracting spin system is to broaden the resonance absorbtion profile. The quantity of interest in a pulsed NMR experiment is *the normalized transverse response function of free induction decay* (FID). The FID signal or its Fourier transform, the absorbtion spectrum, is one of the fundamental problems of NMR. Considerable effort has been dedicated to the solution of this problem using a variety of techniques.

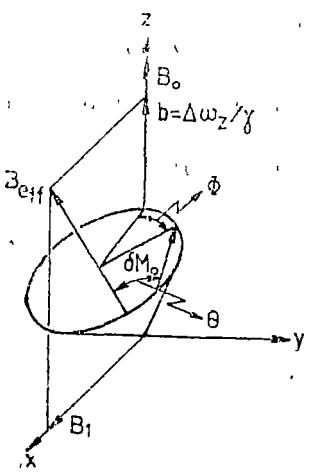

Fig. 3. Precession of elemental spin magnetization δM_0 in the tilted rotating reference frame.

Mansfield [5] and others calculated the effects of aplication of some magnetic field gradients which, as we noted before, may "individualize" the resonance phenomenon in respect of spatial distribution of spins.

For establishing the equation of motion magnetization, Eq. (6), from a certain sample position, we shall use the technique of density matrix developed in reference rotating frame.

2.1. *The magnetization in stationary states.* The Zeeman interaction $\mathcal{H}'$ for an isolated spin at position $\vec{r}$ in the rotating frame is presented

in Eq (3) I can be shown [6] that for an ensemble, in thermal equilibrium, the density matrix is time independent and is given by

$$\hat{\rho} = \exp(-\mathcal{H}'/kT)/Tr\{\exp(-\mathcal{H}'/kT)\} \tag{7}$$

where T is the temperature of the ensemble. Therefore, after the thermal equilibrium is established, the sample will have developed a magnetic moment

$$\langle\vec{m}\rangle = Tr\{\hat{\rho}\vec{m}\} = Tr\{\exp(-\mathcal{H}'/kT)\vec{m}\}Tr\{\exp(-\mathcal{H}'/kT)\} \tag{8}$$

Thus one can see that Eq. (8) agrees with the Langevin case but here there are magnetizations from different parts of the specimen.

2 2 *The magnetization in unstationary states.* All the curent NMR absorption techniques employ a $r f$ magnetic field pulse $\vec{B}_1$ with the components $(B_1 \cos \omega t,\ B_1 \sin \omega t,\ 0)$ in a laboratory frame and of constant amplitude $\vec{B}_1$ in a reference frame rotating with angular frequency ω and t_w the rf pulse length

Assume further that this pulse is of such form that if the wave function for the i^{th} spin is $\Psi_i(0)$ before the pulse, it is

$$\Psi_i'(t_w) = \hat{R}(t_w)\Psi(0) = e^{i\gamma B_1 I_x t}\Psi_i(0) = \hat{R}_x(\beta) \cdot \Psi_i(0) \tag{9}$$

after the pulse is turned off, t_w being the length of time the pulse lasts. Under these conditions the propagator operator becomes the rf. pulse rotation operator $R_i(\beta)$ where β is the Euler nutation angle of the pulse generally given by $\beta = \gamma B_1 t_w = \omega_1 t_w$

Thus, „t'' secondes after the shock is turned off:

$$\hat{\Psi}_i''(t) = \hat{T}(t)\Psi_i'(t_w) = \hat{T}(t)\hat{R}(t_w)\Psi_i(0) \tag{10}$$

$$\text{where } \hat{T}(t) = \exp(-itH'/\hbar) = \exp(i\Delta\omega I_z t) \cdot \exp(i\gamma\vec{G}\vec{r}I_z t) \tag{11}$$

Using the formalisme of density matrix

$$\langle\vec{m}(t)\rangle = Tr\{\exp(-\mathcal{H}'/kT)\hat{R}^+(t_w) \cdot \hat{T}^+(t)\ \vec{m} \cdot \hat{T}(t)\hat{R}(t_w)\}/Tr\{\exp(-\mathcal{H}'/kT)\} \tag{12}$$

Since $Tr(\hat{A} \cdot \hat{B}) = Tr(\hat{B} \cdot \hat{A})$ where A and B are any two operators. By substituting Eq (9) and Eq (11) into Eq (12) we have:

$$\langle\vec{M}(t)\rangle = \sum_i Tr\{\exp(-\mathcal{H}'/kT)\exp(-i\Delta\omega I_{z_i} t)\exp(-i\gamma\vec{G}\vec{r}_i I_{z_i} t) \cdot \cdot \hat{R}_i^+(\beta)\vec{m}\hat{R}_x(\ )\ \exp(i\gamma\vec{G}\vec{r}_i I_{z_i} t)\exp(i\Delta\omega I_{z_i} t)\}/Tr\{\exp(-\mathcal{H}'/kT)\} \tag{13}$$

This equation is a general formulation of magnetization motion or F I D. in the tilted rotating frame about an efective field $\vec{B}_{eff} = B_1\vec{i} + b\vec{k}$ where b is the suplimentary magnetic field due to gradient and which appeares in the vecinity of the spins at exact resonance In Eq (13) we can use the high temperature approximation

3. **The Transverse response.** The transvere NMR response signal in the rotating reference frame where the system of spins is prepared by $\beta = \omega_1 t_w = \gamma B_1 t_w$ pulse in a state described at $t = 0$ a matrix $\hat{\rho}(0) = const.\ I_x$, is the spin autocorrelation function given by [7]

$$S(t) = Tr[I_x(t)I_x]/Tr(I_x^2) \tag{14}$$

where the time dependences of the operator in a rotating reference frame is:

$$I_x(t) = e^{iH''t/\hbar} \cdot I_x \cdot e^{-iH''t/\hbar} \equiv \hat{T}^+(t)\hat{R}^+(\beta)\hat{I}_x\hat{R}(\beta)\hat{T}(t) \tag{15}$$

where

$$\mathcal{H}'' = -\hbar[\Delta\omega I_z + \gamma(\vec{G}\vec{r})I_z + \omega_1 I_x]$$

is whole Hamiltonian in rotating frame

Using the spin raising operator I_+, and by substituting the Eq (15) Eq. (9) and Eq. (11) into Eq (14), we derive the normalized transverse response function or free induction decay in the rotating frame

$$S(t) = \sum_i Tr\{\exp(-i\Delta\omega I_{zi}\, t)\, \exp(-i\gamma\vec{G}\vec{r}_i I_z t)\hat{R}_i^+(\beta)\hat{I}_{zi}\hat{R}_i(\beta) \cdot \exp(i\gamma\vec{G}\vec{r}_i I_{zi}\, t)\, \exp(-i\Delta\omega I_{zi}t)I_{+i}\}/\sum_i Tr\{I_{+i}^2\} \tag{16}$$

4. **Discussion.** The *rf* pulse rotation operator $R_x(\beta) = (exp_{i\beta}I_x)$ corresponds to a rotation of $\beta = \gamma B_1 t_w$ about the x axis When $\beta = \pi/2$, for example, we see that $\hat{R}_x^+(\pi/2)I_z\hat{R}_x(\pi/2) = I_y$, where the sign (+) denotes the Hermitian adjoint

Implicit in Eq (16) is that *rf* field $B_1 \gg b = (\vec{G}\vec{r}) = \frac{\Delta\omega}{\gamma}$ which amounts to saying that the spectral distribution of *rf* pulse is much wider than any gradient shift from exact resonance Because of the linear relationship betwee frequency an displacement imposed by the field gradient, the inverse Fourier transform of $S(t)$ yields directly the distribution of spins wich lie in isochromatic planes normal to $\vec{G}$

Thus resonance spectrum obtained for this configuration corresponds to a projection of the spin density of the substance, on the axis defined by the field gradient vector $\vec{G}$.

REFERENCES

1. P. Mansfield and P. K Grannell, *Phys Rev*, **12**, 3618 (1975)
2 P C Lauterbur, *Nature*, **242**, 190 (1973)
3 Al Nicula, S Nicula, L Giurgiu and I Ursu, *Studia—Physica*, **1**, (1986).
4 Al Nicula, S Nicula, *Studia—Physica*, **2**, p 40, (1986)
5 P Mansfield and P. G "Morris, NMR Imaging in Biomedicine", Acad Press, NY (1982)
6 J M Ziman, "Elements of Advanced Quantum Theory", Cambridge Univ. Press, (1969).
7. A. Abragam, "Principles of Nuclear Magnetism", Oxford, England, (1961)

STUDIA UNIV BABEŞ—BOLYAI, PHYSICA, XXXII, 1, 1987

DEPENDENCES OF THE ELECTRICAL RESISTANCE OF A SYNTTHETIC ZEOLITE UPON THE AMBIENT ATMOSPHERIC PRESSURE

V. CRISTEA*, ELEONORA TRIF* and AL. NICULA*

Received February 5, 1987

ABSTRACT. — On investigated the influence of the influence of the ambient atmospheric pressure on the electrical resistance of a synthetic zeolite The major variation appears for $p > 7 \times 10^3 N/m^2$, which may be described by the equation $Rp =$ const For samples calcined at 1200 K this dependence cannot be evidenced

The scientific interest in zeolite properties has arison up during the last years with regard to the great variety of their applications in industry [1].

The aim of this study was to characterize the thermal stability of Y-type zeolites. In a previous work [2] we have carried out investigations concerning their thermal stability. The DTA, RX and EPR methods revealed the lattice breakdown in the temperature range of 870—960 °C with the maximum at 820 °C In their early studies Freeman and Stamires [3] investigated the electrical conductivity of anhydrous synthetic zeolites, as well Stamires [4] investigated the effect of various adsorbed phases on the electrical conductivity. Some results on the dependence of the electrical conductivity upon the temperature of some natural zeolites have been reported by Rusu et al. [5] al the simposium on "zeolites in modern technology".

In the present work we have investigated the influence of the room temperature water evacuation on the electrical resistance of the synthetic Y-type zeolite with SiO_2/Al_2P_3 'mole ratio of 5.1, containing cations as: 10 1% Na^+, 0.49% Ca^{2+}, 0.34% K^+, 0 28% Fe^{3+}, 0 16% Ti^{2+}, 0 12% Mg^+ and 0.01 Mn^{2+}, required to achieve the electrical neutrality of the crystal

The resistance measurements were performed on compacted cylinders with a diameter of 12 mm and a thickness between 1 and 2 mm A standard pressure of 3×10^8 N/m^2 has been adopted in the preparation of all compact pellets. The Ag electrodes with a diameter of 10 mm were attached by vacuum evaporation The pellet was placed between 2 brass plates in the conductivity cell which is connected to the vacuum system and allows also pretreatments at temperatures up to 1400 K The samples were pretreated in the cell for at least 6h up to 700 K in air.

* *University of Cluj-Napoca, Faculty of Mathematics and Physics, 3400 Cluj-Napoca, Romania*

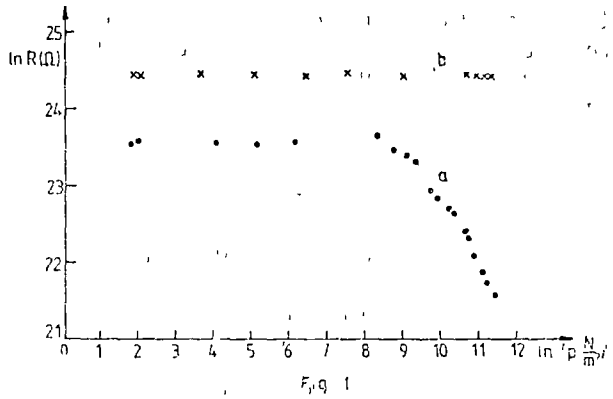

Fig 1 The variation of resistance with pressure a) the pellet submitted to a pretreatment at 700 K, b) the pellet submitted to a pretreatment at 1200 K

The investigation of the influence of the atmospheric pressure decreasing on zeolite resistance was performed at room temperature by stepurise reducing the pressure in the conductivity cell. The measurements were performed with a DC "orion" terraohmmeter.

Caution was taken to insure that equilibrium was reached at each decrement of pressure. During desorption, the attainment of equilibrium was indicated by obtaining constant values of both conductivity and pressure with time. Owing to the high values of the resistance the whole electric circuit was screened.

The variation of resistance with pressure for two types of pellets is shown in Fig 1. The curve (a) shows the behaviour of the pellet submitted to a previous heat treatment at 700 K, whereas the curve (b) is obtained for a pellet submitted to a previous treatment at 1200 K The major variation for the pellet (a) appears for $p > 7 \times 10^3$ N/m².

In Fig. 2 we have plotted $R(p)$ for $p > 2 \times 10^4$ N/m². It appears that for $p \geqslant 2\,67 \times 10^4$ N/m² we are able to describe the resistance variation by the equation of the type:

$$RP = \text{const.} \qquad (1)$$

where the constant value corresponding to the solid line has the value of 2.268×10^4 ΩN/m². In order to explain this relationship we must take into account that

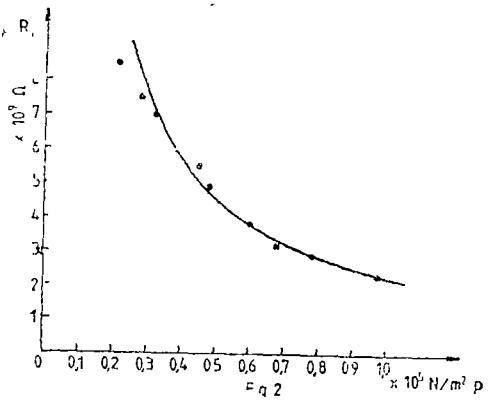

Fig 2 The variation of resistance with pressure, for $p \geqslant 2 \times 10^4 \frac{\text{N}}{\text{m}^2}$

the conductivity of zeolites increases with hydration. The association of the cations with water molecules by electrostatic cation-dipole interaction decreases the framework binding energy of the cations and consequently increases their mobility in the applied electric field. On the other hand we have:

$$R = \frac{1}{neu} \frac{l}{S} \tag{2}$$

where l and S are the thickness of the pellet and the electrod area respectively, n is the ion concentration and u their mobility. For a given pellet maintained at constant temperature, the mobility depends upon the amount of water only. Consequently, we have:

$$Ru = \text{constant}, \tag{3}$$

where u increases with the number of water molecules. Therefore u decreases with the pressure diminution. We suppose that such a conductivity mechanism is adequate for the ions located in the large cavities of zeolite. Therefore in formula (2) n is the number of ions in the large cavities and that is why R becomes constant when the pressure decreases below 10^4 N/m^2. As for pellet (b), we notice that it is contracted after the heat treatment. From Fig. 1.b we may conclude that as a result of high temperature heating, zeolite structure collapses and loses the hydration capacity. Hence the cation mobility is independent of pressure.

REFERENCES

1. D. W. Breck, "Zeolite Molecular Sieves", J. Willey-Interscience Publication, New York, 1973, Chapter 4
2. E. Trif, R. Rusu, G. Gheorghe, D. Strugaru, I. Ivan and Al. Nicula, *Proc. 24-th Congr. AMPERE*, Roma, 1986, p. 462
3. D. C. Freeman and D. N. Stamires, *J. Chem. Phys.* **35**, 799 (1961)
4. D. N. Stamires, *J. Chem. Phys.*, **36**, 3162 (1962)
5. Gh. Rusu, M. Rusu, F. Jacomi, M. Cruceanu, E. Popovici, M. Alexandroaiei and A. Vasile, *Proc. first Symposium on "Zeolites in Modern Technology"*, Iaşi, 1983, p. 130

STUDIA UNIV BABEŞ—BOLYAI, PHYSICA, XXXII, 1, 1987

CRITICAL DYNAMICS OF THE CLUSTER MODEL OF THE SPIN GLASS STATE

M. CRIŞAN*

Received February 6, 1987

ABSTRACT. — The dynamic and static properties of the cluster model for the spin glass state in the critical region are analysed using the dynamic and static scaling hypothesis.

1. **Introduction.** The cluster model for the spin glass state has been succesfully applied to explain the static properties of the short range spin glass state. A b r i k o s o v [1] considered such a model as consisting of "infinit clusters" (at very low temperatures), which is destroyed with the increasing of the temperature by the percolation, and finit size clusters appear in the system. If the temperature is not high enough the thermal fluctuations cannot break the bonds within one cluster, and only the spin orientation of the cluster can change in time. We will consider a model of saturated clusters, which are similar to a superparamagnetic cluster with strong anisotropy. However, near the critical temperature the scaling hypothesis will give us the possibility to show the existence of two distinct contributions: one given by saturated clusters and another given by unsaturated clusters. The same conclusion has been reached from dynamic considerations, and the main result of this paper is that the dynamic and static scaling hypothesis can be applied for the transition from the paramagnetic state into spin glass state. This conclusion is a good argument that this transition is a real "phase transition" but the equilibrium state is stil an open problem. Another problem which has to be clarified is the critical dimension of this transition and the fractal character of the clusters, a fact which seems to be in agreement with the experimental data [2, 3].

2. **The model.** The temperature dependence of the dynamic magnetic susceptibility can be calculated using the following model: (1) the spin glass state contains a finite number of clusters with a magnetic moment M_s, (2) the magnetic moment of a cluster is temperature independent and (3) the relaxation time τ is given by

$$\tau = \tau_0 \exp\ (E/T) \tag{1}$$

where τ_0 is a slowly varying function of temperature and E is the anisotropy barrier height given by

$$E = E_0 v \tag{2}$$

where v is the volume of the cluster and E_0 constant.

* *University of Cluj-Napoca, Faculty of Mathematics and Physics, 3400 Cluj-Napoca, Romania*

We also assume that there is a distribution in the volumes of the clusters, and the susceptibility of the spin glass is given by

$$\chi(T,\ \omega) = \int_0^\infty \chi_v(T,\ \omega) f(v)\, dv \tag{3}$$

where $f(v)$ is the volume distribution and ω is the frequency.

The contribution $M_v(t)$ of the cluster with volume V at the total magnetization is given by

$$M_v(t) = H[\chi_0 - (\chi_0 - \chi_1) \exp(-t/\tau)] \tag{4}$$

where χ_0 is the paramagnetic susceptibility corresponding to thermal equilibrium

$$\chi_0 = \int ds M_s s^y \mathfrak{L}\left(\frac{M_s s^y}{M}\right) \tag{5}$$

where $\mathfrak{L}$ is the Langevin function and $y = 1/2$ for a spin glass, n_s the number of clusters containing "s" spins

The number n_s of clusters depends on the number of spins s but we will take for the begining n_s as constant and (5) it will be approximated by

$$\chi_0 = \frac{M_S^2 V n_s}{3T} \tag{6}$$

The contribution of the anisotropy (2) will be given by

$$\chi_1 = \frac{a M_S^2 n_s}{E_0} \tag{7}$$

In an external magnetic field the spin glass acquires a magnetization in a time which is short compared to the relaxation time τ. Subsequently, the spin glass relaxes via thermal fluctuations to the superparamagnetic state characterized by a susceptibility given by (5)

The Fourier transform of (4) leads to the complex susceptibility

$$\chi_v = \frac{\chi_0 + i(\omega\tau)\chi_1}{1 + i(\omega\tau)} \tag{8}$$

and from this equation the real χ_v' and the imaginary past χ_v'' are

$$\chi_v' = \frac{\chi_0 + (\omega\tau)^2\chi_1}{1 + (\omega\tau)^2} \tag{9a}$$

$$\chi_v'' = \frac{(\omega\tau)(\chi_1 - \chi_0)}{1 + (\omega\tau)^2} \tag{9b}$$

Using these results we can calculate the temperature dependence of the dynamical susceptibility.

3. **The dynamics susceptibility.** We consider the equations (9a — 9b) to calculate the real part χ_v' and the imaginary part χ_v'' for a spin glass consisting from clusters with the volume v and the distribution function $f(v)$ From (9a) we get

$$\chi'(T,\ \omega) = \int dv \chi_v'(T,\ \omega) f(v) = \chi_1 \int dv \frac{[\chi_0 + (\omega\tau_0)^2 \exp 2E_0 V/T]}{1 + (\omega\tau_0)^2 \exp 2E_0 V/T} f(v) \qquad (10)$$

and if $T \gg E_0 V_m$, where V_m is the maximum volume of a cluster the equation (10) can be approximated as

$$\chi'(T,\ \omega) \cong \chi_1 \int_0^\infty dv f(v) \frac{E_0 v}{3aT} = \frac{\chi_1 \overline{V} E_0}{3aT} = \frac{M_s^2 \overline{V} n_s}{3T} \qquad (11)$$

an equation which shows that the system presents a superparamagnetic behaviour

The imaginary par t

$$\chi''(T,\ \omega) = \int dv f(v) \frac{(\omega\tau)(\chi_0 - \chi_1)}{1 + (\omega\tau)^2}$$

$$= \int_0^\infty dv f(v) (\omega\tau_0)^2 \frac{\exp E_0 V}{1 + (\omega\tau_0)^2 \exp \frac{2E_0 V}{T}} \left[1 - \frac{E_0 v}{3aT}\right] \qquad (12)$$

In order to calculate the integrals from (10) and (12) we consider the function

$$F(z) = [1 + (\omega\tau_0)^2 e^z]^{-1} \qquad (13)$$

which can be approximated as

$$F(z) = \begin{cases} 1\ ,\ z < 2\,|\ln \omega\tau_0\,| \\ 0\ ,\ z > 2\,|\ln \omega\tau_0\,| \end{cases} \qquad (14)$$

The equation (14) defines an supper limit for the volume of the cluster as

$$\frac{EV_m}{T} = |\ln \omega\tau_0\,| \qquad (15)$$

and the equation (10) becomes

$$\frac{\chi'(T,\ \omega)}{\chi_1} = 1 + \int_0^\infty dv f(v) \left[\frac{E_0 v}{3aT} - 1\right] F\left(\frac{2E_0 v}{T}\right)$$

$$\cong 1 + \int_0^{T/E_0 |\ln w\tau_0|} f(v) \left[\frac{E_0 V}{3aT} - 1\right] dv \qquad (16)$$

In a similar way we get grom (12)

$$\frac{\chi''(T,\omega)}{\chi_1} = -(\omega\tau_0)\int_0^{T/E_0} f(v)\left[\frac{E_0 V}{3aT} - 1\right]dv \tag{17}$$

If we consider the distribution $f(v) = \delta(v - \bar{v})$ the temperature dependence of $\chi'(T, \omega)$ and $\chi''(T, \omega)$ can be calculated from (16) and (17) as

$$\frac{\chi'(T,\omega)}{\chi_1} = 1 + \frac{|\ln\omega\tau_0|}{2E_0V}\left(\frac{|\ln\omega\tau_0|}{6a} - 1\right)T \tag{18}$$

and

$$\frac{\chi''(T,\omega)}{\chi_1} = -\frac{(\omega,\tau_0)|\ln\omega\tau_0|}{2E_0V}\left(\frac{|\ln\omega\tau_0|}{6a} - 1\right)T \tag{19}$$

The equations (11) and (18) show the existence of a temperature for which $\chi'(T_v, \omega)$ is maximum. The maximum of χ' will be obtained from the function

$$G(T) \equiv \frac{\chi'(T)}{\chi_1} - 1 = \left[\frac{E_0\bar{V}}{3aT} - 1\right]F\left(\frac{2E_0\bar{V}}{T}\right) \tag{20}$$

which has a maximum at

$$T_{\max} = E_0\bar{V}|\ln\omega\tau_0| \tag{21}$$

The effect of the magnetic field on the superparamagnetic relaxation time τ was calculated for a high energy-barrier approximation as

$$\tau^{-1} = C\alpha^{3/2}(1-h^2)\{(1+h)\exp[-\alpha(1+h)^2] + (1-h)\exp[-\alpha(1-h)^2] \tag{22}$$

where C is a numerical constant, $\alpha = E/T$, $h = M_sH/T$, E is the energy barrier in tero field and M_s is the superparamagnetic moment. Expanding (21) to order H^2 and replacing preexponential factor by a constant, one obtains

$$\tau = \tau_0 \exp\frac{E}{T}\left[1 - \left(\frac{M_sH}{T}\right)^2 + \ldots\right] \tag{23}$$

Taking now $\omega \sim 1/\tau$ from (21) we get

$$T_m(H) = \left|\frac{E}{T_m(H)} + \ln\left[1 - \frac{1}{2}\left(\frac{M_sH}{T_m(o)}\right)^2\right]\right|$$

which will be approximated for small magnetic fields as

$$T_m^2(H) - T_m^2(o) \cong \left(\frac{M_sH}{T_m(o)}\right)^2 \tag{24}$$

and if we consider T_m^- as the "freezing temperatur", T_f the field dependence given by (24) is in agreement with the recent results obtained by W e n g e r and M y d o s h [5].

4. **Critical behaviour.** The spin-glass state presents a critical behaviour but until now there are different scalings which have been tested experimentally. The best one seems to be

$$\tau = \tau_0 |\varepsilon|^{-z\nu} g(H/T\varepsilon^{\Phi}) \tag{25}$$

where $\varepsilon = (T - T_f)/T_f$

In this case (18) will be approximated by

$$\frac{\chi'}{\chi_1} = 1 + C_1 \ln |\varepsilon|^{2\nu} \left[\frac{C_2 \ln |\varepsilon|^{z\nu}}{6a} - 1 \right] \tag{26}$$

where C_1 and C_0 are constants, z and ν the standard critical indices It seems to be interesting that the scaling

$$\ln \frac{\tau}{\tau_0} = T^{-z\nu} f(H/T\varepsilon^{\Phi}) \tag{27}$$

is also a good approximation for the dynamic critical behaviour. In this case from (18) one obtains

$$\frac{\chi'}{\chi_1} = 1 + B_1 T^{z\nu+1} \left[\frac{B_2 T^{z\nu}}{6a} - 1 \right] \tag{28}$$

where B_1 and B_2 are constants.

The static critical behaviour can be proved easier from the experimental point of view and if the "cluster picture" for the spin glass is appropriated we have to obtain relevant results for the static critical behaviour. Let us go back to the equation (5) where n satisfies the scaling

$$n_s = s^{-\tau} \quad f]s/s_c) \tag{29}$$

where $\tau = 2 + \delta^{-1}$ (δ is the standard critical exponent), $f(s/s)$ is the distribution function which becomes a constant for $s \to 0$, and s is the characteristic cluster size $s_l \sim l^d(T)$, l, is the correlation length, d the euclidian dimension. As near the "freezing temperature" T_f, $l(T) \sim |\varepsilon|^{-1}$ the cluster size is s n_s (s, ε). Abrikosow showed that the number n_s has to satisfy

$$\sum_s s[n_s(s, \varepsilon) - n_s(s, 0)] = -\theta(-\varepsilon) |\varepsilon|^{\beta} \tag{30}$$

where

$$\beta = (\tau - 2)/\sigma \qquad \sigma = (\gamma + \beta)^{-1}$$

This relation can be written as

$$\int_0^{\infty} ds n_s \sim \int_0^{s_e} d_s s^{1-\tau} = 1, \quad \varepsilon \geqslant 0 \tag{31}$$

$$\int_0^{s_e} d_s s^{1-\tau} = s - \delta s_s^{2-\tau}; \quad \varepsilon \leqslant 0, \; H = 0 \tag{32}$$

In the presence of the magnetic field the size of the cluster has to be scaled as

$$s_e(H) \sim |\varepsilon|^{-\Phi} \; f_e(H^{1/2}/\varepsilon^{\Phi}) \tag{33}$$

and in the limit $H^{1/2}/^{\Phi}\varepsilon \to 0$ we can discuss the behaviour of the susceptibility given by (5) If we use the variable $x = s/s_e$ and $a = M_s s^{1/2} H/3T$ the equation (5) becomes

$$\chi' = \frac{M_s}{H} s_e^{3/2-\tau} \int_0^{\infty} dx \, x^{1/2-x} f(x) \mathfrak{L}(3ax^{1/2}) \tag{34}$$

If in (33) $f(x) \cong 1$ and $\mathfrak{L}(x) \cong x/3$ for $x \in [0, 3)$ and 1 for $x \gg 3$ the equation (34) becomes

$$\chi' = \frac{M_s}{H} \left[\int_0^{s_e/a^2} d_s s^{1-\tau} a \, s_e^{-1/2} + \int_{s_e/a^2}^{s_e} d_s \, s^{1/2-\tau} \right] \tag{35}$$

where the first term is the contribution of the unsaturated clusters and the second the contribution of the field frozen (saturated) clusters. The first term of (34) can be transformed using the equation (3) and

$$\chi' = \frac{M_s^2}{3T} \left[1 + s_e^{2-\tau} \int_{1/a^2}^{1} dx \left(-x^{1-\tau} + \frac{1}{a} x^{1/2-x} \right) \right] \tag{36}$$

which has the scaling behaviour

$$\chi' = \frac{M_s^2}{3T} \left[1 + a \left(\frac{H}{T} \right)^{\tau} - b \left(\frac{H}{T} \right)^{2\tau} \right] |\varepsilon|^{\Phi\delta} \tag{37}$$

where $\varphi = \nu d$.

We get a relation which describes the same qualitative picture as (26) or (28) because there are two terms: one which is negative and describes the contribution of the *unsaturated clusters* and the other which is positive and describes the contribution of the *saturated clusters*.

5. **Conclusions.** The cluster model for the spin glass transition can be succesfully used to describe the static and dynamic properties. The agreement between critical behaviour in the static and dynamic regime is a strong argument for the "scaling" hypothesis near the critical temperature. The existence of the unsaturated and saturated clusters near the critical temperature gives rise to different relaxation times and makes the dynamic scaling more difficult. Then the dynamic critical behaviour of the spin glass state has to be considered only qualitatively and as an argument for the static scaling

REFERENCES

1 A. A Abrikosov, *Adv Phys*, **29,** 869 (1980)
2 N Bonetemps, J Rajchenbach, R Chamberlin and R Orbach, *Phys Rev*, B **30,** 6514 (1984)
3 A P Malozemoff and B Barbara, *J Appl Phys*, **57,** 3410 (1985)
4. W F Brown, *Phys Rev*, **130,** 1677 (1963)
5 L E Wenger and J A Maydosh, *Phys Rev*, **B 29,** 4156 (1984).

STUDIA UNIV BABEŞ—BOLYAI, PHYSICA, XXXII, 1, 1987

SPIN WAVES FOR FERRIMAGNETIC COLLINEAR STRUCTURES

V. CRIŞAN*

Received February 6, 1987

ABSTRACT. — This report sumarizes the calculations, based on the Heisenberg model, of spin wave spectra in ferrimagnetic compounds, using a Green function method with Zubarev decoupling technique. The results are compared with the corresponding ones of other authors.

1 **Introduction.** The standard calculation of the spin waves spectra for ferri-and antiferrimagnetic structures can be done using two magnetic sublattices [1], this procedure being extended even for ferromagnetic Heisenberg structures formed by atoms with different values of magnetic moments [2]

Using the equation of motion method, S a h n i and V e n k a t a r a m a n [3] have calculated the spin waves spectra for collinear magnetic structures, the obtained results being used for the investigation of the spin waves in ferrimagnetic $Ho_2Fe_{17-x}Al_x$ intermetallic compounds [4]

The aim of this paper is the calculation, by the Green function method, of the spin waves spectra for ferrimagnetic collinear structures.

2 **The Hamiltonian.** In order to obtain the equation of motion for the Green function of the collinear magnetic structures it is conveninet to introduce „local coordinate frames" associated with the various spin sites, the z-axes of these frames being along the nominal spin directions and the x and y axes in any convenient directions. The structure contains $N_\downarrow$ spins per primitive magnetic unit cell, l', pointing along and $N_\downarrow$ spins per primitive magnetic unit cell, l, pointing againts the z direction. ($N_\downarrow$ may or may not be equal to $N_\searrow$). We shall refer to these as spins of categoiy $\uparrow$ and $\downarrow$, respectively, and use the indices $\lambda,\lambda'(=\uparrow,\downarrow)$ as labels for them

The cartesian components of the spin operator

$$(S_x^\lambda(lk),\ S_y^\lambda(lk),\ S_z^\lambda(lk))$$

for the k-th spin of category λ in the l-th cell, are specified with respect to the local coordinate system at the site (lk) where k runs over 1, 2 ... $N_\downarrow$, if $\lambda = \uparrow$ and over 1, 2 ... $N_\downarrow$ if $\lambda = \downarrow$.

* *University of Cluj-Napoca, Faculty of Mathematics and Physics, 3400 Cluj-Napoca, Romania*

In the following it will be assumed that local coordinate systems for spins of any given category (↑ or ↓) are parallel to each other and, further, that all the local x-axes are parallel.

The Heisenberg Hamiltonian for the ferrimagnetic spin system has the form :

$$\begin{aligned}\mathcal{H} = \frac{1}{2}\Big\{&\sum_{ll'}\sum_{kk'} \mathcal{J}(lk\uparrow, l'k'\uparrow)\,[S_x^{\uparrow}(lk)S_x^{\uparrow}(l'k') + S_y^{\uparrow}lk)S_y^{\uparrow}(l'k') + S_z^{\uparrow}(lk)S_z^{\uparrow}(l'k') + \\ &+ \sum_{ll'}\sum_{kk'} \mathcal{J}(l'k\uparrow,\ l'k'\downarrow)\,[S_x^{\uparrow}(lk)S_x^{\downarrow}(l'k') - S_y^{\uparrow}(lk)S_y^{\downarrow}(l'k') - S_z^{\uparrow}(lk)S_z^{\downarrow}(l'k')] + \\ &+ \sum_{ll'}\sum_{kk'} \mathcal{J}(lk\downarrow,\ l'k'\uparrow)\,[S_x^{\downarrow}(lk)S_x^{\uparrow}(l'k') - S_y^{\downarrow}(lk)S_y^{\uparrow}(l'k') - S_z^{\downarrow}(lk)S_z^{\uparrow}(l'k')] + \\ &+ \sum_{ll'}\sum_{kk'} \mathcal{J}(lk\downarrow,\ l'k'\downarrow)\,[S_x^{\downarrow}(lk)S_x^{\downarrow}(l'k') + S_y^{\downarrow}(lk)S_y^{\downarrow}(l'k') + S_z^{\downarrow}(lk)S_z^{\downarrow}(l'k')]\Big\} + \\ &+ \sum_{l}\Big[\sum_{k} \mu_B g(k\uparrow)H(k\uparrow)S_z^{\uparrow}(lk) + \sum_{k} \mu_B g(k\downarrow)H(k\downarrow)S_z^{\downarrow}(lk)\end{aligned} \tag{1}$$

where the quantity $H(k\lambda)$ denotes the effective anisotropic field associated with the sublattices $(k\lambda)$ directed along the local z-axes. μ_B is the Bohr magneton and $g(k\lambda)$ the Landé g factor $\mathcal{J}(lk\lambda,\ l'k'\lambda')$ refers to the exchange integral associated with the pair of sites $(lk\lambda,\ l'k'\lambda')$. For the sake of simplicity we have assumed here $\mathcal{J}(lk\lambda,\ l'k'\lambda') = \mathcal{J}$ to be a scalar. The negative signs before the y and z component terms in the second and third summatoins on the right hand side of the equation arise from the relative orientations of the local frames for the two categories of spins, ↑ and ↓, The exchange integrals have permutation symmetry $\mathcal{J}(lk\lambda,\ l'k'\lambda') = \mathcal{J}(l'k'\lambda',\ lk\lambda)$ and translational periodicity. Using the trnaslation invariance and the usual raising and lowering operators, $S_{\pm}$, for each sublattice the Hanmiltonian (1) becomes

$$\begin{aligned}\mathcal{H} = \frac{1}{2}\Big\{&\sum_{ll'}\sum_{kk'} \mathcal{J}(lk\uparrow, l'k'\uparrow)\Big[S_z^{\uparrow}(lk)S_z^{\uparrow}(l'k') + \frac{1}{2}\,[S_+^{\uparrow}(lk)S_-^{\uparrow}(l'k') + S_-^{\uparrow}(lk)S_+^{\uparrow}(l'k')]\Big] + \\ &+ \sum_{ll'}\sum_{kk'} \mathcal{J}(lk\uparrow,\ l'k'\downarrow)\Big[-S_z^{\uparrow}(lk)S_z^{\downarrow}(l'k') + \frac{1}{2}\,(S_+^{\uparrow}(lk)S_+^{\downarrow}(l'k') + S_-^{\uparrow}(lk)S_-^{\downarrow}(l'k'))\,] + \\ &+ \sum_{ll'}\sum_{kk'} \mathcal{J}(lk\downarrow,\ l'k'\uparrow)\,[-S_z^{\downarrow}(lk)S_z^{\uparrow}(l'k') + \frac{1}{2}\,(S_+^{\downarrow}(lk)S_+^{\uparrow}(l'k') + S_-^{\downarrow}(lk)S_-^{\uparrow}(l'k'))\,] + \\ &+ \sum_{ll'}\sum_{kk'} \mathcal{J}(lk\downarrow,\ l'k'\downarrow)\,[S_z^{\downarrow}(lk)S_z^{\downarrow}(l'k') + \frac{1}{2}\,(S_+^{\downarrow}(lk)S_-^{\downarrow}(l'k') + S_-^{\downarrow}(lk)S_+^{\downarrow}(l'k'))\,]\Big\} + \\ &+ \sum_{l}\Big[\sum_{k} \mu_B g(k\uparrow)H(k\uparrow)S_z^{\uparrow}(lk) + \sum_{k} \mu_B g(k\downarrow)H(k\downarrow)\,S_z^{\downarrow}(lk)\end{aligned} \tag{2}$$

3. The equations of motion for Green functions

The Green functions are defined by:

$$G_1 = \begin{bmatrix} G_+^{\uparrow\uparrow}(\alpha\beta,\ ij) & 0 \\ G_-^{\downarrow\uparrow}(\alpha\beta,\ ij) & 0 \\ 0 & G_-^{\uparrow\downarrow}(\alpha\beta,\ ij) \\ 0 & G_+^{\downarrow\downarrow}(\alpha\beta,\ ij) \end{bmatrix};\ G_2 = \begin{bmatrix} G_-^{\uparrow\uparrow}(\alpha\beta,\ ij) & 0 \\ G_+^{\downarrow\uparrow}(\alpha\beta,\ ij) & 0 \\ 0 & G_+^{\uparrow\downarrow}(\alpha\beta,\ ij) \\ 0 & G_-^{\downarrow\downarrow}(\alpha\beta,\ ij) \end{bmatrix} \tag{3}$$

where:

$$G_\pm^{\lambda\lambda'}(\alpha\beta,\ ij) = \ll S_\pm^\lambda(\alpha i);\ (S_-^{\lambda'}(\beta j))^n (S_+^{\lambda'}(\beta j))^{n-1} \gg \tag{4}$$

and n is a positive integer

The equations of motion of these Green functions are

$$E \ll S_\pm^\lambda(\alpha i);\ (S_-^{\lambda'}(\beta j))^n (S_+^{\lambda'}(\beta j))^{n-1} \gg = \frac{1}{2\pi} \langle [S_\pm^\lambda(\alpha i);\ (S_-^{\lambda'}(\beta j))^n (S_+^{\lambda'}(\beta j))^{n-1}] \rangle +$$

$$+ \ll [S_\pm^\lambda(\alpha i),\ \mathcal{H}],\ (S_-^{\lambda'}(\beta j))^n (S_+^{\lambda'}(\beta j))^{n-1} \gg \tag{5}$$

where the Hamiltonian is given by the equation (2) and the first term on the right hand side by

$$[S_+^\lambda(\alpha i),\ S_-^{\lambda'}(\beta j))^n (S_+^{\lambda'}(\beta j))^{n-1}] = [2n\hbar S_z^{\lambda'}(\beta j) + n(n-1)\hbar^2] \prod_{p=1}^{n-1} [S(S+1)\hbar^2 -$$

(6)

$$- (n-p-1)(n-p)\hbar^2 - (2n-2p-1)\hbar S_z^{\lambda'}(\beta j) - (S_z^{\lambda'}(\beta j))^2] \delta_{\lambda\lambda'} \delta_{ij} \delta_{\alpha\beta}$$

and

$$[S_-^\lambda(\alpha i);\ (S_-^{\lambda'}(\beta j))^n (S_+^{\lambda'}(\beta j)^{n-1}] = [2(n-1)\hbar S_z^{\lambda'}(\beta j) + \hbar^2 (n-1)(n-2) \times$$

(7)

$$\times \prod_{p=1}^{n} [S(S+1)\hbar^2 - (n-p)(n-p+1)\hbar^2 - (2n-2p+1) S_z^{\lambda'}(\beta j) - (S_z^{\lambda'}\beta j))^2] \delta_{\alpha\beta} \delta_{ij} \delta_{\lambda\lambda'}$$

with the usual comutation relations and Zubarev decoupling,

$$\ll S_z S_\pm,\ (S_-^{\lambda'}(\beta j))^n (S_+^{\lambda'}(\beta j))^{n-1}) \gg = \langle S_z \rangle \ll S_\pm,\ (S_-^{\lambda'}(\beta j))^n (S_+^{\lambda'}(\beta j))^{n-1} \gg \tag{8}$$

the equation of motion (5) becomes

$$\Big\{\pm E \pm \mu_B g(\imath\uparrow)H(\imath\uparrow) \pm \sum_{l'k'} [\mathfrak{J}(\alpha\imath\uparrow,\ l'k'\uparrow)\langle S_z^{\uparrow}(l'k')\rangle \mp \mathfrak{J}(\alpha\imath\uparrow,\ l'k'\downarrow)\langle S_z^{\downarrow}(l'k')\rangle] \pm$$

$$\pm \sum_{lk} [\mathfrak{J}(lk\uparrow,\ \alpha\imath\uparrow)\langle S_z^{\uparrow}(lk)\rangle \mp \mathfrak{J}(lk\downarrow,\alpha\imath\uparrow)\langle S_z^{\downarrow}(lk)\rangle]\} G_{\pm}^{\uparrow\lambda'}(\alpha\beta,\ \imath\jmath) =$$

$$= \frac{1}{2\pi}\,\delta_{\alpha\beta}\delta_{\imath\jmath}\delta_{\lambda\lambda'} < \{[n(n-1)\hbar^2 + 2n\hbar S_z^{\lambda'}(\beta\jmath)] \prod_{p=1}^{n-1} [S(S+1)\hbar^2 -$$

$$- (n-p-1)(n-p)\hbar^2 - (2n-2p-1)\hbar\, S_z^{\lambda'}(\beta\jmath) - (S_z^{\lambda'}(\beta\jmath))^2]\Big\}$$

or

$$\frac{1}{2\pi}\,\delta_{\alpha\beta}\delta_{\imath\jmath}\delta_{\lambda\lambda'} \Big\langle \Big\{ [2(n-1)\hbar S_z^{\lambda'}(\beta\jmath) + \hbar^2(n-1()n-2)] \prod_{p=1}^{n} [S(S+1)\hbar^2 -$$

$$- (n-p)(n-p+1)\hbar^2 - (2n-2p+1)\hbar S_z^{\lambda'}(\beta\jmath) - (S_z^{\lambda'}(\beta\jmath))^2]\Big\} > \pm \tag{9}$$

$$\pm \langle S_z^{\uparrow}(\alpha\imath)\rangle \Big\{ \sum_{l'} \sum_{k'} [\mathfrak{J}(\alpha\imath\uparrow,\ l'k'\uparrow) G_{\pm}^{\uparrow\lambda'}(l'\beta,\ k'\jmath) + \mathfrak{J}(\alpha\imath\uparrow,\ l'k'\downarrow) G_{\mp}^{\downarrow\lambda'}(l'\beta,\ k'\jmath)] +$$

$$+ \sum_{lk} \mathfrak{J}(lk\uparrow,\ \alpha\imath\uparrow) G_{\pm}^{\uparrow\lambda'}(l\beta,\ k\jmath) + \mathfrak{J}(lk\downarrow,\ \alpha\imath\uparrow) G_{\mp}^{\downarrow\lambda'}(l\beta,\ k\jmath)]\Big\}$$

Changing the spin directoins $\uparrow$ by $\downarrow$ and $\downarrow$ by $\uparrow$ in this relations, the equation of motion for $G_{\pm}^{\downarrow\lambda'}$ is obtained

As a consequence of translation invariance we can write the Fourier transform of the Green functions with respect to the reciprocal lattice

$$G_{\pm}^{\lambda\lambda'}(\pm q,\ \imath\jmath) = \frac{1}{N} \sum_{\beta} G_{\pm}^{\lambda\lambda'}(\alpha\beta,\ \imath\jmath) \exp\,(\mp \imath\vec{q}\ (\vec{\alpha} - \vec{\beta}))$$

and

$$\mathfrak{J}(\vec{q},\ \imath k',\ \lambda\lambda') = \sum_{l} \mathfrak{J}(\alpha l',\ \imath k',\ \lambda\lambda') \exp\,(\imath\vec{q}\ (\vec{\alpha} - \vec{l'})) \tag{10}$$

$$\delta_{\alpha\beta} = \frac{1}{N} \sum_{\beta} \exp\,(\imath\vec{q}\,(\vec{\alpha} - \vec{\beta}))$$

where the wave vector $\vec{q}$ ranges over the first Brillouin zone, $\vec{\alpha}$, $\vec{\beta}$, $\vec{l'}$ denotes vectors of the primitive magnetic lattices and N is the total number of spins in the lattice.

Finally, the equations of motion for the Green functions, (9), can be expresed by

$$\sum_{k'\in\uparrow} B_{ik'}G_{+}^{\downarrow\lambda'}(k'j) + \sum_{k''\in\downarrow} C_{ik''}G_{-}^{\downarrow\lambda'}(k''j) = -\frac{\delta_{ij}\,\delta_{\lambda\lambda'}}{2\pi}\langle[n\hbar^2(n-1) +$$

$$+ 2n\hbar\, S_z^{\lambda'}(\beta j)]\prod_{p=1}^{n-1}[S(S+1)\hbar^2 - (n-p)(n-p-1)\hbar^2 - (2n-2p-$$

$$- 1)\hbar S_z^{\lambda'}(\beta j) - (S_z^{\lambda'}(\beta j)^2]\rangle$$

$$\sum_{k'\in\uparrow} B_{ik'}G_{-}^{\uparrow\lambda'}(k'j) + \sum_{k''\in\downarrow} C_{ik''}G_{-}^{\downarrow\lambda'}(k''j) =$$

$$= \frac{\delta_{ij}\,\delta_{\lambda\lambda'}}{2\pi}\langle[(n-1)(n-2)\hbar^2 + 2(n-1)\hbar\, S_z^{\lambda'}(\beta j)]\prod_{p=1}^{n}[S(S+1)\hbar^2 -$$

$$- (n-p+1)(n-p)\hbar^2 - (2n-2p+1)\hbar S_z^{\lambda'}(\beta j) - (S_z^{\lambda'}(\beta j))^2]\rangle \tag{11}$$

$$\sum_{k'\in\downarrow} D_{ik'}G_{+}^{\downarrow\lambda'}(k'j) + \sum_{k''\in\uparrow} F_{ik''}G_{-}^{\uparrow\lambda'} = -\frac{\delta_{ij}\,\delta_{\lambda\lambda'}}{2\pi}\langle[n\hbar^2(n-1) + 2n\hbar S_z^{\lambda'}(\beta j)]\times$$

$$\times\prod_{p=1}^{n-1}[S(S+1)\hbar^2 - (n-p)(n-p) - 1)\hbar^2 - (2n-2p-1)\hbar\, S_z^{\lambda'}(\beta j) -$$

$$- (S_z^{\lambda'}(\beta j))^2]\rangle$$

$$\sum_{k'\in\downarrow} D_{ik'}G_{-}^{\downarrow\lambda'}(k'j) + \sum_{k''\in\uparrow} F_{ik''}G_{+}^{\uparrow\lambda'} = \frac{\delta_{ij}\,\delta_{\lambda\lambda'}}{2\pi}\langle[(n-1)(n-2)\hbar^2 +$$

$$+ 2(n-1)\hbar S_z^{\lambda'}(\beta j)]\prod_{p=1}^{n}[S(S+1)\hbar^2 - (n-p+1)(n-p)\hbar^2 - (2n-2p+$$

$$+ 1)\hbar S_z^{\lambda'}(\beta j) - (S_z^{\lambda'}(\beta j))^2]\rangle$$

where

$$B_{ik'} = \langle S_z^{\uparrow}(\beta j)\rangle\mathfrak{J}(q;\, ik',\, \uparrow\uparrow) - (E + A_{\uparrow} + Q_{\uparrow})\delta_{ij} \qquad i\in\uparrow,\ k'\in\uparrow$$

$$C_{ik''} = \langle S_z^{\uparrow}(\beta j)\rangle\mathfrak{J}(q,\, ik'',\, \uparrow\downarrow) \qquad i\in\uparrow,\ k''\in\downarrow \tag{12}$$

$$D_{ik'} = \langle S_z^{\downarrow}(\beta j)\rangle\mathfrak{J}(q,\, ik',\, \downarrow\downarrow) - (E + A_{\downarrow} + Q_{\downarrow})\delta_{ij};\qquad i\in\downarrow,\ k'\in\downarrow$$

$$F_{ik''} = \langle S_z^{\downarrow}(\beta j)\rangle\mathfrak{J}(q,\, ik'',\, \downarrow\uparrow) \qquad i\in\downarrow,\ k''\in\uparrow$$

The matrix form of the equations are

$$\begin{bmatrix} -B(\uparrow\uparrow) & -C(\uparrow\downarrow) & 0 & 0 \\ F(\downarrow\uparrow) & D(\downarrow\downarrow) & 0 & 0 \\ 0 & 0 & B(\uparrow\uparrow) & C(\uparrow\downarrow) \\ 0 & 0 & -F(\downarrow\uparrow) & -D(\downarrow\downarrow) \end{bmatrix} \begin{bmatrix} G_{+}^{\uparrow\uparrow} & 0 \\ G_{-}^{\downarrow\uparrow} & 0 \\ 0 & G_{-}^{\uparrow\downarrow} \\ 0 & G_{+}^{\downarrow\downarrow} \end{bmatrix} = \begin{bmatrix} \delta_{ij} & 0 \\ 0 & 0 \\ 0 & 0 \\ 0 & \delta_{ij} \end{bmatrix} \times$$

$$\frac{1}{2\pi} \langle [S_{+}^{\lambda}(\alpha i) ; (S_{-}^{\lambda'}(\beta j))^{n} (S_{+}^{\lambda'}(\beta j))^{n-1}] \rangle \qquad (13)$$

$$\begin{bmatrix} B(\uparrow\uparrow) & C(\uparrow\downarrow) & 0 & 0 \\ F(\downarrow\uparrow) & D(\downarrow\downarrow) & 0 & 0 \\ 0 & 0 & B(\uparrow\uparrow)' & C(\uparrow\downarrow) \\ 0 & 0 & F(\downarrow\uparrow) & D(\downarrow\downarrow) \end{bmatrix} \begin{bmatrix} G_{-}^{\uparrow\uparrow} & 0 \\ G_{+}^{\downarrow\uparrow} & 0 \\ 0 & G_{+}^{\uparrow\downarrow} \\ 0 & G_{-}^{\downarrow\downarrow} \end{bmatrix} = \begin{bmatrix} \delta_{ij} & 0 \\ 0 & 0 \\ 0 & 0 \\ 0 & \delta_{ij} \end{bmatrix} \times$$

$$\frac{1}{2} \langle [S_{-}^{\lambda}(\alpha i) ; (S_{-}^{\lambda'}(\beta j))^{n} (S_{+}^{\lambda'}(\beta j))^{n-1}] \rangle$$

The dispersion relations for spin waves have been calculated from G_1 and G_2 Green functions, the obtained branches number being $2(N_\uparrow + N_\downarrow)$, half of them corresponding to positive frequencies and the other half to negative frequencies. Using the Green function method it seems that the branches of the spectrum is shifted by:

$$\Delta E_1 = A_\uparrow + Q_\uparrow \quad \text{or} \quad \Delta E_2 = A_\downarrow + Q_\downarrow$$

where

$$A_\lambda = \mu_B g(i\lambda)\, H\,(i\lambda)$$

$$Q_\lambda = \sum_{l'k'} \mathfrak{J}(\alpha i\lambda,\ l'k'\lambda) \langle S_z^{\lambda}(l'k') \rangle \mp \mathfrak{J}(\alpha i\lambda,\ l'k'\lambda') \langle S_z^{\lambda'}(lk) \rangle]$$

from the spin waves spectrum calculated by Sahni and Venkataraman [3].

REFERENCES

1. C Kittel, "Quantum Theory of Solids", John Wiley Sons inc, New York—London 79 (1963)
2. M Crişan, M Mc Neil, V Crişan, *Studia Univ. B.B., Ser Phys*, **41**, 1 (1972)
3. V C Sahni, G Venkataraman, *Adv. Phys*, **547**, 23 (1974)
4. V Crişan, *Studia Univ B B. Ser Physica*, **16**, 2 (1978)

STUDIA UNIV BABEŞ—BOLYAI, PHYSICA, XXXII, 1, 1987

4f STATES IN Gd_2Ni_{17} INTERMETALLIC COMPOUND

V. CRIŞAN*, I POP*, T. TOŞA* and M. POPESCU*

Received February 9, 1987

ABSTRACT. — The logarithmic derivatives and the band structure of Gd_2Ni_{17} intermetallic compound are performed using APW nonrelativistic method The muffin-tin potential are calculated using the Matthciss method and χ_α approximation for exchange.

The intermetallic compounds, RT, between rare earth, R, and transmition metal T show many interesting magnetic properties In R = Y and M = Ni, Cr compounds the ferromagnetism becomes weak with increasing Y concentration and disappears in YNi_5 and YCo_2, but a resurgence of the ferromagnetism occurs in Y_2Ni_7 and Y_4Co_3 [1, 2] On the other hand, in Y—Fe compounds, the Curie temperature increases while the average magnetic moment on an Fe atom decreases

The compound Y_2Fe_{17} shows an anomaly in its latice constant below T and pressure dependence of T_c similar to that in Fe—Ni Invar alloys [3—6].

In the Y—Ni system with increasing concentration of Y, the spontaneous magnetisation decreases rapidly from pure Ni YNi_5 is a strongly—exchange—enhanced Pauli paramagnet, YNi_3, a very weak itinerant electron ferromagnet, [2]. Y_2Ni_{17} has a Curie temperature of 150 K and some Ni sites show itinerant electron metamagnetism [7] The magnetic properties can be explained in the itinerant electron model by the special shape of the density of states due to the hybridisation between the 3d band of Ni atoms and 4d band of Y atoms and the position of Y atoms and the position of the Fermi level [8] The effects of pressure in these compounds are well accounted in the itinerant electron model [9]. Other magnetic measurements shows that Y_2N_{17} is ferrimagnetic and the anomaly in magnetisation at lower temperatures may be interpreted as a second order phase transition of order-order type, i e from collinear to non-collinear ferrimagnetic structure according to Yafet and Kittel theory [10].

The magnetic measurements on Dy_2Ni_{17} [10—12] are still a matter of controversy Some of the f systems are heavy-fermion The magnetic properties of these materials are typical of narrowband metals ranging from enhanced Pauli paramagnetism through spin fluctuation and Kondo-lattice behaviour, to itinerant magnetism In some cases superconductivity associated with the heavy electrons has been observed, and the possibility of p-wave pairing has been discussed

* *University of Cluj-Napoca, Faculty of Mathematics and Physics, 3400 Cluj-Napoca, Romania*

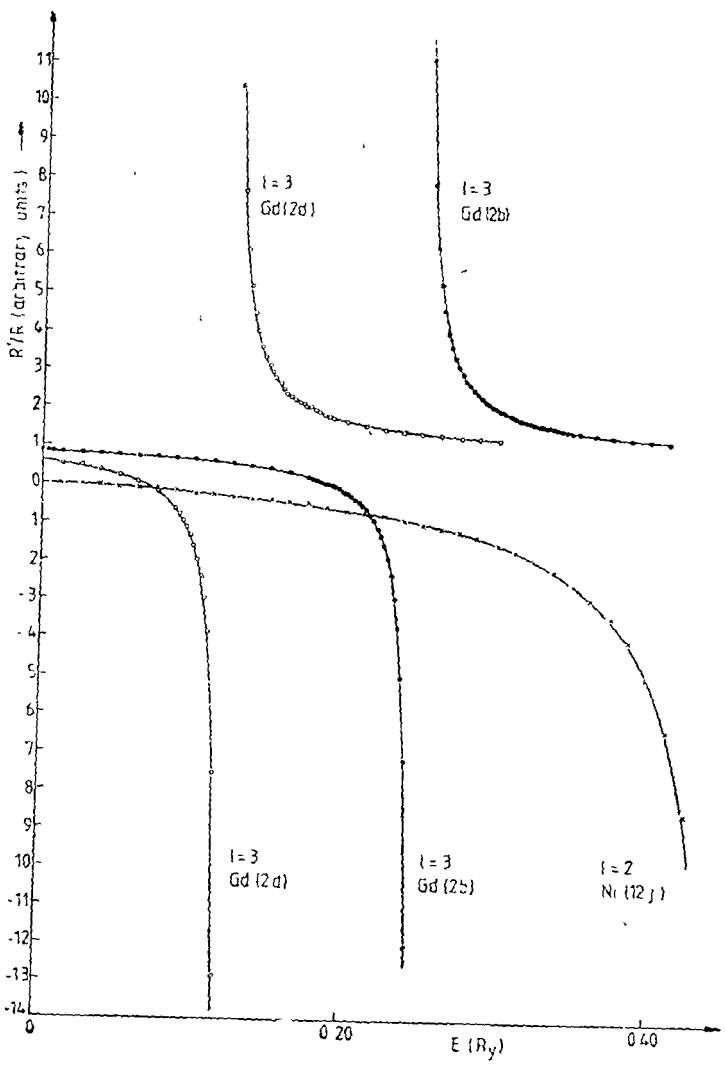
R'/R (arbitrary units)
l = 3
Gd (2d)
l = 3
Gd (2b)
l = 3
Gd (2d)
l = 3
Gd (2b)
l = 2
Ni (12 j)
0
0 20
0 40
E (Ry)

Fig 1

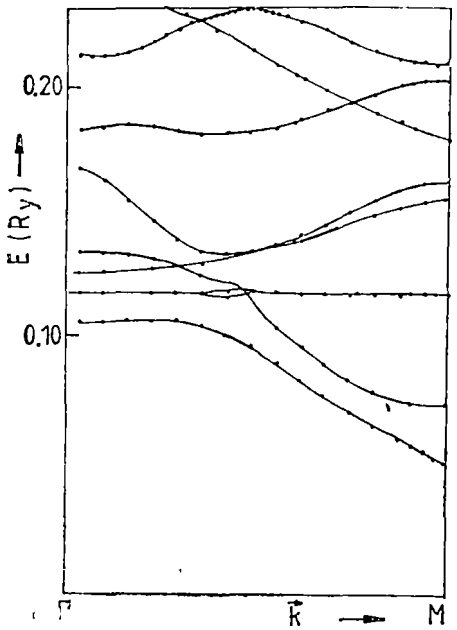

Fig. 2

The aim of this paper is the study of 4f states in the Gd_2Ni_{17} intermetallic compound. The band structure calculation was performed APW method with χ_α approximation by for exchange. The crystalline structure is of the Th_2Ni_{17} type with 38 atmos per unit cell.

Logarithmic derivatives shows the possibility of $f-d$ hybridisation (Fig. 1) in this compound.

The energy bands were computed for the ΓM direction of the Brillouin zone (Fig. 2). The results for this direction show a $d-f$ hybridisationof 3d and 4f energy bands. The gadolinium 4f bands are larger than the nickel 3d bands and are situated at the bottom of them. There is an energy band gap for this direction as that calculated for Y_2Ni_{17} intermetallic compound [1, 2].

REFERENCES

1. J. Inoue, M Shimizu, *J Phys* **E 1511** (1985)
2. M Simizu, J. I noue, S. Nagasawa, *J. Phys*, **14**, 2673 (1984).
3 D. Givord, R. Lemaire, *IEEE Trans Mag* **MAG-10**, 109 (1974)
4. D Givord, F Givord. R Lemaire, *J. Physique Coll*, 32, C1, 668 (1971).
5 M. Brouha, K. H J Buschow, A. R Miedema, *IEEE Trans Mag.* **MAG-10**, 182 (1974).
6 M. Shimizu, *Rep. Prog. Phys*, **44**, 329 (1981).
7 D. Gignoux, R. Lemaire, P Molho, *J. Magn Magn Mater*, **21**, 119 (1980).
8. D. Gignoux, R Lemaire, P Molho, F Tasset, *J Appl Phys*, **52**, 2087 (1981)
9. J. Beille, D. Gignoux, R. Lemaire, M. Shimizu, J Voiron, *Physica* B **119**, 133 (1983).
10 M. Coldea, I. Pop, N Dihoiu, *J Magn. Magn Mater*, **31–34**, 204 (1983).
11. J. Laforest, R. Lemaire, D Paccard, P Pauthenet, *C R Acad. Sci*, *Paris*, B **264**, 676 (1976).
12. P. D. Carfagna, W. E. Wallace, *J Appl Phys*, **39**, 5259 (1968).

STUDIA UNIV BABEŞ—BOLYAI, PHYSICA, XXXII, 1, 1987

ON THE APPLICABILITY OF THE JOOS-WEINBERG EQUATIONS

Z. NÉDA* and Z. GÁBOS*

Received February 10, 1987

ABSTRACT. — The absence of additional conditions is a great advantage, but the high order partial derivates which appear constitute is a disadvantage for the Joos-Weinberg equations This work shows (for the case $s = 1, 3/2$) that these high order partial derivates result from the fact that the Joos-Weinberg equations describe the motion of the center of inertia of particles with high spin, composed of two, or more Dirac particles Thus the Joos-Weinberg formalism is very useful in scattering problems, but unusable in structural ones

1°. For the two helicity states the Dirac equation

$$\left(\gamma_\mu \frac{\partial}{\partial x_\mu} + m_0\right)\Psi = 0, \quad (c = 1,\ \hbar = 1), \tag{1}$$

admits the following solutions:

$$\Psi_\lambda = \frac{1}{\sqrt{2}} \begin{pmatrix} u_\lambda \\ v_\lambda \end{pmatrix} e^{ipx}, \qquad \lambda = \frac{1}{2}, -\frac{1}{2}, \tag{2}$$

where u_λ respectively v_λ are two spinors caracterised by the m quantum number, which quantify the projection of the spin on the 3rd axis, hence the notation $u_{\lambda m}$, respectively $v_{\lambda m}$ $\left(m = \frac{1}{2}, -\frac{1}{2}\right)$. Using λ as index for the rows, and m as index for the columns we define the u and v matrices, so that we may write

$$u_\lambda = ue_\lambda, \quad v_\lambda = ve_\lambda, \tag{3}$$

where

$$e_{\frac{1}{2}} = \begin{pmatrix} 0 \\ 1 \end{pmatrix}, \qquad e_{-\frac{1}{2}} = \begin{pmatrix} 0 \\ 1 \end{pmatrix} \tag{4}$$

* *University of Cluj-Napoca, Faculty of Mathematics and Physics, 3400 Cluj-Napoca, Romania*

Considering the following matrices

$$\gamma_j = \begin{pmatrix} 0 & -i\sigma_j \\ i\sigma_j & 0 \end{pmatrix}, \quad \gamma_4 = \begin{pmatrix} 0 & 1 \\ 1 & 0 \end{pmatrix} \tag{5}$$

we get for u and v:

$$m_0 u + [(\vec{\sigma}, \vec{p}) - E]v = 0, \tag{6}$$

$$-[(\vec{\sigma}, \vec{p}) + E]u + m_0 v = 0. \tag{7}$$

On imposing the condition

$$\overline{\Psi}_\lambda \Psi_\lambda = 1 \tag{8}$$

the solutions of (6) and (7) will be:

$$u = \begin{pmatrix} A\cos\frac{\vartheta}{2} - \frac{1}{A}\sin\frac{\vartheta}{2}\, e^{-i\varphi} \\ A\sin\frac{\vartheta}{2}\, e^{i\varphi} \quad \frac{1}{A}\cos\frac{\vartheta}{2} \end{pmatrix}, \tag{9}$$

$$v = \begin{pmatrix} \frac{1}{A}\cos\frac{\vartheta}{2} - A\sin\frac{\vartheta}{2}\, e^{-i\varphi} \\ \frac{1}{A}\sin\frac{\vartheta}{2}\, e^{i\varphi} \quad A\cos\frac{\vartheta}{2} \end{pmatrix}, \tag{10}$$

where

$$A = \sqrt{\frac{1-v}{1+v}} \tag{11}$$

(ϑ and φ indicate the direction of movement of the Dirac particle). One may notice that u and v only depend on the velocity vector of the particle: v

2°. Let us consider a particle with spin 1, which has no internal orbital angular momentum, and is composed of two Dirac particles. In this case the composition operation for both the state functions, and for the operators is given by the direct-product.

From the product of the wave functions for the two Dirac particles we can separate the following factor:

$$e^{iPx}, \quad P = p_1 + p_2, \tag{12}$$

where P is the momentum four-vector, and x is the position four-vector for the center of inertia where the 1st and 2nd Dirac particles have been combined.

For the two Dirac particles we can write, according to relations (6), (7):

$$m_{01}u^{(1)} + [(\sigma,\ \vec{p}_1) - E_1)]v^{(1)} = 0, \tag{13}$$

$$-[(\vec{\sigma},\ \vec{p}_1) + E_1]u^{(1)} + m_{01}v^{(1)} = 0 \tag{14}$$

and, respectively:

$$m_{02}u^{(2)} + [(\vec{\sigma},\ \vec{p}_2) - E_2]v^{(2)} = 0, \tag{15}$$

$$-[(\vec{\sigma},\ \vec{p}_2) + E_2]u^{(2)} + m_{02}v^{(2)} = 0. \tag{16}$$

The velocity of the 1st and 2nd particles is the same, so

$$u^{(1)} = u^{(2)} = u, \quad v^{(1)} = v^{(2)} = v, \tag{17}$$

and

$$\frac{p_{1\mu}}{m_{01}} = \frac{p_{2\mu}}{m_{02}} = \frac{P_\mu}{m_0} = \frac{1}{\sqrt{1-v^2}}, \quad m_0 = m_{01} + m_{02}. \tag{18}$$

After multiplying equations (13), (14) by m_0/m_{01}, and equations (15), (16) by m_0/m_{02}, these systems become identical:

$$m_0 u + [(\vec{\sigma},\ \vec{P}) - \sigma_4 P_4]v = 0. \tag{19}$$

$$-[(\vec{\sigma},\ \vec{P}) + \sigma_4 P_4]u + m_0 v = 0, \tag{20}$$

where $P_4 = \imath E$ and $\sigma_4 = -\mathrm{i}1$.

Thus, the composition relations can be written in the following way:

$$[m_0 u + (\sigma_j P_j - \sigma_4 P_4)v] \otimes [m_0 u + (\sigma_k P_k - \sigma_4 P_4)v] = 0, \tag{21}$$

$$[-(\sigma_\mu P_\mu)u + m_0 v] \otimes [-(\sigma_\nu P_\nu)u + m_0 v] = 0. \tag{22}$$

Is well known that from two u matrices we can build the U matrix of 3×3 type, using the Clebsch—Gordan coefficients:

$$U_{\Lambda M} = \sum_{\substack{\lambda_1,\ \lambda_2 \\ m_1, m_2}} C^{1\Lambda}_{\frac{1}{2}\lambda_1 \frac{1}{2}\lambda_2} C^{1M}_{\frac{1}{2}m_1 \frac{1}{2}m_2} u_{\lambda_1 m_1} u_{\lambda_2 m_2}, \quad \Lambda = \overline{1,\ 3},\ M = \overline{1,\ 3} \tag{23}$$

Using (23) we may write

$$U = C_1(u \otimes u)\tilde{C}_1, \tag{24}$$

where

$$C_1 = \begin{pmatrix} 1 & 0 & 0 & 0 \\ 0 & \frac{1}{\sqrt{2}} & \frac{-1}{\sqrt{2}} & 0 \\ 0 & 0 & 0 & 1 \end{pmatrix} \tag{25}$$

The matrix elements of $C_1\,(3 \times 4)$ are given by,

$$(C_1)_{ab} = C^{1M}_{\frac{1}{2}\alpha\frac{1}{2}\beta}, \quad a = \overline{1,\ 3}, \quad b = \overline{1,\ 4} \tag{26}$$

with the connection between a, b and M, α given by

$$a = 2 - M, \qquad b = \frac{5}{2} - (M + \alpha). \tag{27}$$

In a quite similar way:

$$V = \mathrm{C}_1(v \otimes v)\tilde{\mathrm{C}}_1. \tag{28}$$

Using the rule:

$$(\mathrm{M}_1\mathrm{M}_2) \otimes (\mathrm{M}_3\mathrm{M}_4) = (\mathrm{M}_1 \otimes \mathrm{M}_3)(\mathrm{M}_2 \otimes \mathrm{M}_4) \tag{29}$$

valid for matrices $(\mathrm{M}_1, \mathrm{M}_2, \mathrm{M}_3, \mathrm{M}_4)$, and after we multiply (21) and (22) from the left with C_1, and from the right with $\tilde{\mathrm{C}}_1$, we obtain.

$$(-P_jP_kS_{jk} + P_jP_4S_{j4} + P_4P_jS_{4j} - P_4^2S_{44})V + m_0^2U = 0 \tag{30}$$

$$-P_\mu P_\nu S_{\mu\nu}U + m_0^2V = 0, \tag{31}$$

In these relations $S_{\mu\nu}$ are defined as:

$$S_{\mu\nu} = \mathrm{C}_1(\sigma_\mu \otimes \sigma_\nu)\tilde{\mathrm{C}}_1. \tag{32}$$

In passing from (21), (22) to (30), (31) one must take into account (19), (20) and the following properties

$$1 = \tilde{\mathrm{C}}_1\mathrm{C}_1 + \mathrm{T}_1, \qquad \mathrm{T}_1 = \frac{1}{2}\begin{pmatrix} 0 & 0 & 0 & 0 \\ 0 & 1 & -1 & 0 \\ 0 & -1 & 1 & 0 \\ 0 & 0 & 0 & 0 \end{pmatrix}, \tag{33}$$

$$\mathrm{T}_1(u \otimes u)\tilde{\mathrm{C}}_1 = 0, \qquad \mathrm{T}_1(v \otimes v)\tilde{\mathrm{C}}_1 = 0. \tag{34}$$

With the help of

$$e_1 = \begin{pmatrix} 1 \\ 0 \\ 0 \end{pmatrix}, \quad e_1 = \begin{pmatrix} 0 \\ 1 \\ 0 \end{pmatrix}, \quad e_1 = \begin{pmatrix} 0 \\ 0 \\ 1 \end{pmatrix} \tag{35}$$

we obtain

$$U_\Lambda = Ue_\Lambda, \quad V_\Lambda = Ve_\Lambda, \qquad \Lambda = \overline{1, 3}. \tag{36}$$

U and V is helpful for usoto form well determined helicity states for $s = 1$:

$$\Psi_\Lambda = \frac{1}{\sqrt{2}} \begin{pmatrix} U_\Lambda \\ V_\Lambda \end{pmatrix} e^{ipx}. \tag{37}$$

Considering now (30) and (31) we find that the quantities from (37) are solutions of the Joos-Weinberg equation for $s = 1$:

$$\left(\gamma_{\mu\nu} \frac{\partial^2}{\partial x_\mu \partial x_\nu} + m_0^2 \right) \Psi = 0, \tag{38}$$

where

$$\gamma_{44} = \begin{pmatrix} 0 & S_{44} \\ S_{44} & 0 \end{pmatrix}, \quad \gamma_{j4} = \gamma_{4j} = \begin{pmatrix} 0 & -S_{j4} \\ S_{j4} & 0 \end{pmatrix}, \quad \gamma_{jk} = \begin{pmatrix} 0 & S_{jk} \\ S_{jk} & 0 \end{pmatrix}. \tag{39}$$

3°. Let us consider now a particle with spin $s = 3/2$, composed of 3 Dirac particles. In the absence of internal angular momentum the possible states for these particle result by combining the states for $s = 1$ and $s = 1/2$.

Following the method from point 2° we can build the U and $V(4 \times \times 4)$ matrices:

$$\mathcal{U} = C_{3/2}(U \otimes u)\tilde{C}_{3/2}, \tag{40}$$

$$\mathcal{V} = C_{3/2}(V \otimes v)\tilde{C}_{3/2} \tag{41}$$

The $C_{3/2}(4 \times 6)$ matrix

$$C_{3/2} = \frac{1}{\sqrt{3}} \begin{pmatrix} \sqrt{3} & 0 & 0 & 0 & 0 & 0 \\ 0 & 1 & \sqrt{2} & 0 & 0 & 0 \\ 0 & 0 & 0 & \sqrt{2} & 1 & 0 \\ 0 & 0 & 0 & 0 & 0 & \sqrt{3} \end{pmatrix} \tag{42}$$

can be built using the Clebsch—Gordan coefficients

$$C^{\frac{3}{2}\,M}_{1\alpha\,\frac{1}{2}\,\beta} \tag{43}$$

For the matrix element

$$(C_{3/2})_{ab}, \quad a = \overline{1,4}, \quad b = \overline{1,6} \tag{44}$$

the connection between a, b, and M, α is given by.

$$a = \frac{5}{2} - M, \qquad b = \frac{7}{2} - (M + \alpha) \tag{45}$$

Combining Eqs. (30) and (6), respectively (31) and (7), by taking into account property (29) and the equalities

$$1 = \tilde{C}_{3/2} C_{3/2} + T_{3/2}, \tag{46}$$

$$T_{3/2}(U \otimes u)\tilde{C}_{3/2} = 0, \quad T_{3/2}(V \otimes v)\tilde{C}_{3/2} = 0, \tag{47}$$

where

$$T_{3/2} = \frac{1}{3}\begin{pmatrix} 0 & 0 & 0 & 0 & 0 & 0 \\ 0 & 2 & -\sqrt{2} & 0 & 0 & 0 \\ 0 & -\sqrt{2} & 1 & 0 & 0 & 0 \\ 0 & 0 & 0 & 1 & -\sqrt{2} & 0 \\ 0 & 0 & 0 & -\sqrt{2} & 2 & 0 \\ 0 & 0 & 0 & 0 & 0 & 0 \end{pmatrix} \tag{48}$$

we come to the conclusion that the wave functions

$$\Psi_\Lambda = \frac{1}{\sqrt{2}}\begin{pmatrix} u_\Lambda \\ v_\Lambda \end{pmatrix} e^{iPx}, \quad \mathcal{U}_\Lambda = \mathcal{U} e_\Lambda, \quad \mathcal{V}_\Lambda = \mathcal{V} e_\Lambda \tag{49}$$

are plane wave solutions with determined helicity for the Joos-Weinberg equation, valid for $s = 3/2$:

$$\left(\gamma_{\mu\nu\rho}\frac{\partial^3}{\partial x_\mu \partial x_\nu \partial x_\rho} + m_0^3\right)\Psi = 0. \tag{50}$$

Matrices e_Λ are given by

$$e_{3/2} = \begin{pmatrix} 1 \\ 0 \\ 0 \\ 0 \end{pmatrix}, \quad e_{1/2} = \begin{pmatrix} 0 \\ 1 \\ 0 \\ 0 \end{pmatrix}, \quad e_{-1/2} = \begin{pmatrix} 0 \\ 0 \\ 1 \\ 0 \end{pmatrix}, \quad e_{-3/2} = \begin{pmatrix} 0 \\ 0 \\ 0 \\ 1 \end{pmatrix} \tag{51}$$

The matrices

$$\gamma_{444} = \begin{pmatrix} 0 & -iS_{444} \\ -iS_{444} & 0 \end{pmatrix}, \quad \gamma_{j44} = \begin{pmatrix} 0 & iS_{j44} \\ -iS_{j44} & 0 \end{pmatrix} \tag{52}$$

$$\gamma_{jk4} = \begin{pmatrix} 0 & -iS_{jk4} \\ -iS_{jk4} & 0 \end{pmatrix}, \quad \gamma_{jkl} = \begin{pmatrix} 0 & iS_{jkl} \\ -iS_{jkl} & 0 \end{pmatrix} \tag{53}$$

contain matrices $S_{\mu\nu\rho}$ defined by:

$$S_{\mu\nu\rho} = \frac{1}{3} C_{3/2} [(S_{\mu\nu} \otimes \sigma_\rho) + (S_{\nu\rho} \otimes \sigma_\mu) + (S_{\rho\mu} \otimes \sigma_\nu)]. \tag{54}$$

4°. If one performs the calculus based on the general results established, one can obtain results already found in other ways. At the same time some conclusions can be drawn on the applicability field of the Joos-Weinberg equations. These equations describe the kinetics of the centre of inertia of a higher spin particle, which has no internal orbital angular momentum, and are composed of Dirac particles. As an example we give the deuteron ($s = 1$) and the Δ resonance ($s = 3/2$).

REFERENCES

1. M. Jacob, *Annals of Phys.*, **7**, (1959), 404.
2. H. Joos, *Fortschritte der Physik*, **10**, (1962), 65
3. H. Stapp, *Phys. Rev*, **125**, (1962), 2139
4. A. O. Barut, I. Muzinich, D N. Williams, *Phys. Rev.*, **130 (1963)**, 442.
5. A J. Macfarlane, *Revs Mod. Phys*, **34** (1962), 41; *Journ. Math. Phys.*, **4** (1963), 490
6. D Zwanziger, *Phys Rev*, **133** B, (1964), 1036.
7. S Weinberg, *Phys. Rev.*, **133** B, (1964), 1318
8. A. McKerrell, *Nuovo Cimento*, **34** (1964), 1289
9. Wu-Ki Tung, *Phys. Rev.*, **156** (1967), 1383
10. Z Gábos, *Acta Physica Polonica*, **34** (1968), 231

STUDIA UNIV BABEŞ—BOLYAI, PHYSICA, XXXII, 1, 1987

MAGNETIC RESONANCE ON BORATE GLASSES WITH HIGH COPPER OXIDE CONTENT

S. SIMON*, V. SIMON* and AL. NICULA*

Received February 10, 1987

ABSTRACT. — Soda borate glasses with high CuO content are studied by means of nuclear magnetic resonance (NMR) and of electron paramagnetic resonance (EPR) It was followed and compared the effect of the CuO content on the shape and parameters of the spectra obtained by using the two magnetic resonance methods It was concluded on the structural effect of this oxide and on the distribution of the Cu^{2+} ions in the vitreous soda borate matrix

1 **Introduction.** The glasses with high content of transition metal oxides represente one of the class of vitreous materials of spécial scientific and practical interest due to their magnetic and electric properties confered by the presence of the paramagnetic ions in high concentrations. The magnetic and electric properties of the glasses with high V_2O_5 [1—4], Fe_2O_3 [5—7] and CuO content [8, 9] were studied in several papers, but the investigation of the structural effects of these oxides on the local order existing in the vitreous matrices are unsignificant The mentioned studies generally treated the properties of the glasses with high content of transition metal oxides starting from the identification of the microenvironment structure of the paramagnetic ions and from the identification of the type and intensity of the interactions between them, without following the manner in which these oxides modify the shape and share of the different structural units existing in the matrices in their absence.

The high limit for the concentration of the transition metal oxides in vitreous matrices depends on the nature of the matrices, on the type of the transition metal and on the preparation conditions The parameters characterizing the preparation process of the samples are also very important, and first the cooling rate of the melts It is possible, at large cooling rates, to obtain vitreous samples with extremely high content of transition metal oxides, practically without clasical glass formers (B_2O_3, SiO_2, P_2O_5) [10—13].

2 **Experimental.** In order to evidence by NMR the structural effects of the transition metal oxides on the local order from glasses we prepared soda borate vitreous samples with a CuO content ranging from 0 to 25% mol, where R is the ratio between the soda oxide and boric oxide contents

The samples were prepared by the melting of the oxide mixtures corresponding to the desired composition, at 1000°C, with a maintaining time at this temperature of 30 minutes followed by the undercooling of the melts at the room temperature The magnetic resonance spectra were recorded on powder samples, at the room temperature, on JEOL NMR and EPR spectrometers

3. **Results and discussion. NMR.** The nuclear magnetic resonance studies on soda borate glasses with high content of transition metal oxides

* *University of Cluj-Napoca, Faculty of Mathematics and Physics, 3400 Cluj-Napoca, Romania*

allowed us to evidence for the first time [14—17] the structural effects of these oxides on the type and fraction of structural units existing in the borate glasses. In this way one remarked significant differences between the effects induced by the different oxides. Thus, wile TiO_2 and MoO_3 do not determine changes in the structural units fraction, up to 35 mol%, the increase of the concentration of the other transition metal oxides leads to evident changes of the ratio between the intensities of the narrow and wide line from the ^{11}B NMR spectra, reflecting changes in the number of the boron nuclei disposed in sites without electric field gradient. Similar structural effects were also observed by other authors [18] which studies glasses from $x\%B_2O_3 \cdot y\%PbO$ system with high Fe_2O_3 content.

In order to appreciate how much from these changes are effectively caused by the structural modifications it is first necessary to estimate the effect determined by the increase of the paramagnetic centers number in the vitreous matrices on the ^{11}B NMR lineshape. The presence of the paramagnetic ions in the vitreous matrices modifies the local fields where the ^{11}B nuclei are disposed so that the resonance lines appear broadened in comparison with the lines observed in the ^{11}B NMR spectra from samples without paramagnetic ions

The main mechanism of the line broadening in the absence of paramagnetic ions is the dipole interaction between like nuclear spins In this case the line broadening, estimated from the increase of peak-to-peak width in the derivative curve, may be written [19].

$$\Delta B_{pp}^{I} = \text{cosnt.} \left[3/5I(I+1) \sum_{k} r_{jk}^{-6} \right]^{1/2} \tag{1}$$

where ΔB_{pp}^{I} is the peak-to-peak field, r_{jk} is the distance between the nuclei j and k, and the sum is made on all the sites occupied by ^{11}B nuclei.

The dipolar broadening due to the interaction between like nuclear spins has a gaussian shape. It depends on the spatial distribution of the ^{11}B nuclei and does not depend on the applied magnetic field.

The presence of paramagnetic ions in samples produces an additional line broadening, due to the dipole interaction between the magnetic moments of ^{11}B nuclei and of paramagnetic ions. This broadening has a lorentzian shape [20] and depends on the applied magnetic field, so that in the high temperature approximation it may be written

$$\Delta B_{pp}^{\mu_p} = K \cdot B \tag{2}$$

where B is the applied magnetic field, the constant K depends on temperature, on effective magnetic moment of paramagnetic ion μ_p and on the spatial arrangement of these ions. The relationship (2) is valid only when between the paramagnetic ions there is no exchange interaction

In addition to this lorentzian broadening shape the presence of paramagnetic ions also determines a gaussian broadening shape, due to the large distribution of the values corresponding to the local magnetic field

at the sites where the ^{11}B nuclei are located. This line broadening is also proportional to the applied magnetic field [21].

$$\Delta B'_{pp} = K' \cdot B \tag{3}$$

where the constant K' is proportional to the volume magnetic susceptibility of the sample. Therefore, in the case of ^{11}B NMR spectra from samples containing paramagnetic ions we have two types of line broadening, a lorentzian and a gaussian broadening shape, so that the resonance line will be a line of Voight type [22] obtained by the convolution of gaussian and lorentzian broadening shapes.

A possibility to estimate the two contributions of the paramagnetic ions to the line broadening of the narrow line from the ^{11}B NMR spectra is to determine the ratio between the narrow line width $\Delta B''_{pp}$ and the distance between the peaks of the large line $\Delta B'_{pp}$, corresponding to boron nuclei disposed in sites with electric field gradient. This distance modifies unsignificantly with the concentration of transition metal oxides. The deviation of the value calculated by dividing the areas corresponding to the two lines from the real value of the fraction of boron atoms disposed in sites without electric field gradient at nucleus increases continously with the ratio $\Delta B''_{pp}/\Delta B'_{pp}$. Making for every sample the necessary correction after the estimation tof he ratio $\Delta B''_{pp}/\Delta B'_{pp}$ we obtained the results presented in Figure 1. One remarks that in the first part of the composition range the copper oxide determines a pronounced increase of the fraction of boron atoms dispoded in sites with high symmetry, while at higher concentrations it determines a decrease of this fraction. It may be appreciated that up to concentrations of 15 mol%, for the samples with $R = 0.2$, and up to 5 mol%, for the samples with $R = 0.5$, the cooper oxide has the role of the alkali oxide and favours the increase of the number of network formers disposed in sites without electric field gradient (N_{WEFG}). Above the mentioned concentrations the copper oxide produces the distorsion of a large number of microenvironments of the boron atoms.

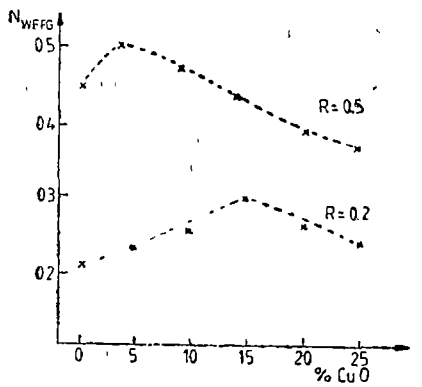

Fig. 1. The dependence of the fraction of the boron atoms disposed in sites without electric field gradient on the copper oxide content in soda borate glasses

EPR. The increase of the density of paramagnetic centers with the increase of concentration of trasnition metal or rare earth oxides determines important changes in the shape of the EPR spectra. For relatively low contents of transition metal oxides, the increase of the density of paramagnetic centers leads to a line broadening due to the augmentation of dipole interaction between these centers. If the concentration increases further, the distance between the paramagnetic ions

decreases down to the limit for wihch between them the exchange interaction appears. This has as effect the narrowing of the resonance lines. The concentration limits above which the exchange interaction occurs depend on several parameters characterizing the preparation process of the vitreous samples and first on the homogenity of the samples regarding the distribution of the paramagnetic ions. If in a vitreous matrix the paramagnetic ions are not uniformly distributed, then the exchange interaction will already manifests at low concentrations of the transition metal oxides

The diminution of the intensity of the EPR signals above certain value of the concentration of transition metal oxides is a consequence of the fact that the valency state of these ions modifies, or, in the most cases this is a consequence of the fact that the paramagnetic ions form antiferromagnetically coupled pairs.

The study of the magnetic properties of some oxide glasses with high copper oxide content [8] also confirmed the occurence of the antiparallelly coupled Cu^{2+} ion pairs For every type of matrix there is a high limit of the paramagnetic center density, for which it can still be obtained vitreous samples By means of electron paramagnetic resonance it was followed the manner in which the maximum density of paramagnetic centers depends on the composition of the vitreous samples in the range from $R = 0$ to $R = 0\,5$, with a step of 0 05 The EPR signals modify with the increase of the copper concentration. In the case of the samples with less than 1 mol%, CuO the hyperfine structure in the parallel band is well resolved [23]. For higher CuO concentrations the signals are large, asymmetrical having $g_{\parallel} = 2\,3$ and $g_{\perp} = 2\,0$ The asymmetry of this large signal decreases with the CuO concentration, while its width becomes maximum for the samples in which the density of the paramagnetic centers is maximum.

In order to estimate the density of the paramagnetic centers we determined the shape of the large line, considering that this line is a convolution of Lorentzian and Gaussian shapes [22, 24]·

$$f(B, \xi) = \xi \cdot f_L(B) + (1 - \xi) f_G(B) \tag{4}$$

The share of the lorentzian shape is given by the parameter $\xi (0 \leqslant \xi \leqslant 1)$ and increases with the copper oxide content The EPR signals obtained for the samples with intermediate concentrations of CuO may be considered as the result of the superposition of asymmetrical lines with hyperfine structure partially resolved, arising from isolated Cu^{2+} ions, octahedrically coordinated with oxygen ions, the octahedron being tetragonally distorted (D_{4h}) and of large asymmetrical lines with the hyperfine structure unresolved, arising from Cu^{2+} ions coupled in pairs The strength of the couplage depends on the distance between them and increases with the density of the Cu^{2+} ions, hence with the CuO concentration.

As may be observed from Figure 2, the intensity of the Cu^{2+} EPR signal depends substantialy on the alkali oxide content from the vitreous matrix In this way the signal intensity is maximum for the sample with $0\,05 \leqslant R \leqslant 0\,15$ and minimum for those with $0.25 \leqslant R \leqslant 0.4$ The most

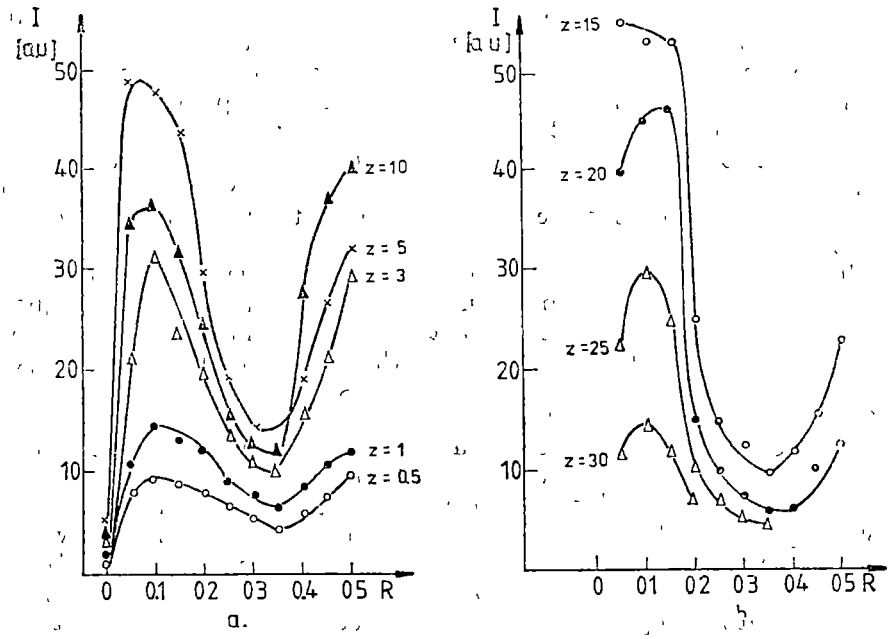

Fig. 2. The composition dependence of the intensity of Cu^{2+} EPR signal from soda borate glasses containing copper oxide.

a) 0.5 mol% $\leqslant z \leqslant$ 10 mol% CuO

b) 15 mol% $\leqslant z \leqslant$ 30 mol% CuO

pronounced effect occurs for the samples with the CuO concentration comprised between 5 mol% and 20 mol%.

The diminution of the EPR signal intensity for the samples with $0.25 \leqslant R \leqslant 0.4$ is a consequence of the fact that the copper oxide tends to occupy preponderently the sites from the microphase rich in soda oxide. This leads to the existence of an effective density of Cu^{2+} ions more larger in this microphase and thus there will here occur more pairs of Cu^{2+} ions in comparison with isolated Cu^{2+} ions.

A similar conclusion was also obtained from the EPR study of some soda borate glasses [25] ($0.1 \leqslant R \leqslant 0.5$) with high nickel oxide content ($\leqslant$15 mol% NiO).

The spectacular increase of the density of isolated Cu^{2+} ions in the samples with low alkali oxide content ($R = 0.05$) in comparison with the samples without alkali oxide represents a consequence of the structural changes induced by the addition of the alkali oxide. These changes are more pronounced than those evidenced by nuclear magnetic resonance which consists in the breaking of the network specific to the vitreous boric oxide, without affecting pronouncedly the microenvironment of the boron atoms.

The maximum values of the paramagnetic center density depends

on the nature of the vitreous matrix and are obtained for different concentration of copper oxide. Thus, for the samples with $0.05 \leqslant R \leqslant 0.15$ (Fig. 3a) the highest intensity for the Cu^{2+} EPR signals is obtained for the concentration of 15 mol% CuO. In this concentration range the effect of the alkali oxide is unsignificant. For the samples with $0.2 \leqslant R \leqslant 0.3$ (Fig. 3b) this maximum is less pronounced and it occurs between 5 mol% and 15mol% CuO, while for the samples with $R \geqslant 0.35$ it occurs at the concentration of 5 mol% CuO (fig. 3 c)

The position of these maxima indicates that in the case of the investigated samples the highest concentration of copper oxide for which one obtaines still vitreous samples with paramagnetic properties decreases with R. For higher concentrations of CuO the phenomenon of clustering occurs. On the other hand one observes that the values of the CuO concentrations at which the intensity of the EPR signals decreases are the same with the concentrations from which the structural effect of the copper oxide evidenced by NMR (Fig. 1) changes its sign. One may state that up to these values of the CuO concentration between the matrix and the paramagnetic ion the effect of the matrix on the Cu^{2+} ions is prevalent and at higher concentrations the effect of the copper oxide on the vitreous matrix is prevalent.

4. Conclusions. The magnetic resonance studies carried out on soda borate glasses with high copper oxide content permitted to evidence the structural effect of the copper oxide on the vitreous samples. At small concentrations

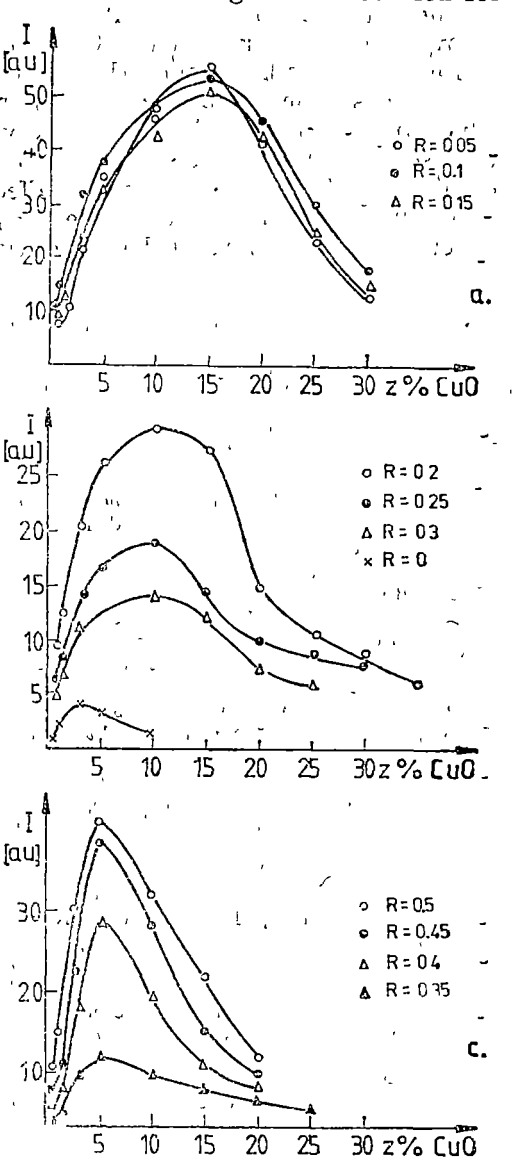

Fig 3 The dependence of the intensity of Cu^{2+} EPR signal from soda borate glasses on the copper oxide content.
a) $0.05 \leqslant R \leqslant 0.015$; b) $R = 0$ and $0.2 \leqslant R \leqslant 0.3$, c) $0.35 \leqslant R \leqslant 0.5$.

of CuO as the Cu^{2+} ions are uniformly distributed in the matrix, the boron atoms are disposed in sites without electric field gradient. The uniform distribution of the Cu^{2+} ions is confirmed by the increase of the intensity of the EPR signal attributed to Cu^{2+} isolated ions. Above certain values of the CuO concentrations, which depend on the content of the alkali oxide, the homogeneus distribution is destroyed and in this case the occurence of clusters formed by Cu^{2+} ions is favoured which perturb the local order in the vitreous matrix. The copper ions are disposed in similar sites with hose occupied by the vitreous network modifiers. The whole structural effects of the copper oxide are similar with those of the nickel oxide [25] and differ pronouncedly from the effects observed for the other transition metal oxides [16].

REFERENCES

1. E. J. Friebele, L. K. Wilson, D. L Kinser, *J. Am Ceram Soc*, 55, 164 (1972)
2. Al Nicula, E. Culea, L. Stănescu, *Studia, Physica*, **23**, 1, 55 (1978)
3. E. Culea, Al Nicula, C Sîrbu, M. Culea, *Mat Chem Phys*, 13, 517 (1985)
4. Al. Nicula, E Culea, *Solid State Comun.*, **50**, 1, 929 (1984)
5. E J. Friebele, L K. Wilson, D L Kinser, *Physica Status Solidi* (b), **45**, 323 (1971)
6. I Ardelean, E Burzo, I Pop, *Solid State Comun*, **23**, 211 (1977)
7. E Burzo, I. Ursu, I Ardelean, *J Mater Sci*, **15**, 581 (1980)
8. A R. Lusis, J G Kliava, „Fiz Chem Steklo Sist," Riga, 1974, p 68
9. I. Ardelean, O Cozar, Gh Ilonca, *Rev Roum Phys*, **28**, 451 (1983)
10. A M Glass, N. E Lines, K Nassau, J W Shiever, *Appl Phys Lett*, **31**, 249 (1977)
11. T. Nakamura, M. Takashige, T Mitsui, *Ferroelectrics*, **37**, 582 (1981)
12. S Simon, Al Nicula, *Rev. Roum Phys*, **28**, 1, 57 (1983)
13. Al. Nicula, S Simon, *Glastechn Ber*, **56K**, 2, 904 (1983)
14. S Simon, V. Simon, Al. Nicula, *Studia, Physica*, **24**, 1, 77 (1979)
15. S Simon, Al. Nicula, *Studia, Physica*, **25**, 1, 63 (1980)
16. S Simon, V Simon, Al Nicula, *Studia, Physica*, **26**, 1, 11 (1981)
17. S Simon, V Simon, Al. Nicula, *Mat de Constr*, **12**, 3, 159 (1982)
18. P J Bray, F. Bucholtz, A E Geissberger, J A Harris, *Nucl Instr and Methods*, **199**, 1 (1982)
19. A Abragam, „The Principles of Nuclear Magnetism," Oxford Univ Press, London, 1961
20. D Freude, H Schmiedel, *Phys Status Solidi* (b), **54**, 631 (1972)
21. R E Behringer, *J Phys, Chem Solids*, **2**, 209 (1957)
22. C Poole, „Electron Spin Resonance", Publ Joler Weley, 1967
23. S Simon, Al Nicula, *Studia, Physica*, **25**, 2, 39 (1980)
24. C B Azzoni, G L Del Nero, A Krajewski, A Ravaglioli, *Litt Nuovo Cimento*, **26**, 2, 55 (1979)
25. S Simon, Al Nicula, *Studia, Physica*, **27**, 50 (1982)

STUDIA UNIV BABEŞ—BOLYAI, PHYSICA, XXXII, 1, 1987

DISPOZITIV DE MĂSURARE A FAZEI IN AMPLIFICATORUL — DETECTOR SINCRON

V. IONCU*, S. SIMON*, V. SIMON*, E. TĂTARU* şi I. ARDELEAN*

Intrat în redacţie la 12 februarie 1987

ABSTRACT. — Device for the Measurement of Phase Relation in the Sinchron Amplifier-Detector. It is presented a device for the measurement of the phase relation (advance or delay) between the reference signal and the signal which carries the information, processed in synchron amplifiers-detectors

In studierea fenomenului de rezonanţă zgomotele limitează precizia măsurării şi chiar posibilitatea detectării fenomenului. Problema extragerii semnalului purtător de informaţie, semnal înecat în zgomot, este de mare importanţă. Pentru soluţionarea problemelor ridicate de extragerea informaţiei dintr-un semnal înecat în zgomot au fost utilizate diverse metode [1—5] de la măsurători de precizie de laborator pînă la experimente de rutină.

Unul dintre cele mai utilizate aparate pentru extragerea unui semnal înecat în zgomot, exceptînd prelucrarea datelor pe calculator şi care funcţionează după principiul intercorelaţiei este amplificatorul cu eşantionare sau amplificatorul-detector sincron. Un astfel de aparat utilizează două căi de semnal care prelucrează (intercorelează) semnalul de referinţă şi pe cel purtător de informaţie, rezultînd la ieşire un semnal lent variabil care reprezintă informaţia căutată.

Pentru realizarea procesului de intercorelare a celor două semnale este important a se cunoaşte relaţia reală de fază a celor două semnale. În scopul realizării acestui deziderat şi al eliminării unor aparate auxiliare (osciloscoape, voltmetre electronice, etc) am completat amplificatorul-detector sincron, realizat de noi, cu un bloc care permite cunoaşterea permanentă a relaţiei reale de fază

Montajul descris în continuare face posibilă măsurarea relaţiei de fază (avans sau întîrziere) a celor două semnale prelucrate în amplificatorul-detector sincron Instrumentul de la ieşire este etalonat în grade ($0 - \pm 180°$).

Schema circuitului este prezentată în Figura 1 şi cuprinde două tranzistoare MOSFET (T_1 şi T_2) conectate ca repetoare pe sursă, două comparatoare cu histereză (A_1 şi A_4), două circuite de temporizare A_2 şi A_5 şi un integrator de ieşire A_3. Pentru o mai exactă apreciere a principiului de funcţionare a acestui dispozitiv asociem Figurii 1 diagrama evoluţiilor în timp ale tensiunilor în punctele de interes ale schemei (Fig. 2).

Rolul tranzistoarelor MOSFET (T_1 şi T_2) este de a asigura o impedanţă de intrare mare la intrările acestui dispozitiv, respectiv de suprimare a

* *Universitatea din Cluj-Napoca, Facultatea de matematică şi Fizică, 3400 Cluj-Napoca, Romania*

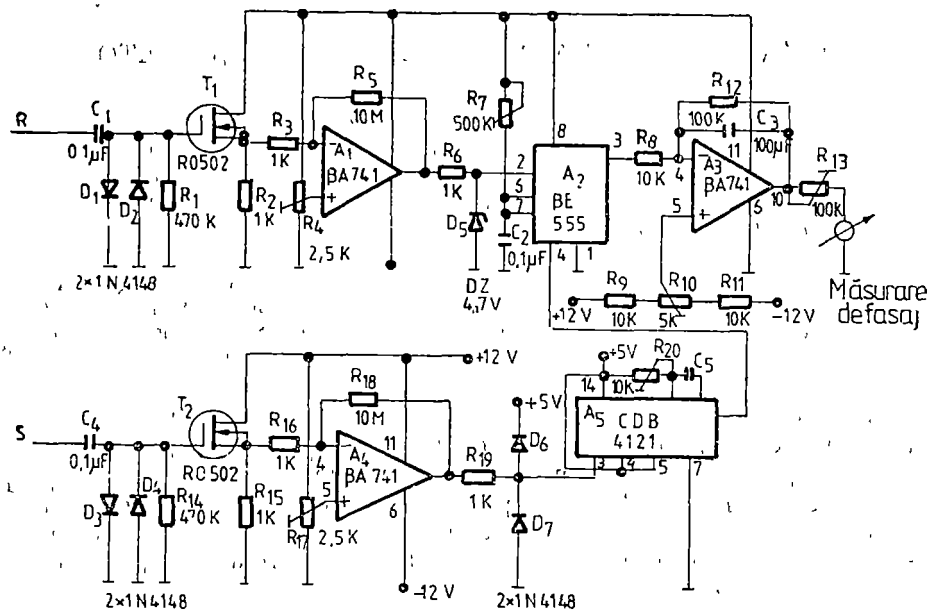

Fig 1 Schemade principiu a dispozitivului de măsurare a fazei în amplificatorul-detector sincron

influențelor posibile rezultate din conectarea acestuia asupra caracteristicilor semnalului purtător de informație (S) și de referință (R) analizate în amplificatorul-detector sincron. Pentru protecția acestor tranzistoare a fost prevăzut grupul diodelor D_1—D_4.

Cele două comparatoare (A_1 și A_4) sînt soluționate în mod clasic, la ieșirile lor obținîndu-se semnale dreptunghiulare cu fronturi abrupte. Acestea permit o ajustare inițială a histerezei, impusă de regimul static de funcționare a celor două tranzistoare MOSFET. Limitele de evoluție impuse impulsurilor dreptunghiulare de la ieșire se selectează cu ajutorul diodelor D_5, D_6 și D_7 fiind determinate de tipul circuitelor integrate utilizate pentru realizarea celor două circuite basculante monostabile: βF 555 pentru A_2 și CDB 4121 pentru A_7. Aceste circuite formează detectorul de fază propriu-zis.

Impulsurile dreptunghiulare pe canalul semnalului de referință, avînd limitele de evoluție +5,6 V respectiv —0,7 V, servesc la declansarea circuitului βE 555, conectat într-o variantă de circuit basculant monostabil. Așa cum se poate urmări pe figura 2, la trecerea semnalului de referință în domeniul valorilor pozitive este comutat comparatorul A_1 (—0,7 V la terminalul 2 al circuitului basculant monostabil A_2). Această valoare a tensiunii se situează sub valoarea de prag ($1/3\ U_{alimentare}$) necesară declanșării prin terminalul 2. Tensiunea de la ieșirea circuitului basculant monostabil (terminal 3) este acum aproape egală cu tensiunea de alimentare și în principiul ar trebui să se mențină la această valoare pînă ce

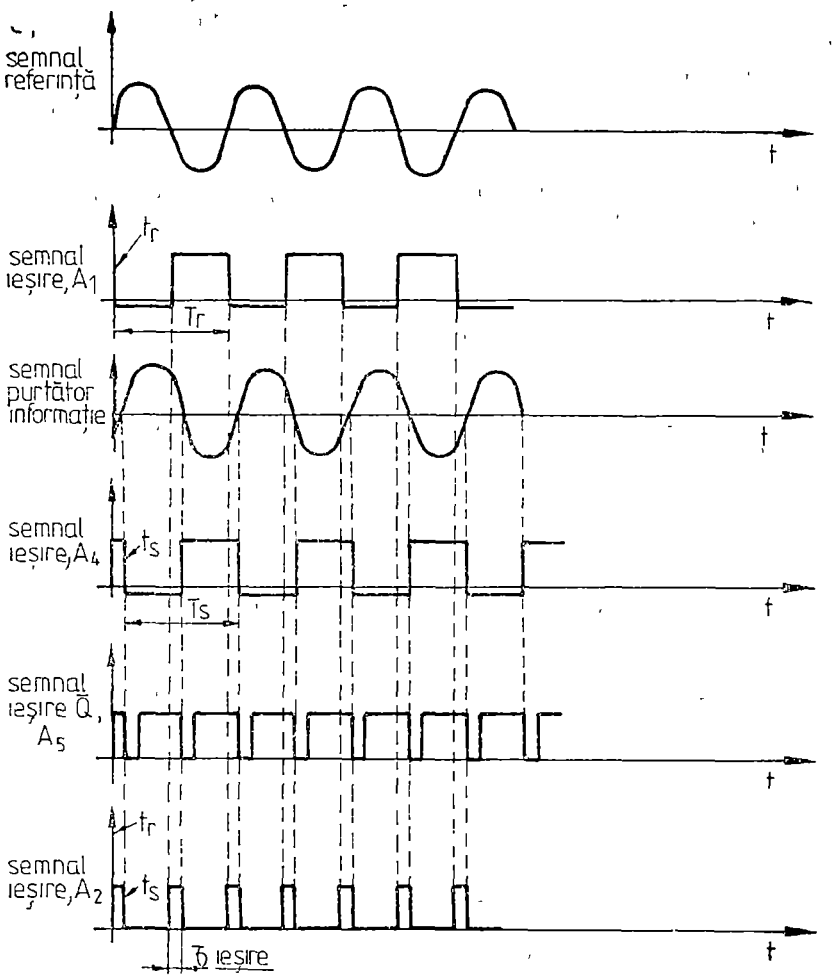

Fig 2 Diagrama evoluțiilor tensiunilor în punctele de interes ale dispozitivului

tensiunea de pe condensatorul de încărcare (C_2) atinge cel de-al doilea nivel de prag (2/3 $U_{alimentare}$) pentru readucerea monostabilului în starea inițială. Durata temporizării poate fi determinată cu ajutorul relației $\tau_v = 1{,}1\ R_7C_2$ și se reglează astfel încît să fie întotdeauna mai mare decît perioada T_r a semnalului de referință.

Varianta de canal pentru semnalul purtător de informație are aceleași principii constructive, deosebirile apar la selectarea componentelor de realizare practică S-a utilizat circuitul integrat CDB 4121 în calitate de circuit basculant monostabil (A_6), acesta oferind avantajul celor două ieșiri negate ($\bar{Q}$ și $\bar{\bar{Q}}$) necesare pentru acționarea aducerii la zero a lui A_2.

Ieşirea circuitului A_2 nu rămîne în stare H pe întreaga durată a procesului de temporizare τ_v deoarece va fi comutat din nou în starea iniţială de nivelul logic al impulsului de la ieşirea lui A_{15} (front negativ) care acţionează asupra terminalului 4 prevăzut pentru aducerea forţată la zero (nivel logic zero la ieşirea lui A_2).

Cel de-al doilea circuit basculant monostabil este declanşat de impulsurile dreptunghiulare (tot pe front negativ) de la ieşirea comparatorului A_4, deci de semnalul purtător de informaţie.

Momentele de declanşare ale celor două circuite basculante monostabile sînt notate t_r şi t_s în Figura 2. Durata reală a impulsului de la ieşirea monostabilului A_2 este, din acest motiv, direct proporţională cu intervalul de timp definit de momentele trecerilor prin zero ale celor două semnale (de referinţă şi purtător de informaţie: $\tau_{ieşire} = t_s - t_r$) şi nu depinde de constantele de timp ale circuitelor basculante monostabile. Evoluţia în timp a semnalului de ieşire este caracterizată cu ajutorul perioadelor, de aceea se defineşte exact diferenţa de fază a semnalului R faţă de S:

$$\Phi = 360 \frac{\tau_{ieşire}}{T_r} = 360 \frac{t_s - t_r}{T}$$

Modul de apreciere al acestei relaţii presupune o prelucrare analogică într-un circuit de integrare (A_3). Pentru un proces de retardare al lui S în raport cu R, tensiunea de la ieşirea integratorului creşte. Tensiunea de la ieşirea integratorului va scădea pentru variantă de retardare inversată. Tensiunea de ieşire are aceeaşi valoare pentru un unghi de fază $\Phi = 180°$ între cele două semnale, deci în mijlocul domeniului, acesta fiind unicul caz în care sensul deplasării nu influenţează tensiunea de ieşire.

Cu ajutorul potenţiometrului P_4 se reglează mărimea tensiunii de ieşire (curentul prin instrument) pentru o deviaţie maximă, funcţie de domeniul frecvenţei de lucru.

Dispozitivul realizat prezintă calitatea importantă de a permite identificarea relaţiei reale de fază a semnalelor din cele două canale urmărind caracterul evoluţiei semnalului de la ieşirea integratorului şi elimină totodată utilizarea unor aparate auxiliare (osciloscoape, voltmetre electronice, etc.) cărora le rămîn tributare alte variante de amplificatoare-detectoare sincron.

BIBLIOGRAFIE

1 Wainstein, L A, Zubakov V. D, „Extraction of signals from noise", Prentince-Hall, Inc Englewood Cliffs, New Jersey, 1962
2. Chaykowsky O C, Moore R D, Signal-to-noise considerations in experimental research, „Princeton Applied Research, Technical Notes T — 196", Thompson Publ Inc, 1968
3 Spătaru Al, „Teoria Transmisiei informaţiei", Ed tehnică, Bucureşti, 1971
4. Widrow B, şa, „Adoptive noise concelling", *Proc of the IEEE*, Vol 63, N 12, p. 1692—1716, 1975
5. Rădoi C, Metode de corelaţie utilizate în măsurători industriale *Teză de doctorat I P B*, Bucureşti, 1980

STUDIA UNIV BABEŞ—BOLYAI, PHYSICA, XXXII, 1, 1967

PHOTOTHERMAL METHODS FOR THE STUDY OF THE SOLIDS

D. DĂDÂRLAT* AND EUGENIA DĂDÂRLAT*

Received January 30, 1987

ABSTRACT. — Two photothermal methods are proposed for investigating the properties of solids Using a direct pyroelectric detection method, we investigated the optical absorption of some non-transparent anodized Al samples, in the 1—14 μm range It is found that the anodized Al has a selective optical absorption. A photothermal deflection method was proposed in order to investigate some electrical properties of PbSe thinfilms. A spatial conductivity profile was drawn and the ohmic behaviour of the electrical contacts (Au and Ag) was tested.

I. **Introduction.** The so called „photothermal effects" are caused by the heating of a sample after the absorbtion of optical enegry. If the quantity of the heat from the sample can be measured, then one obtaines informations about the optical absorbtion [1] the thermal diffusivity and conductivity [2, 3], or about other properties (electrical properties [4, 5], phase transitions [6]) of the sample. It is possible to detect the heating of a sample by measuring the temperature rise of the sample, the thermal refractive-index gradients produced by the heat, the surface deformations, or the increase of the total radiant energy of the sample. The methods which use these phenomena caused by the heat, in order to investigate physical properties of a sample, are called photothermal methods or techniques and they are the following [7]: the optical calorimetry, the thermal lens spectroscopy, the photothermal displacement spectroscopy and the photothermal radiometry.

In this paper we report on two photothermal methods used in our laboratory in order to investigate the optical and electrical properties of the solids. In section 2 we present how photopyroelectric spectroscopy can be used in investigating the optical absorption of the non transparent materials In section 3 some photothermal deflection measurements on thin-film semiconductors are presented. Section 4 is devoted to some concluding remarks

II. **The Photopyroelectric Detection of Optical Absorption in Non-transparent Materials.** The pyroelectric effect consists in the induction of spontaneous polarization in a noncentrosymmetric crystal, as a result of a temperature change in the crystal The charge accumulated in the pyroelectric, due to a change ΔT in the temperature, is given by

$$Q = p \cdot \Delta T \qquad (1)$$

* *Institute of Isotopic and Molecular Technology, 3400 Cluj-Napoca 5, P O BOX 700, Romania*

The average pyroelectric voltage due to this charge has the following form

$$V(\omega_0) = \frac{pL\theta(\omega_0)}{K\varepsilon_0} exp\ (i\omega_0 t) \tag{2}$$

where p is the pyroelectric coefficient, L and K are the thickness and the dielectric constant of the detector, ω_0 is the modulation frequency of the radiation, and $\theta(\omega_0)$ is given by [7]

$$\theta(\omega_0) = \frac{1}{L}\int_L T(\omega_0, x)dx \tag{3}$$

For a one-dimensional geometry of a photopyroelectric system composed by a pyroelectric in good thermal contact, with a solid sample the function $T(\omega_0, x)$ is a solution of coupled, one dimensional thermal transport equations Using (3) in (2) one can obtain the pyroelectric signal as a function of some sample-related parameters. Mandelis and Zver [7] have found the general expression for $V(\omega_0)$, but the result is too complex for practical interest. Fortunately, the general result can be much simplified in some special cases, according to the relative magnitudes of three characteristic lengths in the sample and the pyroelectric, namely, the thickness, the optical absorption depth and the thermal diffusion length.

In an experimental situation, when the pyroelectric sensor is a 250 μm thick TGS, the samples are 50 μm thick anodised Al plates and the modulation frequency of the radiation is 7 Hz, the pyroelectric voltage is directly proportional to the optical absorption coefficient of the sample.

Using the experimental set-up presented in Fig. 1, we investigated the optical absorption of some Al samples anodized in H_2SO_4 and $H_2C_2O_4$ [1], in the 1—14 μm range.

The results are presented in Fig 2 together with the theoretical black-body radiation curve normalized at its maximum value.

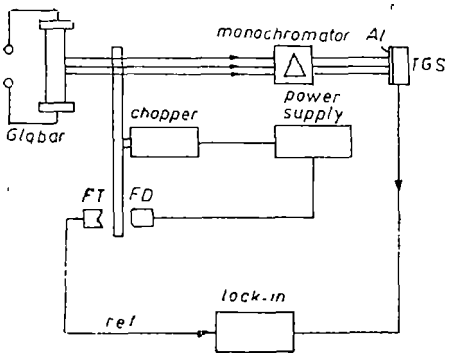

Fig 1 The experimental set-up used for photopyreolectric measurements

As one can see from fig 2 the anodized Al has a selective optical absorption strong absorption bands at 2.5—4 and 6—12 μm for Al anodized in H_2SO_4 and at 2.5—4, 5—8 and 9—13 μm for Al anodized in $H_2C_2O_4$

III. **Photothermal Deflection Measurements on Thin-Film Semiconductors.** In a photothermal deflection detection experiment, to compute the thermal energy of a heated region by processing a detector signal means to correlate the temperature distribution of the investigated region

with the optical beam propagation through this nonhomogeneous medium and with the detector response [8] In recent years, new techniques, based on photothermal deflection, were developed in order to investigate surface or intrinsic properties of thin-film semiconductors. In this paper we present a method used in our laboratory in investigating the Joule and Peltier heat, generated by electric currents through thin-film semiconductors The physics! of the method consists of the following [4, 5]. When the heat generated in a thin-film semiconductor by an applied oscillating voltage $U = U_0 \cos(\omega t)$ is probed by a laser beam skimming the surface of the sample, perpendicular to the current direction, a detector able to measure the deflection of the laser beam will detect two oscillating signals: one signal oscillating at twice the applied voltage frequency, with amplitude $\sim U_0^2/2R$ (R sample usitance) which is a measure of the Joule heat, and another signal oscillating at the same frequency as U, with the amplitude $\sim \Pi\, U_0/R$ (Π Peltier coefficient) which is a measure of the Peltier heat. This method can be used in obtaining information about the uniformity of the electrical conductivity, the type of the majority carriers, and the ohmic behaviour of the electrical contacts.

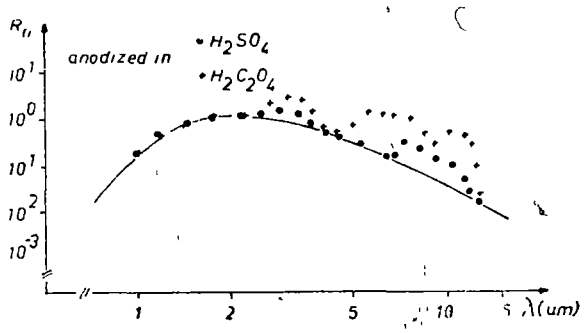

Fig 2 Normalised spectral responsivity of the detector anodized Al System in the 1 — 14 μm range

Using the experimental set-up presented in Fig 3, we performed conductivity measurements on PbSe films

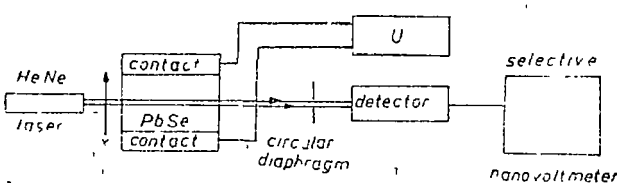

Fig 3 The experimental set-up used for the photothermal deflection measurements

The results are presented in Fig. 4

As one can see from Fig. 4 the PbSe films obtained in our laboratory present a uniform electrical conductivity in a direction perpendicular to the electrical contacts. The evaporated Au and Ag electrical contacts present an ohmic behaviour.

IV **Conclusions.** IV.1 *The Photopyroelectric Method.* The method proposed in this paper for measuring the optical absorption of the nontransparent materials is simple and direct. It is important to point out that for nontransparent samples the clasical spectrophotometric method can

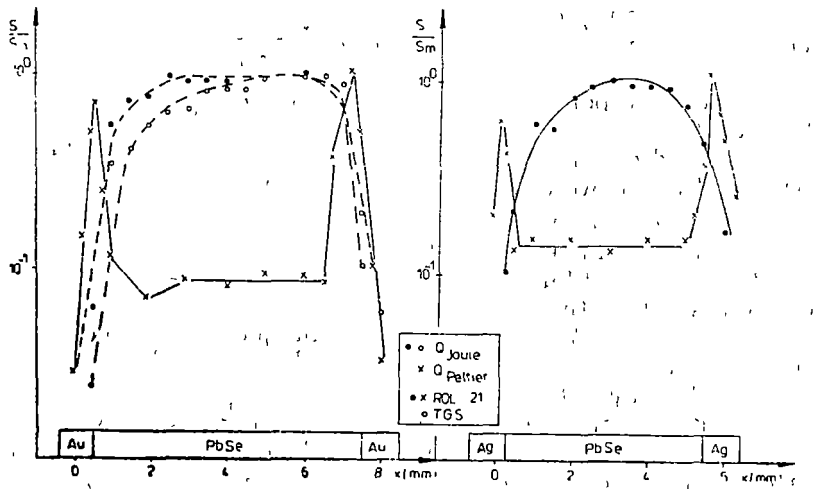

Fig. 4 The magnitude of the detector's signals, normalized at their maximum values, for PbSe films prepared by chemical deposition (left) and by vacuum evaporation (right).

not be applied, and thatos why the photopyroelectric method is very useful in compairing different nontransparent materials used as absorbent layers for IR detectors

IV 2 *The Photothermal Deflection Method.* The transverse photothermal deflection method proposed in this paper can give accurate spatial conductivity and Peltier effect profiles for thin-film semiconductors. The resolution of the method depends on the diameter of the laser beam. The method gives only qualitative results because the detector signal is strongly dependent on the geometry of the detection configuration.

REFERENCES

1 D Dădârlat, M Chirtoc, R. M Cândea, I. Bratu, *Infrared Phys*, **24**, 469 (1984)
2 C. C Ghizoni, L C M. Miranda, *Phys. Rev*, **B 32**, 8392 (1985)
3. C E Yeack, R L Melcher, S S. Jha, *J. Appl. Phys*, **53**, 3947 (1982)
4 H. Dersch, N M Amer, *Appl Phys Lett*, **45**, 272 (1984)
5. D Dădârlat, M Chirtoc, R M. Cândea, *Phys. Stat. sol.* (*a*) **98**, 279 (1986)
6 A. Mandelis, F Care, K. K Chan, L C M Miranda, *Appl. Phys.*, A **38**, 117 (1985)
7 See for example: A. C Tam, *Rev. Mod Phys*, **58**, 381 (1986)
8 W. B Jackson, N. M. Amer, A C Boccara, D. Fournrier, *Appl. Opt*, **20**, 1333 (1981)

STUDIA UNIV BABEŞ—BOLYAI, PHYSICA, XXXII, 1, 1987

CONTRIBUTIONS TO THE ELECTRICAL AND MAGNETICAL METHODS OF THE PHYSICAL-MECHANICAL PARAMETER DETERMINATION OF THE MACHINE PARTS MADE OF FERROMAGNETIC AND NON-FERROUS MATERIALS

HUBA SZŐCS*

Received : November 27, 1987

ABSTRACT. — In this paper the dependence between the hardness of ferromagnetic metals and the coercive field is treated, on the basis of the physical theory of metal microstructure The conclusion is that between the H_c coercive field and the HB hardness there is a striaght relation

$$H_c = k \cdot HB$$

where k is constant.

So, measuring the hysteresis curve diameter for the induction $B = 0$ we obtain an imediate information upon hardness The measurement shows a good concordance with reality in the limits of a relatively smaller variation of hardness

The quality of products is a desideratum of the products competition both in our country and abroad

Among the technical parameters that determine the quality of metalic products we can mention their hardness.

Among the methods of hardness static determination there is also used the method of the mark left by a harsh body on the surface of the machine-part to be measured (the Brinell, Wickers and Rockwell Method).

The hardness is calculated out of the relation between the marked surface area and the press force (N/mm^2 or Brinell units of measurement etc.).

The advantage of these methods is their high precision, their shortcoming consisting in the fact that they are laborious and need a long time, so that they are not suitable for the line of high productivity (machine parts such as screws, nuts etc.).

I. For these reason an automatic measurement of hardness is necessary, or at least a sensitive shortening of the measurement lenght of time.

This problem is still in the process of being solved, and there are few patents worlduride that are available, reason for which agreement No. 1874/1984 with the productive units has been concluded.

A mean of automatic and semiautomatic evaluation and measurement of hardness is offered to us by the magnetising curve — the hysteresis — of the ferromagnetical material (Fig. 1) that can be raised with the help of ballistic galvanometer or with the help of a cathodic oscilloscope — a dinamical and fast method (Fig 2)

* Liceul cu Clasele I—VIII Nr. 6 Engineering Institute of Baia Mare, 4800 Baia Mare, Romania

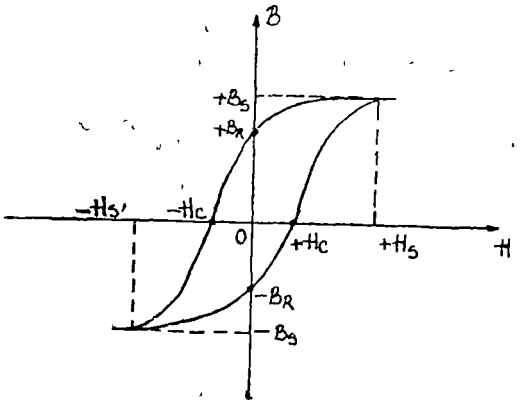

Fig 1 Hysterezis-curve of ferromagnetic substances

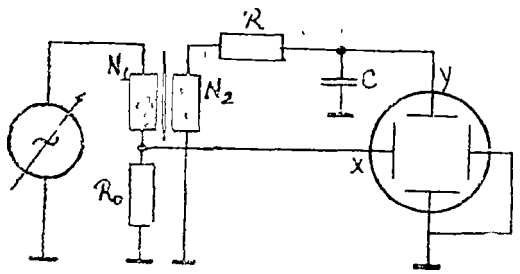

Fig 2 Electronic-scheme for the obtaining of the hysterezis-curve

The signal applied on the X input (horizontally) of the H magnetising field, and the signal applied on the Y input (vertically) is proportional to the B magnetic induction, this signal is obtained at the output of an integration circuit due to relation (1)

$$\int u_i(t)dt = \int \frac{d\Phi}{dt} dt = \Phi_B = n \cdot B \quad S = k \cdot B \tag{1}$$

where u_i is the signal got at the output of the N_2 measurement bobbin, Φ_B being the flux of the magnetic induction vector $\bar{B}$, n being the number of helix, S being the bobbin surface and $\bar{B}$ the magnetic induction The hysteresis curve thus obtained is stable and it nearly does not depend on the position of the machine part in the N_1 exitation bobbin, B_r is the remanence induction, B_s is the saturation induction, H_s is the saturation field, H_c *is the corcive field.*

Between the coercive field and the saturation field there is relation (2)

$$H_s = k \cdot H_c \tag{2}$$

where k is a constant that can take values between 2 and 3.

Due to the reference material [1, 2, 3] there is a tight connection between the coercive field H_c and several physical and technical parameters of the substance

Thus between d medium diameter of the crystal grain and the coercive field there is the relation inferred from theory (3)

$$H_c = \frac{A}{d} \tag{3}$$

where $A = \pi\gamma/\mu_0 M_s$ (which in the case of iron $\gamma = 10^{-3}$J/m, where M_s is the value of the magnetising vector at saturation) has the value $A = 1{,}5 \times 10^{-3}$ A (Ampère) that is well verified in praxis

Generally, the coercive field is determined by the shift of the Block walls and the rotation of M_s vector (H_c respectivelly) but it also depends of some other elements (internal mechanical tension, the degree of hardening — return — recrystallising, magnetic anisotropy, inclusions etc.).

In these condition the comparison is possible among the parts of the same composition and structure, the variation of the coercive field being owed to the hardness variation only. Indeed, out of the analyses of the parameters of the hardness of the ferromagnetic substance it results that there is a tight connection between the middle diameter of the grain and HB (4) hardness [4]

$$HB = \frac{C}{d} \tag{4}$$

where C is an experimental constant. Thus out of (3) and (4) results

$$H_c = A \cdot C \cdot HB \tag{5}$$

so, a dependence of the H_c coercive field on the hardness of the part in HB, that and the same substance may vary according to the applied thermic treatement

But a difficult problem is represented by the obtaining of magnetic magnetic saturation of the parts that regurarly form open magnetic circuit.

That is why, our reserch work will be centred upon the weak magnetising theory.

II The results of the measurements are included in Table 1, in which d' is the diameter of the histeresis curve for $B = 0$, and HB being hardness in Brinell.

Table nr 1

Hardness HB	360	363	366,33	373	376,33	383	389,33	477
Diameter d', mm (medium values, I = 1,5 A, R_0 = 5 — 10 Ohm)	32	32,5	32,5	33,5	434	34,5	35	37

Comment The corresponding diameter was taken instead of the H_c coercive field.

Thus

$$HB = k_1 \cdot d' \tag{6}$$

The results are in good concordance with reality in the limits of a relativelly restricted variation of hardness (sensitivity $S = 23{,}4\ HB/mm$).

REFERENCES

1 M Ursache, D. Chircă, „The Metal Properties", EDP, Bucureşti, 1982
2 H Szőcs, Experimental Investigation on the Automatic Measurement of the Hardness of steel Screws, *Cooperation Contract* 1874/1984.
3 S V Vonsovski, „Magnetism", E. St Enc, Bucureşti, 1981
4 H Schumann, „Physical Metallurgy", E then, Bucureşti, 1962

STUDIA UNIV. BABEŞ–BOLYAI, PHYSICA, XXXII, 1, 1987

HIGH TEMPERATURE SUPERCONDUCTIVITY IN Y—Ba—Cu—O SYSTEM

T. PETRIŞOR*, A. GIURGIU and I. POP*****

Received. April, 10, 1987

ABSTRACT. A high temperature superconductor $YBa_2Cu_3O_{9-\delta}$ was obtained with the critical temperature $T_c = 105$ K. The temperature dependence of the static magnetic susceptibility was investigated. This temperature dependence has a caracteristic jump at the temperature transition from the normal state in the superconductive state.

Recently Ba-Y-Cu-O compound exibit high T_c superconducting transition about 90 K [1]. For Ba-La-Cu-O compounds it was recognised [2] that the superconducting transition is bound up with the composition. The $Ba_xLa_{1-x}CuO_{4-y}$ ($x < 0,1$) phase with the K_2NiF_4 type layer perovskite structure and the $LaBaCu_2O_{5-y}$ phase with the superstructure based on the simple cubic perovskite structure show the superconducting transition at about 40 K and 15 K respectively.

A stable and reproductible superconductivity transition between 80 K and 93 K has observed in $(Y_{1-x}Ba_x)_2CuO_{4-\delta}$ system [3; 4]. As pointed out by R.J. Cava et. all. [5] the superconducting material reported in [3] consisted in a mixture of several phases.

They find that the $YBa_2Cu_3O_{9-\delta}$ phase (black) is superconducting and that the Y_2BaCuO_5 phase (green) is semiconducting.

Cava et. all. reported bulk superconductivity in the $YBa_2Cu_3O_{9-\delta}$ pure phase below 91 K.

We prepared single phase $YBa_2Cu_3O_{9-\delta}$ compound through solid state reaction of appropriate amounts of Y_2O_3; $BaCo_3$ and CuO in similar fashion to that described by Cava [5].

The samples showed superconducting properties in liquid nitrogen. Magnetic susceptibility measurements were carried out with a Weiss-Forrer equipment between 80 K and 300 K in a 0.9 T magnetic field intensity.

* *Institute of Metrology, Cluj-Napoca, 3400 Cluj-Napoca, Romania*
** *Polytechnical Institute of Cluj-Napoca, 3400 Cluj-Napoca, Romania*
*** *University of Cluj-Napoca, Faculty of Mathematics and Physics, 3400 Cluj-Napoca, Romania*

Fig 1

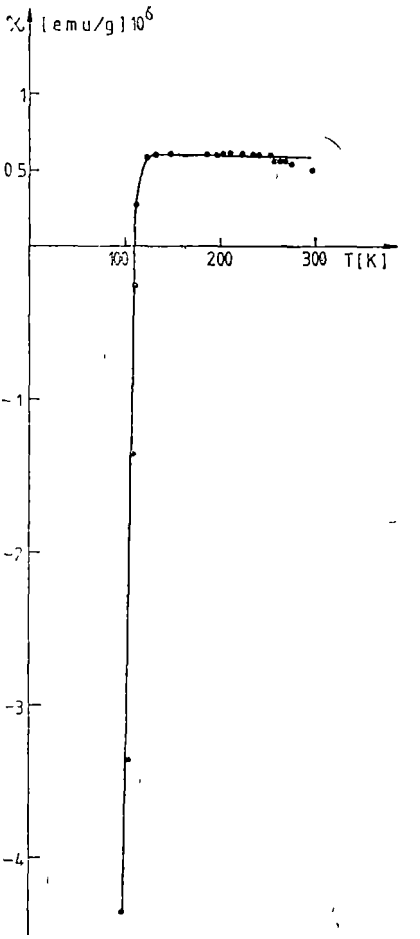

The temperature dependence of the magnetic susceptibility is showed in the Fig. 1.

The sample is diamagnetic below 105 K, showing a sharp drop of the magnetic susceptibility. This behaviour is specific for the superconducting transition. Above the critical temperature ($T_c = 105$ K) the magnetic susceptibility is weelky temperature dependent and about $0\,5\ 10^{-6}$ emu/g.

The small value of the magnetic susceptibility and the week temperature dependence shows that the magnetic moments of Cu^{2+} ions, even if present, do not show their presence in a static measurement This fact supports the idea of valence fluctuation of Cu ions in the CuO_2 layer of $YBa_2Cu_3O_{9-\delta}$ compound

REFERENCES

1. J. G. Bednorz and K Muller, *Z. Phys. B* **64**, 189 (1986)
2. C. W Chu, P. H Hor, R L Meng, L Gao, J. Huang, Y. Q. Wang, J. Behtold, D C Campbell, M. K Wu, J. Ashburn, C. Y. Huang, *Phys, Rev. Lett* **98**, 4 (1987)
3. M. K. Wu, J R Ashburn, C J Torng, P. H Hor, R. L. Meng, L. Gao, Z H Huang, Y. Q Wang, C W. Chu, *Phys. Rev. Lett*, **58**, 908 (1987)
4. P. H Hor, L Gao, R L. Meng, Z. J. Huang, Y. Q. Wang, K. Forster, J. Vassilious, C W Chu, M. K Wu, J. R. Ashburn, C. J. Torng, *Phys Rev Lett*, **58**, 9 (1987)
5 R J Cava, B Batlogg, R B van Dover, D. W. Murphy, S. Sunshine, T. Siegrist, J. P Remeica, E. A. Rietman, S. Zahurak, G. P. Espinosa, *Reprint* (1987)

STUDIA UNIV BABEŞ–BOLYAI PHYSICA, XXXII, 1, 1987

PHYSICAL AND CHEMICAL STUDIES OF THE POLYMERIZATION PRODUCT OF PYROL WITH PHOSPHORIC ACID

ION CĂPLĂNUŞ,* MELANIA GUŢUL**, CRISTINA MANDRAVEL** and ALEXANDRU NICULA***

Received June 15, 1987

ABSTRACT. — The polymerization product obtained from pyrol and phosphoric acid is investigated by elemental chemical analysis, IR spectroscopy and differential thermal analysis

1. **Introduction.** The combinations of pyrol with HCl, HBr, HI, CH_3COOH are unstable [1—4] because they polymerize very easily. Due to the fact that we could not find data on the behaviour of pyrol in the presence of phosphoric acid, the purpose of this work is to give a physical and chemical characterization of the product obtained by polymerization in this case.

2 **Experimental.** The reagents used were pyrol p a Riedel der Haen, redistiled for every charge of product and phosphoric acid p a 85% UCB-Belge The preparation method was similar to that described by Treibs [3]. The IR spectra were recorded on a IR-10-Zeiss Jena spectrometer, in the frequency range from 400 cm^{-1} to 4 000 cm^{-1}, at the room temperature, on samples obtained by the pastillation technique in KBr

The differential thermal analysis (DTA), differential thermogravimetric (DTG), thermogravimetric (TG) and temperature (T) curves were simultaneously recorded on a MOM derivatograph, type Paulik, using samples with a mass of 0,09 g, at a heating rate of 10 degrees/minute.

3. **Results.** The polymerization product of the pyrol with phosphoric acid has black colour, brown in fresh section, and has a density of 1,3308 g/cm^2. It is onctuous, insoluble in acetone, benzene, ethyl alcohol, carbon tetrachloride and ethyl ether For this reason it was not possible to determine the molecular mass using colligative properties.

The elemental chemical analysis leads to the following data . C 28,40% ; H . 3,34% ; N · 8,80% , P , 18,80%.

Typical IR spectra are presented in Figure 1 The frequencies corresponding to the maxima of the absorption bands are indicated in Table 1. The IR spectrum of the polymerized product is expected to have a com-

* *University of Bucharest, Faculty of Physics, 7 Bucharest, Romania*
** *Polytechnic Institute — Bucharest, 7 Bucharest, Romania*
*** *University of Cluj-Napoca, Faculty of Mathematics and Physics, 3400 Cluj-Napoca, Romania*

plex character, in view of the fact that pyrol alone has 24 normal vibrations, ranging between 618 cm^{-1} and 3133 cm^{-1} [5]

In order to assign the observed frequencies we tried a judicious correlation with the data from the literature [6—8] on the vibrational spectra In Table 1, the sites where more assignments of the frequencies are possible are mentioned between accolades, because the respective possibilities are not always exclussive For example, the maximum from 1080 cm^{-1} is compatible both with $\nu_2 = 1076$ cm^{-1} and with $\nu_{13} = 1074$ cm^{-1}, due to the fact that both values are normal frequencies of the pyrol molecule [6, 7].

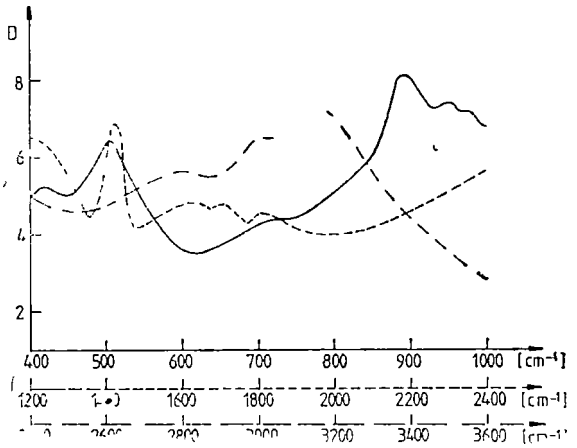

Fig 1 The IR spectra of the studied samples.

Table 1

The frequencies of the absorption maxima from the IR spectra and their assignments.

ν max [cm^{-1}]	Assignment
495	δ_{O-P-O} (in PO_4^{3-} at 500 cm^{-1})
720	γ $(CH_2)_n$ at $n > 4$ β ring (711 cm^{-1})
980	δCH (unplanar) $\nu_{12}(B_1)$ CH pyrol (1015 cm^{-1})
1080	$\nu_2(A_2)$ CH pyrol (1076 cm^{-1}) $\nu_{13}(B_1)$ NH pyrol (1074 cm^{-1})
1140	$\nu_3(A_1)$ pyrol pulsation (1140 cm^{-1})
1410	δCH planar (CH_2-N^+) group, $(CH_2-C=C)$ group $\nu_{14}(B_1)$ pyrolic ring (1418 cm^{-1})
1640	$\nu_{C=C}$
2810	ν_{OH} in H_2PO_4 $\nu_{O\ H-N}$ (by the shift of ν_{R-N-H} in the aromatic cycle)
3030	ν_{CH}
3130	$\nu_8(A_1)$ ν_{CH} pyrol (3133 cm^{-1})
3400—3700	ν_{NH}
2500—3200	intramolecular hydrogen bonds

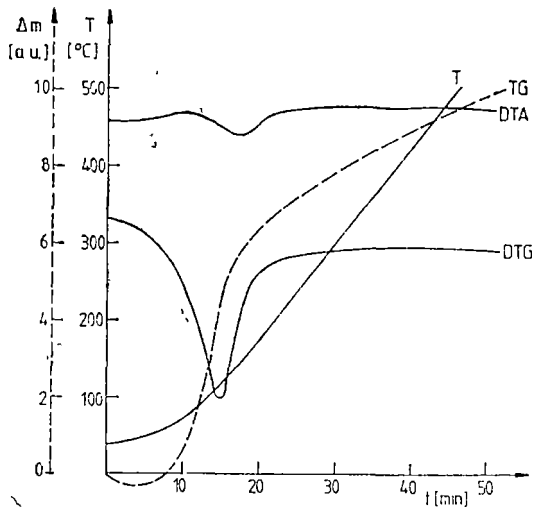

Fig. 2. The DTA, DTG, TG and T curves for the polymerization product.

The DTA, DTG, TG and T curves for the studied polymerization product are presented in Figure 2. One notices from the differential thermal analysis an endothermal effect corresponding to a partial thermal degradation. The maximum transformation rate with the temperature was recorded at 160 °C. The evaluation of the kinetic parameters of the thermal decomposition based on thermogravimetric data was made using the Freeman — Caroll and Coats — Redfern [9—11] methods on the same thermogram, as the conditions of low deviation from the liniarity for the T curve was fullfilled. Figures 3 and 4 represent the Freeman — Caroll and Coats — Redfern curves which lead to the following kinetic parameters for the thermal decomposition of the studied product:

Freeman — Caroll method

$m_p = 0{,}0970$ g

$W_c = 0{,}0685$

Coats — Redfren method

$m_p = 0{,}0970$ g

$W_c = 0{,}0685$

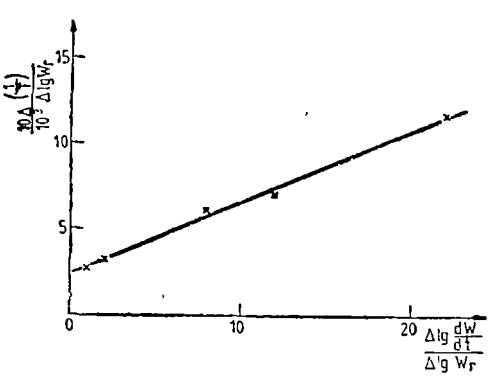

Fig. 3. The Freeman—Caroll curve for the thermal decomposition of the polymerization product.

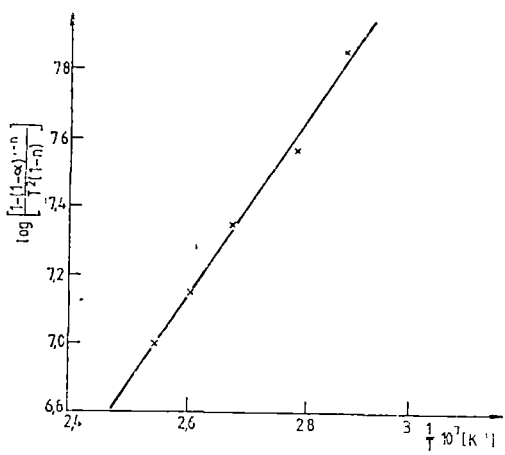

Fig. 4 The Coats—Redfern curve for the thermal decomposition of the polymerization product.

$n = 0,9$	$n = 0,9$
$E = 12,19$ kcal	$E = 13,12$ kcal

where m_p is the mass of the sample, W_c is the amount of the volatile component which may be elliminated from the reaction, n is the reaction order and E is the value of the activation energy.

The value of the reaction order n obtained by Freeman — Caroll method is used as test in the Coats — Redfern method and permits, by an iterative process, to evaluate more accurately the reaction order n and the activation energy E.

4. **Discussion.** Due to the fact that the maxima of more bands observed in the IR spectra of the polymerized samples from pyrol and phosphoric acid are very near to the frequencies corresponding to the normal vibration modes of the pyrol, the unambiguous identification of the pyrolic cycle [8] is based on the simultaneous presence of the absorption bands in the range 3130 cm^{-1} — 3100 cm^{-1}, of the band corresponding to the vibrations —C=C at 1410 cm^{-1} and of the absorption in the range of 3410 cm^{-1}. The intensity of the absorption band which appears near the frequency of 3490 cm^{-1} is diminished, this phenomenon being specific to the spectra obtained on pastillated samples.

On the other hand, in the works which investigate the aging effects in pyrol [1] it is shown that qualitatively the IR spectra of the polypyrol films are practically indistinguishable from the spectrum of the pure pyrol. The structure of the polymer is apparently the same to that of the liquid pyrol, and no modifications are observable

The occurence in the polymerized compound of the radicals derived from the phosphoric acid is proved by the IR spectral analysis, particularly by the existence of the band corresponding to the deformation vibrations δ_{P-O-P} at a frequency very close to the ν_4 frequency of the PO_4 radical and the existence the band from 1140 cm^{-1}, which may be assigned to the shift of the valency vibration P-O (1160 cm^{-1}). As regards the bonding manner of the two specific structural groups, the IR spectra offer information about the presence of bonds such as PO bonded to cycles with aromatic character and about the presence of the hydrogen bonds. The existence of the bonds P-O-aromatic cycle is supported by the absorption from the 1240 cm^{-1} — 1190 cm^{-1} (ν_{CO}) range and by the absorption maximum observed at 1140 cm^{-1} (ν_{PO}). The absorption band with the maximum at 2810 cm^{-1} may arise from the shift of the band R-N-H, where R has aromatic character, like in the case of the pyrol implicated in hydrogen bonds [8].

The kinetic study carried out by differential thermal analysis of the polymerization product of pyrol with phosphoric acid indicates a maximum transformation rate at 160°C and denotes an endothermal effect corresponding to a partial thermal distruction.

REFERENCES

1. R. H. Linell, S. K Umar, *Archiv Biochem Biophys.*, **57**, 264 (1955)
2. A. Pieroni, A. Maggi, *Gazetta Chim. Ital*, **53**, 120 (1923)
3. A. Treibs, H. G Kohn, *Ann.*, **606**, 166 (1957)
4. A. Treibs, *Rev. Roum. Chim. T VII*, **2**, 1345 (1962)
5. Gh. Mateescu, „Aplicațiile spectroscopiei de IR în chimia organică", E,d. Acad. București, 1966
6. K. Nakamoto, „Infrared Spectra of Inorg Coord. Compounds", Loudon, 1966, p. 388
7. A. Cross, „An Introduction to Practical IR Spectroscopy", London, 1960, p 103
8. K. Nakamishi, „IR Absorption Spectra", London, 1962
9. D. W. Coats, P. Redfern, *Nature*, **201**, 4914 (1964)
10. E. S. Freeman, E. Caroll, *J. Phys. Chem.*, **62**, 394 (1958)
11. E. Segal, C. Vasile, *An Univ. Buc.*, **1**, 17 (1966).

ÎNTREPRINDEREA POLIGRAFICĂ CLUJ,
Municipiul Cluj-Napoca, Cd nr 132/1987

În cel de al XXXII-lea an (1987) *Studia Universitatis Babeş—Bolyai* apare în specialităţile:

matematică
fizică
chimie
geologie-geografie
biologie
filosofie
ştiinţe economice
ştiinţe juridice
istorie
filologie

In the XXXII-nd year (1987) of its publication, *Studia Universitatis Babeş—Bolyai* is issued as follows:

mathematics
physics
chemistry
geology-geography
biology
philosophy
economic sciences
juridical sciences
history
philology

Dans sa XXXII-e année (1987), *Studia Universitatis Babeş—Bolyai* paraît dans les spécialités:

mathématiques
physique
chimie
géologie-géographie
biologie
philosophie
sciences-économiques
sciences juridiques
histoire
philologie

43 904

Abonamentele se fac la oficiile poștale, prin factorii poștali și prin difuzorii de presă, iar pentru străinătate prin „ROMPRESFILATELIA", sectorul export-import presă, P. O. Box 12—201, telex. 10376 prsfir, București Calea Griviței nr. 64—66.

Lei 35